Space domain analysis of inhomogeneous waveguides of the microstrip and inset guide families

Izzat, N.

Award date:
1991

Awarding institution:
University of Bath

SPACE DOMAIN ANALYSIS OF INHOMOGENEOUS WAVEGUIDES OF THE MICROSTRIP AND INSET GUIDE FAMILIES

Submitted by

N. Izzat

for the degree of PhD

of the University of Bath

1991

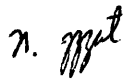

ProQuest LLC
789 East Eisenhower Parkway
P.O. Box 1346
Ann Arbor, MI 48106-1346

ABSTRACT

This thesis is concerned with the analysis of generalised microstrip and inset dielectric guide structures. A large class of structures is considered, including boxed, covered and open multilayered microstrip, multilayered inset dielectric guide, and microstrip loaded inset dielectric guide.

In addition a number of different microstrip circuits house within the inset dielectric guide are also considered.

The emphasis of the work is on obtaining the dispersion characteristics of these devices using a fully rigorous hybrid method. The analysis is carried out in the space domain and is based on the Transverse Resonance Diffraction method.

Particular advantages and characteristics of these structures as transmission line and antenna media are identified and discussed.

ACKNOWLEDGEMENTS

The author would like to thank Professor T. Rozzi and Dr. S. R. Pennock for their expert supervision and advice during the course of this work.

The author also thanks fellow Postgraduate students for helpful discussions and contributions to the theoretical and experimental aspects of the work.

PUBLICATIONS ARISING FROM THIS WORK

1. T. Rozzi, S. R. Pennock and N. Izzat, "Bandwidth Control in multilayer Inset Dielectric Guide", Paper Pl.19, Proc. 20th European Microwave Conf., Budapest, Hungary, Sept. 1990.

2. S. R. Pennock, N. Izzat and T. Rozzi, "Operating Parameters of the Inset Dielectric Guide", IEE Colloquium - "Field Analysis of Microwave Devices and Circuits", London, January 1991.

To Nazli and Nart

CONTENTS

CHAPTER 1

INTRODUCTION

1.1 GENERAL DEVELOPMENTS IN PLANAR WAVEGUIDES

Research was conducted, following the second world war, into alternative waveguides to the rectangular waveguide. The aim was to achieve wider bandwidth than was possible with rectangular waveguide. Microstrip was suggested as a possible alternative [1]. Wider bandwidth is achieved due to the zero cutoff frequency of the fundamental mode. However, the fundamental mode is not TEM, and as a result the transmission line parameters are frequency dependent. This complicated analysis and design procedures. Microstrip was therefore not initially popular, but, interest in a miniaturised form of microstrip was rekindled in the 1960s and the miniaturisation paved the way for the use of microstrip in microwave integrated circuits.

Research into new waveguide structures continues, particularly as the operating frequencies increase. Higher frequency applications can be simply achieved by scaling down of lower frequency designs. However, additional problems arise at higher frequencies which create the need for new alternative designs. At higher operating

frequencies, microstrip transmission line suffers from an increase in radiation loss, conduction loss and from overmoding. The miniaturization which is an asset at the microwave range can become a liability at higher frequencies due to the more stringent manufacturing tolerance. The maximum practical frequency limit for microstrip is 90 Ghz [2].

Fin-line transmission line has been suggested for use at higher frequencies [3]. Mechanical tolerances are less stringent than for microstrip. The fundamental mode of fin-line has no propagating mode at zero frequency and there is greater freedom from overmoding. Losses in fin-line are less than in microstrip. In addition the device is compatible with beam-lead and chip devices, thus offering the potential for integration with monolithic integrated ciruits.

A variant on microstrip which exhibits lower loss is suspended substrate microstrip (SSS) [4]. The substrate in SSS is used only to support the strip conductors. The removal of the ground plane from the dielectric and reduced field confinement causes a reduction in loss compared to microstrip.

Another waveguide which is becoming of increasing importance is the coplanar waveguide [5]. The earthed "side-planes" in the guide, reduce the effect of coupling

between neighbouring lines, and facilitate the connection of active components such as the diode across the line.

1.2 THE INSET DIELECTRIC WAVEGUIDE

A number of different dielectric waveguide structures, such as imageline [6], have been suggested for use in the millimetric wave spectrum (30-300 GHz). Each waveguide has its own particular advantages and disadvantages and a comparative study of a range of these waveguide is given in [7].

The inset dielectric guide (IDG) [8] has been investigated for its suitability as a transmission media in the microwave and millimetric region [9]. The advantages of IDG include:

1. Low transmission loss.
2. Ease of fabrication.
3. The ability to negotiate bends with minimal loss.
4. Easy inclusion of devices such as diodes.

In addition to its suitability as a transmission line media, the IDG has also demonstrated its usefulness as an antenna media [10-14]. The advantages of IDG realized antennas include, in addition to the above advantages:

1. Field confinement of the electromagnetic field in the slot.
2. Low cross polarization.

1.3 MICROSTRIP ANTENNAS

Reference to a microstrip antenna array can be found as far back as 1955 [15], only three years after the conception of the microstrip transmission line itself [1]. Early interest in radiation from microstrip, however, was aimed at avoiding radiation in order to minimise loss in transmission line applications, and active interest in microstrip antennas did not emerge until the 1970s. The main advantages of microstrip antennas are considered to be:

1. Light weight.
2. Thin profile allowing the antenna to mounted on the surface of missiles and aircraft.
3. Low fabrication cost and simple manufacture.
4. Easy integration with circuits

Since the 1970s, extensive research has been carried out into a very wide range of microstrip antennas [16].

1.3.1 LIMITATIONS OF MICROSTRIP ANTENNA

1.3.1.1 The Presence of Substrate Surface Waves

The existence of substrate surface waves in microstrip becomes evident when one considers the fact that the dielectric substrate together with its ground plane in microstrip, can support dielectric slab-type modes [17], these waves may be launched to some degree from discontinuities in the circuit. It is thought that the effect of these waves in transmission line applications is of secondary importance [16]. However, substrate surface waves impose a severe limitation on microstrip antenna applications at higher frequencies, where two problems are encountered: the power efficiency of the antenna is degraded due to power lost to the surface waves, and stray coupling resulting from the scattering of the waves of discontinuities in their path, and of the edge of the assembly.

1.3.1.2 Narrow Bandwidth

A major problem with microstrip antennas is their typically narrow VSWR bandwidth. This is due to the radiation mechanism in the open-circuited lines or patches. A variational method of analysis of the microstrip open-circuit termination which models the behaviour of the termination over a wide frequency range is given in [18].

An estimate of bandwidth of radiation from a dipole using the variational method [18] gives the following simple relationship for the bandwidth (B) [16]:

$$B \propto \frac{1}{\epsilon_r}\frac{h}{\lambda_0} \qquad (1.1)$$

Where, ϵ_r is the relative permittivity of the material, and h is the thickness of the substrate. Thus the bandwidth is expected to increase for lower permittivity, thicker substrate and at higher frequencies.

Several methods for improving the bandwidth in microstrip antenna have been suggested. Radiation from curved microstrip lines avoid the open-circuit radiation mechanism. Very wide bandwidth for circularly polarized antenna is reported in [19] where a spiral transmission line is used as the radiating element.

Wide bandwidth has also been achieved by introducing parasitic elements in the vicinity of the radiating patch in order to damp the Q-factor of the patch (Figure 1.1) [20].

1.4 THE ELECTROMAGNETICALLY COUPLED MICROSTRIP ANTENNA

Energy can be coupled into a patch radiator by placing it above a microstrip line, where coupling would occur due to the interactions of fringe fields between the two

conductors. Such a form of antenna is referred to as an electromagnetically coupled antenna. Early examples of such an antenna are given in [21,22]. Figure 1.2 shows possible forms of such resonators. The advantages of the electromagnetically coupled antenna include:

1. The reduction of unwanted radiation from the feed
2. A large degree of control over the coupling which can be achieved by varying the circuit dimensions and permittivities.
3. Reduced size of the antenna.

These advantages are offset by the increase in difficulty of manufacture.

An electromagnetically coupled antenna with a log periodic array of elements that has a wide bandwidth is given in [23], where a bandwidth of 8-10.75 GHz (30%) is achieved.

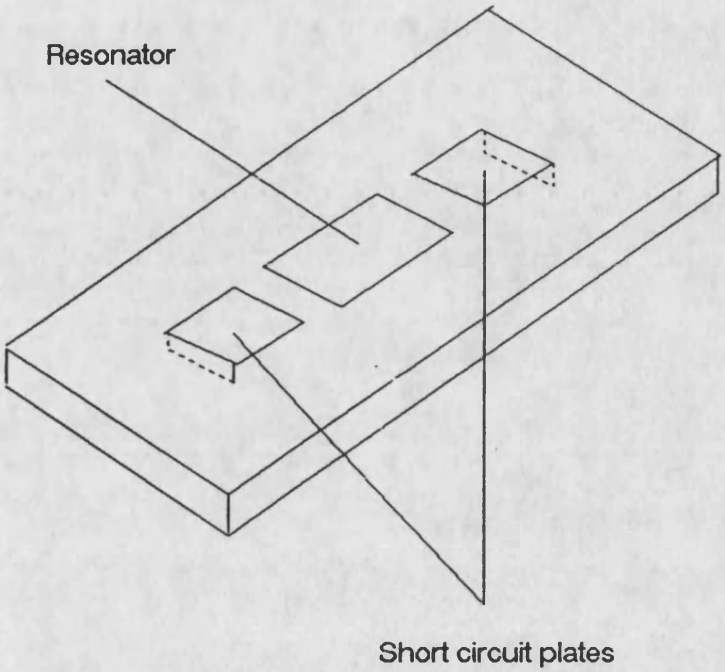

Figure 1.1 Bandwidth increase using parasitic elements

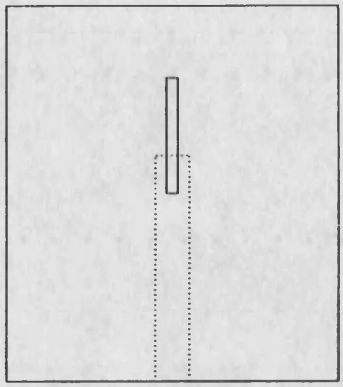

(a)

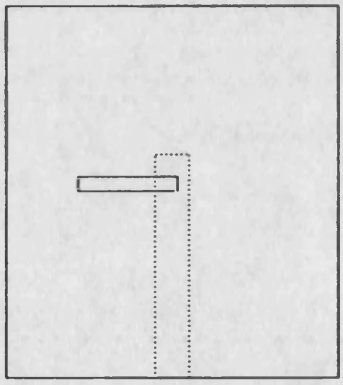

(b)

Figure 1.2 Examples of electromagnetically coupled resonators
(a) Radiator coupled to microstrip feed line
(b) Radiator orthogonally coupled to microstrip feed line

1.5 SURVEY OF NUMERICAL METHODS OF ANALYSIS

A wide variety of methods have been used in the past to analyze waveguide structures, and a complete review of these methods would be difficult. However, in general two approaches can be identified. One general approach is to adopt a numerical method that assumes no prior knowledge of the field behaviour in the guide and to arrive at solutions using purely iterative processes. Examples of such an approach include Finite Element methods [24] and Finite Difference methods [25]. The advantage of such methods is their generality, but slow convergence may result in using these methods thus requiring extensive computer resources and introducing numerical errors. On the other hand an analytic approach may be adopted where knowledge of the field behaviour is sought and were algebraic manipulation is used in order to reduce the computational effort involved. The latter approach may provide very accurate results with minimal computation, however the methods used tend to be complex and limited to specific types of structures.

1.5.1 SPECTRAL DOMAIN METHODS

The Spectral Domain approach [26] is an analytic approach that has recently gained in popularity. The term Spectral Domain refers to the application of integral transform methods such as the Fourier and Hankel transforms, to the

solution of boundary-value and initial-value problems. An early example of a Spectral Domain method for microstrip dates back to 1957 [27] where a Fourier transform method was used to analyze microstrip. Several other Spectral Domain methods have been introduced since [28..31].

A Spectral Domain method widely adopted by the microwave community, and referred to as the "Spectral Domain Immitance Approach" is given in [32] for the analysis of generalised microstrip circuits. In this approach the dyadic Green's functions are obtained in the transformed domain by expressing the Fourier transforms of the field components in terms of LSE and LSM wave potentials. This leads to a natural decoupling of the hybrid (transformed) field into the superposition of TE and TM transmission lines acted on by a suitable coordinate transformation. The hybrid field is considered to be generated from current or field sources located at the interfaces between the various layers of the circuit. Where several sources exist in the circuit, the field generated from each source is first considered independently and the total field is then expressed as the superposition of the fields from all the sources, and is made to be obey the boundary conditions at the various interfaces in the circuit. The particular advantages of the spectral domain immitance approach is the simplicity of the formulation process, which can be accomplished almost by inspection, as well as computational efficiency provided transforms of the various current and

field sources in the circuit are obtainable in a closed form.

While the Spectral Domain Immitance approach is very efficient for analysing generalised microstrip and slotline structures, it cannot be applied to waveguide structures where the cross-sectional geometry is non-uniform (such as the IDG) since the Fourier transform variable for such structures is different for the various layers.

A Mixed Spectral Domain approach is given in [33], where an attempt is made to overcome the above mentioned difficulty. In this method, which has been used to analyze structures with non-uniform cross-sectional geometry, such as the pedestal-supported stripline (Figure 1.3a) [34] and pedestal-supported fin-line (Figure 1.3b) [35], the waveguide structure is replaced by an equivalent structure, the elements of which can be individually analyzed using the spectral domain immitance approach. The total field is then expressed as the superposition of the fields in each of the elements of the equivalent structure, and is made to obey the various boundary conditions in the circuit [33].

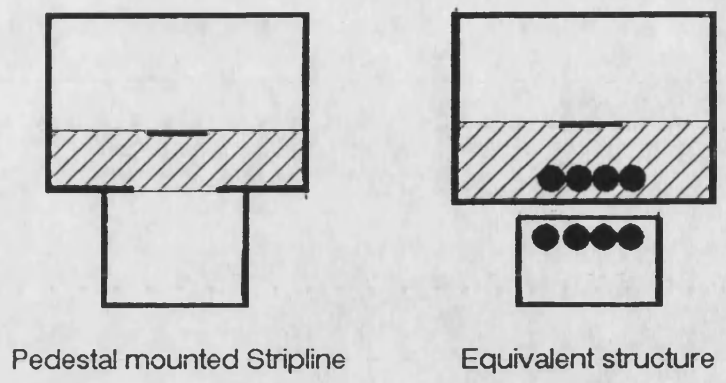

(a)

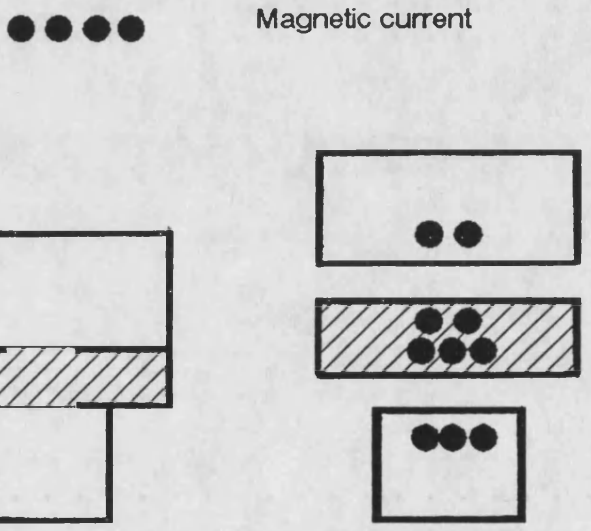

(b)

Figure 1.3 The pedestal supported strip-line and pedestal supported fin-line and their equivalent structures

1.5.2 TRANSVERSE RESONANCE DIFFRACTION

Transverse Resonance Diffraction (TRD) is a space domain method, which has been used to analyse efficiently a number of different waveguides including image-line [36], fin-line [37], IDG [38], and microstrip [39]. The technique has the advantage of its applicability to waveguide structures that may have a non-uniform cross-sectional geometry. The elements of the TRD method can be summarised as follows:

1. The structure is divided into distinct regions, and the fields in each region are expressed in terms of a complete set of potential functions.

2. Admittance operators are derived in the space domain relating the various field components to each other, in each of the regions.

3. Boundary conditions are imposed on the field components at the interface between the various regions of the guide.

4. A scalar equivalent circuit is then introduced for the waveguide.

1.6 STRUCTURE OF THE THESIS

A brief outline of the content of this work is given in

this section. The thesis is devoted to the analysis of several different waveguide structures with a view of identifying particular characteristics and advantages of these waveguides for use as antenna elements, antenna feeds as well as transmission lines.

In chapter 2 a method of analysis of generalised microstrip circuits considering the case of boxed, open or covered microstrip structures (Figure 1.4a).

Chapter 3 considers the Inset Dielectric Guide (IDG) (Figure 1.4b) where in particular the presence of several dielectric layers in the IDG slot is considered.

Chapter 4 consider the Microstrip Loaded IDG (MLIDG) (Figure 1.4c), where the dispersion characteristics including higher order modes are presented together with measured and calculated values of characteristic impedance.

Chapter 5 considers a new range of waveguide structures including the partially filled MLIDG, Embedded Strip IDG, and Multiple Strip IDG (Figure 1.4d). Possible useful applications for these waveguides are discussed and an accurate method for the analysis of these guides is presented.

Finally in Chapter 6, a summary of the work undertaken

herein is given with suggestions for future research.

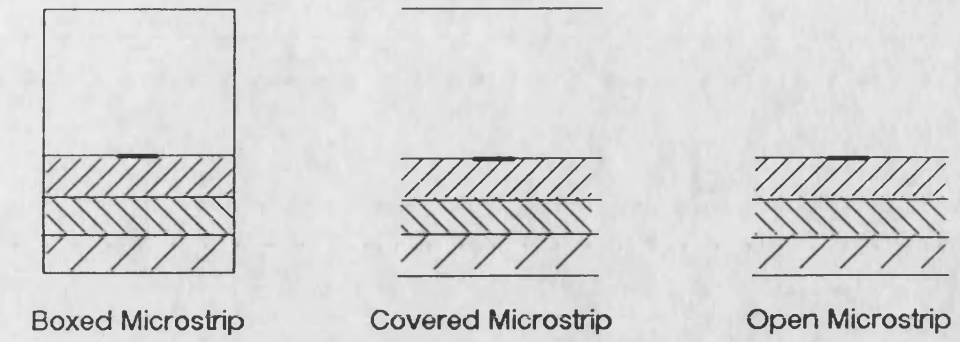

(a)

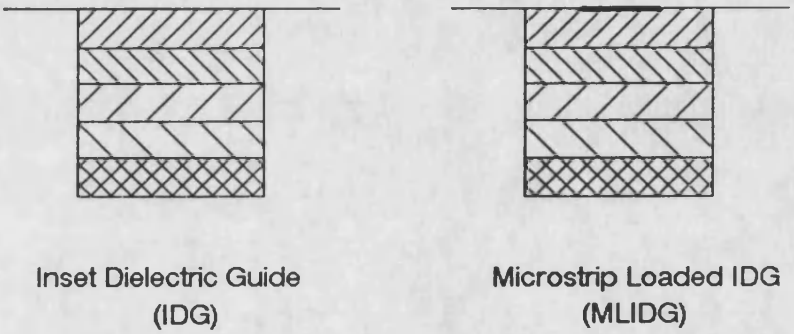

(b)

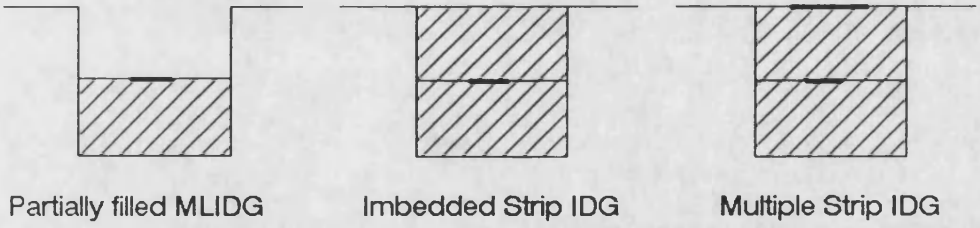

Figure 1.4 Waveguide structures analyzed in this thesis

REFERENCES

1. D. D. Greig and H. F. Englemann, "Microstrip - a New Transmission Technique for the Kilomegacycle Range", Proc. IRE, Vol. 40, 1952, pp. 1644-1650.

2. T. C. Edwards, "Foundations for Microwave Circuit Design", Wiley, 1981.

3. P. J. Meier, "Integrated Fin-Line Millimetre Components", IEEE Trans. Microwave Theory Tech., Vol. MTT-22, No. 12, Dec. 1974, pp. 1209-1216.

4. M. V. Schneider, "Dielectric Loss in Integrated Microwave Circuits", The Bell Syst. Tech. Journal, Sept. 1969, pp. 2325-2332.

5. K. C. Gupta et al. "Microstrip Lines and Slotlines", Artech 1979.

6. D. D. King, "Properties of Dielectric Image Lines", IRE Trans. Microwave Theory Tech., vol. MTT-3, March 1955, pp. 75-81.

7. W. Brunner et al., "100-300 Ghz Transmission Media Evaluation and Component Development", Proc. 14th Eur. Mic. Conf. 1984.

8. D. D. King and S. P. Schlesinger, "Dielectric Image Lines", IRE Trans. Microwave Theory Tech. Vol. MTT-6, July 1958, pp. 291-299.

9. T. E. Rozzi and S. Hedges, "Rigorous Analysis and Network Modelling of Inset Dielectric Guide", IEEE Trans. Microwave Theory Tech. Vol. MTT-35, Sept. 1987, pp. 823-834.

10. T. Rozzi and L. Ma, "Scattering of Dipoles in Inset Dielectric Guide and Applications to Millimetric Leaky Wave Applications", Proc 17th Eur. Mic. Conf., Sept. 1987.

11. T. E. Rozzi and L. Ma, "Mode Completeness, Normalization and Green's Function of the Inset Dielectric Guide", IEEE Trans. Microwave Theory Tech., Vol. MTT-36, March 1988, pp. 542-551.

12. T. Rozzi, R. Deleo and A. Morini, "Analysis of the Microstrip Loaded Inset Dielectric Waveguide", IEEE MTT-S Digest 1990, pp. 923-925.

13. L. Ma, S. R. Pennock and T. Rozzi, "Linear Arrays Realized in IDG", Paper 6, IEE Colloquium "Components for Novel Transmission Lines", London 26th March, 1990 (Digest No. 1990/048).

14. T. E. Rozzi, R. De. Leo, L. Ma. and A. Morini, "Equivalent Network of Transverse Dipoles on Inset Dielectric Guide : Applications to Linear Arrays", IEEE Trans. on A.P., 1989.

15. H. Gutton and G. Baissinot, G. "Flat Ariel for Ultra High Frequency", French Patent No. 703113, 1955.

16. J. R. James, P. S. Hall, and C. Wood, "Microstrip Antenna Theory and Design", IEE Electromagnetic Wave Series 12, Peter Pereguins Ltd., 1981.

17. R. E. Collin, "Field Theory of Guided Waves", McGraw-Hill, 1960.

18. J. R. James and A. Henderson, "High Frequency Behaviour of Microstrip Open-circuit Terminations", IEE J. Microwave Optics and Acoustics, Vol. 3, pp. 205-211.

19. C. Wood, "Curved Microstrip Lines as Compact Wideband Circularly Polarised Antennas", IEE J. Microwave Optics and Acoustics, Vol. 3, pp. 5-13.

20. C. Wood, "Improved Bandwidth of Microstrip Antennas using Parasitic Elements", Proc. IEE, Pt. H., Vol. 127, pp. 231-234.

21. H. G. Oltmann, "Electromagnetically Coupled Microstrip

Dipole Antenna Elements", Proc. 8th Eur. Mic. Conf., Paris, 1978, pp. 281-285.

22. H. G. Oltmann, D. M. Weems, G. M. Lindgren, and F. D. Walton, "Microstrip Components for Low Cost Millimetre Wave Missile Seekers", Millimetre and Sub-millimetre Wave Propagation and Circuits, AGARD Conf. Proc. 245, 1978, Munich, Germany.

23. S.P Hall, "New Wideband Microstrip Antenna using Log-periodic technique", Elect. Lett., Vol. 16, pp. 127-128.

24. J.S. Hornby and A. Gopinath, "Numerical Analysis of a Dielectric Loaded Waveguide with a Microstrip Line - Finite Difference Methods", IEEE Trans. Microwave Theory Tech., Vol. MTT-17, 1969, pp. 684-690.

25. P. Dally, "Hybrid Mode Analysis of Microstrip by Finite Elements Methods", IEEE Trans. Microwave Theory Tech., Vol. MTT-19, 1971, pp. 19-25.

26. R.H. Jansen, "The Spectral Domain Approach for Microwave Integrated Circuits", IEEE Trans. Microwave Theory Tech., Vol. MTT-33, pp. 1043-1054.

27. T.T. Wu, "Theory of Microstrip", J. Appl. Phys., Vol. 28, 1975, pp. 299-302.

28. E. Yamashita and R. Mittra, "Variational Method for the Analysis of Microstrip Lines", IEEE Trans. Microwave Theory Tech., Vol. MTT-16, 1968, pp. 251-256.

29. E. J. Denlinger, "A Frequency Dependent Solution for Microstrip Transmission Lines", IEEE Trans. Microwave Theory Tech., Vol. MTT-19, 1971, pp. 30-39.

30. T. Itoh and R. Mittra, "Spectral Domain Approach for Calculating the Dispersion Characteristics of Microstrip Lines", IEEE Trans. Microwave Theory Tech., Vol. MTT-21, 1973, pp. 496-499.

31. A. R. Van de Cappelle and P.J. Luypaert, "Fundamental and higher-order modes in Open Microstrip", Elect. Lett., Vol. 9, 1973, pp. 345-346.

32. T. Itoh, "Spectral Domain Immitance Approach for Dispersion Characteristics of Generalized Printed Transmission Lines", IEEE Trans. Microwave Theory Tech., Vol. MTT-28, 1980, pp. 981-985.

33. C.H. Chan, K.T. Kwong and A.B. Kouki, "A Mixed Spectral-Domain Approach for Dispersion Analysis of Suspended Planar Transmission Lines with Pedestals", IEEE Trans. Microwave Theory Tech., Vol. MTT-37, 1989, pp. 1716-1722.

34. J.W. Archer, "An Efficient 200-290 GHz Frequency Triple Incorporating a Novel Stripline Structure", IEEE Trans. Microwave Theory Tech., Vol. MTT-32, 1984, pp. 416-420.

35. K. Solbach, "The Status of Printed mm-wave E-Plane Circuits", IEEE Trans. Microwave Theory Tech., Vol. MTT-31, , 1983, pp. 107-121.

36. J. Kot and T. Rozzi, "Rigorous Modelling of Single and Coupled Rectangular Dielectric Waveguides by Transverse Resonance Diffraction", Proc. 14th Eur. Mic. Conf. (Liege), 1984, pp. 424-429

37. C.A. Olley and T. Rozzi, "Characterisation of Unilateral Fin-line Mode Spectrum Including Loss Analysis", Proc. 16th Eur. Mic. Conf. (Dublin), 1986, pp. 551-516.

38. T. Rozzi and S.J. Hedges, "Rigorous Analysis and Network Modelling of the Inset Dielectric Guide", IEEE Trans. Microwave Theory Tech., Vol. MTT-35, 1987, pp. 823-833.

39. C.J. Railton, T. Rozzi and J. Kot, "The Efficient Calculation of Higher Order Shielded Microstrip Modes for use in Discontinuity Problems", Proc. 16th Eur. Mic. Conf. (Dublin), 1986, pp. 529-534.

CHAPTER 2

ANALYSIS OF BOXED AND OPEN MICROSTRIP

2.1 INTRODUCTION

In this chapter, a generalised method of analysis is presented for microstrip. The case were several dielectric layers may exist in the structure is considered and where side walls are present (boxed microstrip) or are removed (covered and open microstrip).

It is recognised that covered and open microstrip are open waveguide structures which are capable of supporting radiation as well as bound modes. The cutoff condition for the bound modes is identified and the spectrum of radiation modes is found to be separated into two regions: a region where the radiation modes are unbound in all directions and a second region, referred to as the "substrate leakage" region where the radiation modes are unbound along the lateral direction only. Since the energy of these substrate modes is concentrated within the vicinity of the guiding structure, their excitation will result in stray coupling between isolated circuit components.

Results for dispersion and substrate leakage are presented for some typical geometries.

2.2 ANALYSIS OF BOXED MICROSTRIP

2.2.1 INTRODUCTION

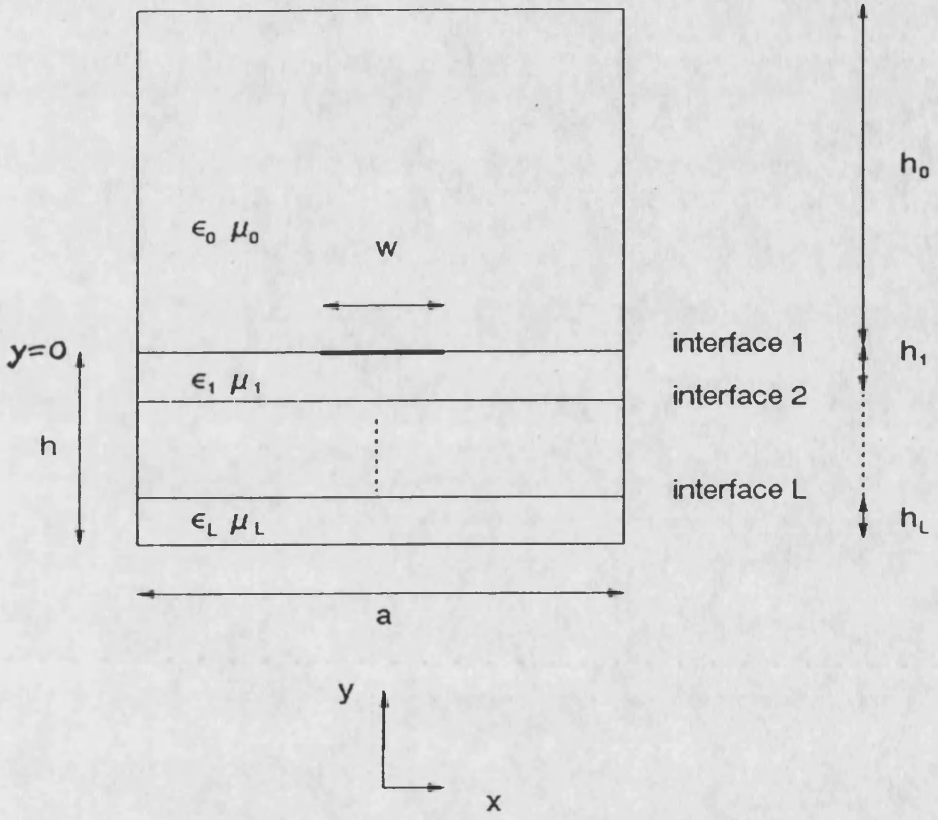

Figure 2.1 Cross section of a boxed microstrip structure

Figure 2.1 above gives the cross section of a boxed microstrip structure. The full six component hybrid field in the air region and each of the dielectric layers can be expressed as the superposition of TM-to-y (e-mode) and TE-to-y (h-mode) fields [1]. The e-mode and h-mode fields can

in turn be derived from y-directed electric and magnetic Hertzian potential functions respectively. Thus

$$E=-j\omega\mu_0\nabla\times\Pi_h+\epsilon_r K_0^2\Pi_e+\nabla\nabla\cdot\Pi_e \tag{2.1a}$$

$$H=j\omega\epsilon_0\epsilon_r\nabla\times\Pi_e+\epsilon_r K_0^2\Pi_h+\nabla\nabla\cdot\Pi_h \tag{2.1b}$$

where

$$\Pi_h=\hat{y}\ \psi_h(x,y)\,e^{-j\beta z} \tag{2.2a}$$

$$\Pi_e=\hat{y}\ \psi_e(x,y)\,e^{-j\beta z} \tag{2.2b}$$

The Hertzian potential functions must satisfy the Helmholtz equation [2]:

$$(\nabla^2+K_i^2)\Pi_{e,h}=0 \qquad K_i^2=\omega^2\epsilon_i\mu_0 \tag{2.3}$$

Substituting (2.2) into (2.1) and dropping the propagation factor $e^{-j\beta z}$ gives the following expressions for the individual field components

$$E_y=(\epsilon_r K_o^2+\partial_y^2)\,\psi_e(x,y) \tag{2.4a}$$

$$H_y=(\epsilon_r K_o^2+\partial_y^2)\,\psi_h(x,y) \tag{2.4b}$$

$$E_x=(\partial_x\partial_y\psi_e(x,y)+\omega\mu_0\beta\psi_h(x,y)) \tag{2.4c}$$

$$E_z=(-j\beta\partial_y\psi_e(x,y)-j\omega\mu_0\partial_x\psi_h(x,y)) \tag{2.4d}$$

$$H_x=(-\omega\epsilon_0\epsilon_r\beta\psi_e(x,y)+\partial_x\partial_y\psi_h(x,y)) \tag{2.4e}$$

$$H_z=(j\omega\epsilon_0\epsilon_r\partial_x\psi_e(x,y)-j\beta\partial_y\psi_h(x,y)) \tag{2.4f}$$

The potential functions are given a z-dependence of the form (2.2) since modes propagating in the z-direction are being considered. The z-dependence will be omitted in the

following sections for the sake of simplicity. The potential functions must be chosen so that the resultant fields will obey the boundary conditions for each region. Any possible field distribution, subject to the boundary conditions, must be expressible in terms of the potential functions except at the location of sources.

Due to the symmetry of the structure, modal solutions will either be symmetric or anti-symmetric with respect to x.

2.2.2 CHOICE OF POTENTIAL FUNCTIONS

Consider the two regions at either side of the conducting strip, which is assumed to be infinitely thin. Based on the previous discussion, the potential functions for the air region, $0<y<h_0$, are chosen as

$$\psi_e(x,y)=\sum_n^{\infty}\frac{I'_{0n}}{j\omega\epsilon_0}\frac{1}{\sqrt{((n\pi/a)^2+\beta^2)}}\phi_{en}(x)\frac{\cos k_{0n}(h_0-y)}{\cos(k_{0n}h_0)} \qquad (2.5a)$$

$$\psi_h(x,y)=\sum_n^{\infty}\frac{V''_{0n}}{j\omega\mu_0}\frac{1}{\sqrt{((n\pi/a)^2+\beta^2)}}\phi_{hn}(x)\frac{\sin k_{0n}(h_0-y)}{\sin k_{0n}h_0} \qquad (2.5b)$$

where for modes with even-Ez symmetry

$$\phi_{hn}(x)=\frac{2}{\sqrt{a}}\sin(n\pi/a)x \qquad (2.6a)$$

$$\phi_{en}(x)=\frac{2}{\sqrt{a}}\cos(n\pi/a)x \qquad (2.6b)$$

and

$n=1,3,\ldots$ (2.6c)

while for modes with odd-Ez symmetry

$$\phi_{hn}(x)=\frac{2\delta_n}{\sqrt{a}}\cos(n\pi/a)x \qquad n=0,2,4 \tag{2.7a}$$

$$\phi_{en}(x)=\frac{2}{\sqrt{a}}\sin(n\pi/a)x \qquad n=2,4,\ldots. \tag{2.7b}$$

where

$$\begin{aligned}\delta_n&=1/\sqrt{2} \qquad n=0\\ &=1 \qquad n=2,4,\ldots\end{aligned} \tag{2.7c}$$

The potential functions are thus expressed as the sum of discrete fourier components with x-dependence such that the boundary conditions at the side walls are satisfied. The functions $\phi_{hn}(x)$, $\phi_{en}(x)$ each form a complete set, and since the fields are symmetrical with respect to x are normalised so that

$$\int_0^{a/2}\phi_{en,hn}(x)\,\phi_{em,hm}(x)\,dx=\delta_{nm} \tag{2.8}$$

It is noted that n starts at 2 in (2.7b) since for $n=0$, $\phi_{en}(x)$ reduces to zero and this gives a trivial solution to the Helmholtz equation (2.3) [1].

The conservation of wavenumber equation is given by

$$\epsilon_{ir}\,K_0^2=\left(\frac{n\pi}{a}\right)^2+k_{in}^2+\beta^2 \tag{2.9}$$

The y-dependence, for each spectral component in (2.5) was derived by treating the air region as a length of transmission line with input at y=0, terminated with a short circuit at $y=h_0$ [3].

Similarly the potential functions for the dielectric layer 1 are chosen as

$$\psi_e(x,y) = \sum_{n=}^{\infty} \frac{I'_{1n}}{j\omega\epsilon_1} \frac{1}{\sqrt{((n\pi/a)^2+\beta^2)}} \phi_{en}(x) \frac{jY'_1(n)\sin k_{1n}(y+h_1) + Y'^D_2(n)\cos k_{1n}(y+h_1)}{jY'_1(n)\sin k_{1n}h_1 + Y'^D_2(n)\cos k_{1n}h_1} \qquad (2.10a)$$

$$\psi_h(x,y) \sum_{n}^{\infty} \frac{V''_{1n}}{j\omega\mu_0} \frac{1}{\sqrt{((n\pi/a)^2+\beta^2)}} \phi_{hn}(x) \frac{Y''_1(n)\cos k_{1n}(y+h_1) + jY''_{(}n)\,{}^D_2\sin k_{1n}(y+h_1)}{Y''_1(n)\cos k_{1n}h_1 + jY''^D_2(n)\sin k_{1n}h_1} \qquad (2.10b)$$

Where the y-dependence for the e-mode and h-mode functions is derived by treating the region $0<y<-h$ as a section of cascaded transmission lines with the input at $y=0$, terminated by a short circuit at $y=-h$.

$Y'_i(n)$ and $Y''_i(n)$ are the characteristic admittances of the e-mode and h-mode functions respectively for the i^{th} dielectric layer and are given by

$$Y'_i(n) = \frac{\omega\epsilon_0\epsilon_{ir}}{k_{in}} \qquad (2.11a)$$

$$Y''_i(n) = \frac{k_{in}}{\omega\mu_0} \qquad (2.11b)$$

while $Y'^{D}_{2}(n)$ and $Y''^{D}_{2}(n)$ are the input admittances looking down at interface 2.

The general expressions for the input admittances looking down at interface i are given by

$$Y'^{D}_{i}=Y'_{i}\frac{jY'_{i}\tan k_{in}h_i+Y'^{D}_{i-1}}{jY'^{D}_{i-1}\tan k_{in}h_i+Y'_{i}} \tag{2.12a}$$

$$Y''^{D}_{i}=Y''_{i}\frac{jY''_{i}\tan k_{in}h_i+Y''^{D}_{i-1}}{jY''^{D}_{i-1}\tan k_{in}h_i+Y''_{i}} \tag{2.12b}$$

The input admittances looking down at the lower metallic boundary are infinite and hence for the L^{th} interface (see Figure 2.1)

$$Y'^{D}_{L}=\frac{\omega\epsilon_0\epsilon_{Lr}}{k_{Ln}}\frac{1}{j\tan k_{Ln}h_L} \tag{2.13a}$$

$$Y''^{D}_{L}=\frac{k_{Ln}}{\omega\mu_0}\frac{1}{j\tan k_{Ln}h_L} \tag{2.13b}$$

2.3 GENERALIZATION TO OPEN AND COVERED MICROSTSRIP

2.3.1 INTRODUCTION

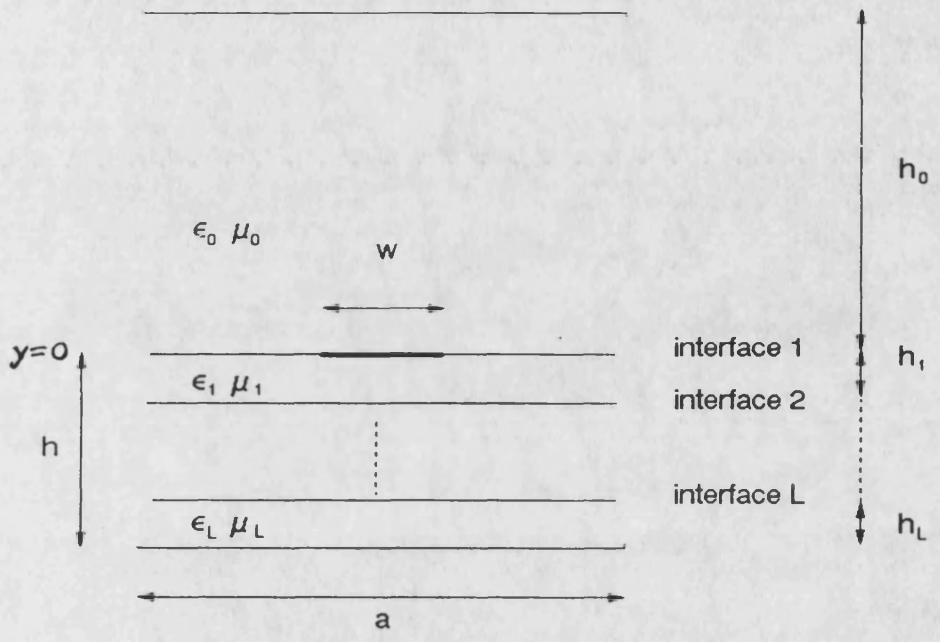

Figure 2.2 Cross section of a covered microstrip structure

Figure 2.2 above gives the cross section of a covered microstrip structure. For open microstrip the top cover at $y=h_0$ is removed.

Whereas the fields in boxed microstrip are confined by the presence of conducting walls, covered and open microstrip are open waveguide structures capable of supporting guided as well as radiation modes [4]. The guided modes are discrete and the energy of the modes is concentrated in the region of the conducting strip. The radiation modes however are continuous and are composed of plane waves that

can transport energy in all directions away from the guiding structure.

Any possible field distribution arising in open or covered microstrip can be expressed as the superposition of guided and radiation modes [4].

The analysis of the radiation modes is beyond the scope of the thesis, and only the solutions for the discrete, guided modes is given. However, it is important to consider the cutoff condition for the guided and radiation modes.

The potential functions for covered microstrip are chosen by considering the potential functions for boxed microstrip and removing the side walls to infinity.

In the limit as $x \to \infty$

$$\phi_{en}(x) \to \phi_e(\rho, x) = \frac{2}{\sqrt{\pi}} \cos \rho x \qquad (2.14a)$$

$$\phi_{hn}(x) \to \phi_h(\rho, x) = \frac{2}{\sqrt{\pi}} \sin \rho x \qquad \rho > 0 \qquad (2.14b)$$

for modes with even-Ez symmetry, while for modes with odd-Ez symmetry,

$$\phi_{en}(x) \to \phi_e(\rho, x) = \frac{2}{\sqrt{\pi}} \sin \rho x \qquad \rho > 0 \qquad (2.15a)$$

$$\phi_{hn}(x) \rightarrow \phi_h(\rho, x) = \frac{2}{\sqrt{\pi}} \cos \rho x \tag{2.15b}$$

The functions $\phi_{e,h}(x)$ now satisfy the normalization condition

$$\int_0^{\infty} \phi_{e,h}(\rho, x)\, \phi_{e,h}(\rho', x)\, dx = \delta(\rho - \rho') \tag{2.16}$$

The x-directed wavenumber which is discrete for boxed microstrip now becomes continuous and the potential functions are expressed in terms of continuous fourier transform components. The potential functions for the air region and the first dielectric layer become:

for $h_0 < y < 0$

$$\psi_e(x, y) = \int_0^{\infty} \frac{I'_0(\rho)}{j\omega\epsilon_0} \frac{1}{\sqrt{(\rho^2+\beta^2)}} \phi_e(\rho, x) \frac{\cos k_0(\rho)\,(h_0 - y)}{\cos(k_0(\rho)\, h_0)}\, d\rho \tag{2.17a}$$

$$\psi_h(x, y) = \int_0^{\infty} \frac{V''_0(\rho)}{j\omega\mu_0} \frac{1}{\sqrt{(\rho^2+\beta^2)}} \phi_h(\rho, x) \frac{\sin k_0(\rho)\,(h_0 - y)}{\sin(k_0(\rho)\, h_0)}\, d\rho \tag{2.17b}$$

while for $0 < y < -h_1$

$$\psi_e(x, y) = \int_0^{\infty} d\rho \frac{I'_1(\rho)}{j\omega\epsilon_1} \frac{1}{\sqrt{(\rho^2+\beta^2)}} \phi_e(x, \rho) \frac{jY'_1(\rho) \sin k_1(\rho)\,(y+h_1) + Y'^{D}_2(\rho) \cos k_1(\rho)\,(y+h_1)}{jY'_1(\rho) \sin k_1(\rho)\, h_1 + Y'^{D}_2(\rho) \cos k_1(\rho)\, h_1} \tag{2.18a}$$

$$\psi_h(x,y)=\int_0^\infty d\rho\,\frac{V''_1(\rho)}{j\omega\mu_0}\,\frac{1}{\sqrt{(\rho^2+\beta^2)}}\,\phi_h(\rho,x)$$
$$\frac{Y''_1(\rho)\cos k_1(\rho)\,(y+h_1)+jY''^{D}_2(\rho)\sin k_1(\rho)\,(y+h_1)}{Y''_1(\rho)\cos k_1(\rho)\,h_1+jY''^{D}_2(\rho)\sin k_1(\rho)\,h_1} \qquad (2.18b)$$

The conservation of wavenumber equation is now given by

$$\epsilon_{ir}\,K_0^2=\rho^2+k_i^2(\rho)+\beta^2 \qquad (2.19)$$

For the case of open-microstrip, the potential functions for the air region must be chosen such that the fields will decay. Thus the potential functions for y > 0 are chosen as

$$\psi_e(x,y)=\int_0^\infty \frac{I'_0(\rho)}{j\omega\epsilon_0}\,\frac{1}{\sqrt{(\rho^2+\beta^2)}}\,\phi_e(\rho,x)\,e^{jk_0(\rho)y}\,d\rho \qquad (2.20a)$$

$$\psi_h(x,y)=\int_0^\infty \frac{V''_0(\rho)}{j\omega\mu_0}\,\frac{1}{\sqrt{(\rho^2+\beta^2)}}\,\phi_h(\rho,x)\,e^{jk_0(\rho)y}\,d\rho \qquad (2.20b)$$

2.3.2 FORMULATION OF ADMITTANCE OPERATORS

Consider the case of covered microstrip, substituting the expressions for the potential functions into (2.4), the following expressions are obtained for the fields at $y=0^-$ (see Appendix 2.A)

$$E_x(x,0^-)=\int_0^\infty E_x^1(\rho)\,\phi_h(\rho,x)\,d\rho \qquad (2.21a)$$

$$E_z(x,0^-)=\int_0^\infty E_z^1(\rho)\,\phi_e(\rho,x)\,d\rho \tag{2.21b}$$

where

$$\begin{bmatrix} E_x^1(\rho) \\ -E_z^1(\rho) \end{bmatrix} = T(\rho) \begin{bmatrix} Z'^D_1(\rho) & 0 \\ 0 & 1 \end{bmatrix} \begin{bmatrix} -I'_1(\rho) \\ V''_1(\rho) \end{bmatrix} \tag{2.22}$$

$T(\rho)$ is a coordinate transformation given by

$$T(\rho)=\begin{bmatrix} \cos\alpha & -j\sin\alpha \\ -j\sin\alpha & \cos\alpha \end{bmatrix} \tag{2.23a}$$

where

$$\cos\alpha=\frac{\rho}{\sqrt{\rho^2+\beta^2}} \qquad \sin\alpha=\frac{\beta}{\sqrt{\rho^2+\beta^2}} \tag{2.23b}$$

Z'^D_1 and Z''^D_1 are the respective e-mode and h-mode input impedances looking down at interface 1.

The following expressions are also obtained for the tangential magnetic fields

$$H_x(x,0^-)=\int_0^\infty H_x^1(\rho)\,\phi_e(\rho,x)\,d\rho \tag{2.24a}$$

$$H_z(x,0^-)=\int_0^\infty H_z^1(\rho)\,\phi_h(\rho,x)\,d\rho \tag{2.24b}$$

where

$$\begin{bmatrix} H_z^1(\rho) \\ H_x^1(\rho) \end{bmatrix} = T(\rho) \begin{bmatrix} 1 & 0 \\ 0 & Y''^D_1(\rho) \end{bmatrix} \begin{bmatrix} -I'_1(\rho) \\ V''_1(\rho) \end{bmatrix} \tag{2.25}$$

Using expressions (2.22) and (2.25), the tangential magnetic field components can be expressed in terms of the tangential electric field components as

$$\begin{bmatrix} H_z^1(\rho) \\ H_x^1(\rho) \end{bmatrix} = T(\rho) \begin{bmatrix} Y'^D_1(\rho) & 0 \\ 0 & Y''^D_1(\rho) \end{bmatrix} T(\rho)^{-1} \begin{bmatrix} E_x^1(\rho) \\ -E_z^1(\rho) \end{bmatrix} \tag{2.26}$$

Following a similar procedure for the fields at $y=0^+$ the following expression is also obtained

$$-\begin{bmatrix} H_z^0(\rho) \\ H_x^0(\rho) \end{bmatrix} = T(\rho) \begin{bmatrix} Y'^U_1(\rho) & 0 \\ 0 & Y''^U_1(\rho) \end{bmatrix} T(\rho)^{-1} \begin{bmatrix} E_x^0(\rho) \\ -E_z^0(\rho) \end{bmatrix} \tag{2.27}$$

Y'^U_1 and Y''^U_1 are the input admittances looking up at interface 1. For covered microstrip these are given by

$$Y'^U_1(\rho) = \frac{\omega\epsilon_0}{k_0(\rho)} \frac{1}{j\tan k_0(\rho) h_0} \tag{2.28a}$$

$$Y''^U_1(\rho) = \frac{k_0(\rho)}{\omega\mu_0} \frac{1}{j\tan k_0(\rho) h_0} \tag{2.28b}$$

while for open microstrip

$$Y'^U_1(\rho) = \frac{\omega\epsilon_0}{k_0(\rho)} \tag{2.29a}$$

$$Y''^U_1(\rho) = \frac{k_0(\rho)}{\omega\mu_0} \tag{2.29b}$$

2.3.3 SETTING UP THE DISPERSION EQUATION

In the previous section, general expressions have been obtained for the tangential electric and magnetic field components at either side of the conducting strip at y=0. The boundary conditions at y=0, have not yet been enforced on these fields. These boundary conditions are satisfied only for particular values of the propagation wavenumber β which are the required solutions for the discrete modes.

The boundary conditions on the tangential electric and magnetic fields are

1) The tangential electric fields must be continuous at y=0. This implies that

$$E_x^1(\rho) = E_x^0(\rho) = E_x(\rho)$$
$$E_z^1(\rho) = E_z^0(\rho) = E_z(\rho) \qquad (2.30)$$

2) For the tangential magnetic fields, we must have

$$H_z(x,0^+) - H_z(x,0^-) = I_x(x)$$
$$H_x(x,0^+) - H_x(x,0^-) = -I_z(x) \qquad (2.31)$$

Where $I_x(x)$, $I_z(x)$ are the x and z-directed current components on the strip, respectively. Applying these boundary conditions to (2.26,2.27) gives

$$\begin{bmatrix} I_x(\rho) \\ -I_z(\rho) \end{bmatrix} = T(\rho) \begin{bmatrix} \overleftrightarrow{Y'}_1(\rho) & 0 \\ 0 & \overleftrightarrow{Y''}_1(\rho) \end{bmatrix} T(\rho)^{-1} \begin{bmatrix} E_x(\rho) \\ -E_z(\rho) \end{bmatrix} \tag{2.32}$$

where

$$\overleftrightarrow{Y'}_1(\rho) = Y'_1(\rho)^{U} + Y'_1(\rho)^{D} \tag{2.33a}$$

$$\overleftrightarrow{Y''}_1(\rho) = Y''_1(\rho)^{U} + Y''_1(\rho)^{D} \tag{2.33b}$$

and

$$I_x(\rho) = \int_0^{w/2} I_x(x)\,\phi_h(\rho, x)\,dx \tag{2.34a}$$

$$I_z(\rho) = \int_0^{w/2} I_x(x)\,\phi_e(\rho, x)\,dx \tag{2.34b}$$

The dispersion relation can be set up with either the strip currents or the tangential electric fields as the independent variables. It has been shown that for boxed microstrip, faster convergence to the solutions of the dispersion equation can be obtained with the strip currents as the independent variables [5]. To achieve this aim, (2.32) is rearranged to give

$$\begin{bmatrix} E_x(\rho) \\ -E_z(\rho) \end{bmatrix} = T(\rho) \begin{bmatrix} \overleftrightarrow{Z'}_1(\rho) & 0 \\ 0 & \overleftrightarrow{Z''}_1(\rho) \end{bmatrix} T(\rho)^{-1} \begin{bmatrix} I_x(\rho) \\ -I_z(\rho) \end{bmatrix} \tag{2.35}$$

where

$$\overleftrightarrow{Z}'_1(\rho) = Z'_1(\rho)^{U} + Z'_1(\rho)^{D} \tag{2.36a}$$

$$\overleftrightarrow{Z}''_1(\rho) = Z''_1(\rho)^{U} + Z''_1(\rho)^{D} \tag{2.36b}$$

Finally the following expression is obtained for the tangential electric fields

$$\begin{bmatrix} E_x(x,0) \\ E_z(x,0) \end{bmatrix} = \begin{bmatrix} \tilde{Z}_{xx}(\beta) & \tilde{Z}_{xz}(\beta) \\ \tilde{Z}_{zx}(\beta) & \tilde{Z}_{zz}(\beta) \end{bmatrix} \begin{bmatrix} I_x(x) \\ I_z(x) \end{bmatrix} \tag{2.37}$$

where the operators $\tilde{Z}_{ii}$ are defined by

$$\tilde{Z}_{xx}(\beta)\, I_x(x) = \int_0^{\infty} \left(\cos^2\alpha \overleftrightarrow{Z}'_1(\rho,\beta) + \sin^2\alpha \overleftrightarrow{Z}''_1(\rho,\beta) \right) \phi_h(\rho,x) \langle I_x(x), \phi_h(\rho,x) \rangle d\rho \tag{2.38a}$$

$$\tilde{Z}_{zx}(\beta)\, I_x(x) = \int_0^{\infty} -j\sin\alpha\cos\alpha \left(\overleftrightarrow{Z}'_1(\rho,\beta) - \overleftrightarrow{Z}''_1(\rho,\beta) \right) \phi_e(\rho,x) \langle I_x(x), \phi_h(\rho,x) \rangle\, d\rho \tag{2.38b}$$

$$\tilde{Z}_{xz} I_z(x) = \int_0^{\infty} j\sin\alpha\cos\alpha \left(\overleftrightarrow{Z}'_1(\rho,\beta) - \overleftrightarrow{Z}''_1(\rho,\beta) \right) \phi_h(\rho,x) \langle I_z(x), \phi_e(\rho,x) \rangle d\rho \tag{2.38c}$$

$$\tilde{Z}_{zz}(\beta)\, I_z(x) = \int_0^{\infty} \left(\sin^2\alpha \overleftrightarrow{Z}'_1(\rho,\beta) + \cos^2\alpha \overleftrightarrow{Z}''_1(\rho,\beta) \right) \phi_e(\rho,x) \langle I_z(x), \phi_e(\rho,x) \rangle d\rho \tag{2.38d}$$

2.3.4 APPLICATION OF THE GALERKIN PROCEDURE

In the dispersion relation (2.37), the strip currents which are treated as the independent variables are unknown. Therefore in order to obtain the solution of the dispersion equation, the procedure known as the Galerkin procedure is applied [6]. The unknown currents are represented in terms of a complete orthonormal basis of functions. Any arbitrary current distribution can be represented as a linear superposition of a set of basis functions, provided the functions satisfy the conditions of completeness and, preferably, orthonormality. The unknown strip currents are then represented as

$$I_x(x) = \sum_{i=0}^{\infty} X_i I_{xi}(x) \tag{2.39a}$$

$$I_z(x) = \sum_{i=0}^{\infty} Z_i I_{zi}(x) \tag{2.39b}$$

In practice, the summations in (2.39) are truncated and, as a result, the solutions obtained are approximate.

The Galerkin procedure is completed by taking the inner product of the basis functions with both sides of (2.37). This reduces the LHS of (2.37) to zero since the tangential electric fields must vanish over the strip giving the transformed dispersion equation

$$\begin{bmatrix} \langle I_{x0}, \tilde{Z}_{xx}E_{x0}\rangle & \cdots & \langle I_{x0}, \tilde{Z}_{xx}I_{xi}\rangle & \langle I_{x0}, \tilde{Z}_{xz}I_{z0}\rangle & \cdots & \langle I_{x0}, \tilde{Z}_{xz}I_{zj}\rangle \\ \vdots & & \vdots & \vdots & & \vdots \\ \langle I_{xi}, \tilde{Z}_{xx}I_{x0}\rangle & \cdots & \langle I_{xi}, \tilde{Z}_{xx}I_{xi}\rangle & \langle I_{xi}, \tilde{Z}_{xz}I_{z0}\rangle & \cdots & \langle I_{xi}, \tilde{Z}_{xz}I_{zj}\rangle \\ \\ \langle I_{z0}, \tilde{Z}_{zx}I_{x0}\rangle & \cdots & \langle I_{z0}, \tilde{Z}_{zx}I_{xi}\rangle & \langle I_{z0}, \tilde{Z}_{zz}I_{z0}\rangle & \cdots & \langle I_{z0}, \tilde{Z}_{zz}I_{zj}\rangle \\ \vdots & & \vdots & \vdots & & \vdots \\ \langle I_{zj}, \tilde{Z}_{zx}I_{x0}\rangle & \cdots & \langle I_{zj}, \tilde{Z}_{zx}I_{xi}\rangle & \langle I_{zn}, \tilde{Z}_{zz}I_{z0}\rangle & \cdots & \langle I_{zn}, \tilde{Z}_{zz}I_{z0}\rangle \end{bmatrix} \begin{bmatrix} X_0 \\ \vdots \\ \vdots \\ X_i \\ Z_0 \\ \vdots \\ \vdots \\ Z_j \end{bmatrix} = \underline{0} \qquad (2.40)$$

The matrix equation (2.40) has a non-trivial solution if and only if the determinant of the matrix is zero. The determinant is a function of β. Therefore a search for the zeros of the determinant gives the required propagating wavenumbers for the discrete modes.

Once the required propagating wavenumbers are obtained, the unknown eigenvectors in (2.39) can be recovered as follows. One of the amplitudes in (2.39) is set arbitrarily equal to unity. This results in an 'over-determined ' matrix equation which can then be solved using a least mean square error technique [7].

2.3.5 CHOICE OF BASIS FUNCTIONS

As outlined in the previous section, the basis functions in (2.39) is

1) Preferably orthonormal

2) Sufficiently complete

Two further requirements are important when making the choice of basis functions. These are:

3) It is important to be able to achieve rapid convergence to the solutions of (2.40) using as few a number of terms in the basis functions as possible. This can reduce computer run-time considerably. In addition, errors are introduced in evaluating the matrix elements of (2.40) as a result of the numerical computation of the integrals in the impedance expressions (2.38). Since the order of the matrix increases with the number of basis functions used, the error in evaluating the determinant would increase accordingly.

Rapid convergence can be achieved by choosing a set of basis functions which closely models the actual distribution of current on the strip. In the vicinity of the metal edge, the current normal to the edge varies as the square root of the distance from the edge and the transverse current varies as the reciprocal of this [2]. To obtain good convergence, this behaviour must be included in the basis functions.

Furthermore $I_z(x)$ and $\partial_x I_x(x)$ have the same singular behaviour and can therefore be efficiently represented by the same set of basis functions.

4) The evaluation of the matrix elements in (2.40)

involves the computation of the fourier transforms of the basis functions. Therefore a further important requirement on the basis functions is that they have fourier transforms which are relatively simple to compute.

In order to take into account the factors mentioned above, the matrix equation (2.40) is first reformulated in terms of $I_{zi}(x)$ and $\partial_x I_{xi}(x)$. This can be accomplished as follows. It is evident from (2.38) that two identities must be computed:

$$\langle I_{xi}, \phi_h(\rho, x) \rangle = I_{1i}(\rho) \tag{2.41a}$$

$$\langle I_{z_i}, \phi_e(\rho, x) \rangle = I_{2i}(\rho) \tag{2.41b}$$

Considering the even modes for example, (2.41) are given by

$$I_{1i}(\rho) = \frac{2}{\sqrt{(\pi)}} \int_0^{w/2} I_{xi}(x) \sin(\rho x)\, dx \tag{2.42a}$$

$$I_{2i}(\rho) = \frac{2}{\sqrt{(\pi)}} \int_0^{w/2} I_{zi}(x) \cos(\rho x)\, dx \tag{2.42b}$$

Integrating $I_{1i}(\rho)$ by parts:

$$I_{1i}(\rho) = -[I_{xi}(x) \cos\rho x] + \frac{1}{\rho} \int_0^{w/2} \partial_x I_{xi}(x) \cos(\rho x)\, dx \tag{2.43}$$

The first term on the RHS of (2.43) reduces to zero since $I_x(x)$ must be zero at the edges of the strip. Thus

$$I_{1i}(\rho) = \frac{2}{\rho\sqrt{\pi}} \int_0^{w/2} \partial_x I_{xi}(x) \cos(\rho x)\, dx \tag{2.44a}$$

$$I_{2i}(\rho) = \frac{2}{\sqrt{\pi}} \int_0^{\infty} I_{zi}(x) \cos(\rho x)\, dx \tag{2.44b}$$

Since $I_z(x), \partial_x I_x(x)$ have the same singular behaviour, the same set of function can be used for both $I_{zi}(x)$ and $\partial_x I_{xi}(x)$.

In order to achieve rapid convergence, the following weight function is introduced into the basis functions

$$W(2x/w) = \sqrt{(1-(2x/w)^2)} \tag{2.45}$$

The weight function $W(2x/w)$, insures that the basis functions incorporate the required singular behaviour at the strip edge.

A set of functions which are orthogonal to the weight function $W(2x/w)$ are the Tchebyschev polynomials [8], $T_m(x)$. The basis functions are thus chosen as

$$\begin{aligned} f_m(2x/w) &= \frac{1}{N_m} \frac{T_m(2x/w)}{W(2x/w)} && |x| \le w/2 \\ &= 0 && |x| > w/2 \end{aligned} \tag{2.46}$$

Where N_m is a normalisation factor given by

$$N_m^2 = \int_0^{\infty} \frac{[T_m(2x/w)]^2}{W(2x/w)}\, dx \tag{2.47}$$

The normalisation factor N_m is evaluated as follows: from mathematical tables [8];

$$\int_{-1}^{1} \frac{1}{\sqrt{(1-t^2)}} T_m(t)\, T_n(t)\, dt = 0 \qquad (m \neq n)$$
$$= \frac{\pi}{2} \qquad (m=n\neq 0) \qquad (2.48)$$
$$= \pi \qquad (m=n=0)$$

substituting $x=wt/2$ in (2.48) gives

$$4/w \int_{0}^{w/2} \frac{1}{\sqrt{1-(2x/w)^2}} T_m(2x/w)\, T_m(2x/w)\, dx = \frac{\pi}{2} \qquad (m\neq 0) \qquad (2.49)$$
$$= \pi \qquad (m=0)$$

from which the normalisation factor is found to be

$$N_m^2 = \frac{\pi w}{8} \qquad m\neq 0$$
$$= \frac{\pi w}{4} \qquad m=0 \qquad (2.50)$$

The fourier transforms of the functions $f_m(2x/w)$ are found as follows. From mathematical tables [8]:

$$\int_{0}^{1} \frac{1}{\sqrt{1-t^2}} T_m(t) \cos\rho t\, dt = (-1)^m \frac{\pi}{2} J_m(\rho) \qquad (m=0,2,4,\ldots) \qquad (2.51)$$
$$= 0 \qquad \textit{otherwise}$$

Substitute $x=wt/2$ in (2.51) gives

$$\frac{2}{w} \int_{0}^{w/2} T_{2m}(2x/w) \cos\frac{2\rho x}{w} \frac{1}{\sqrt{1-(2x/w)^2}} dx = (-1)^{2m} \frac{\pi}{2} J_{2m}(\rho) \qquad (m=0,1,2,..) \qquad (2.52)$$

from which the following result is obtained

$$
\begin{aligned}
&= \frac{1}{N_{2m}} \frac{W}{2} (-1)^{2n} \\
\int_0^{w/2} f_{2m}(2x/w) \cos\rho x dx &= C_{2m} J_{2m}(\rho w/2) \\
&= \frac{N_{2m}}{2} (-1)^{2m} \frac{\pi}{2} J_{2m}(\rho w/2) \\
&= C_{2m} J_{2m}(\rho w/2)
\end{aligned}
\tag{2.53}
$$

where $J_m(\rho)$ are bessel functions of order m

Thus the expressions for the identities (2.42) are

$$I_{1i}(\rho) = C_{2i+2} \frac{1}{\rho} J_{2i+2}(\rho w/2) \tag{2.54a}$$

$$I_{2i}(\rho) = C_{2i} J_{2i}(\rho w/2) \tag{2.54b}$$

Note that for I_{1i} the first term starts from 2 since for the zeroth term $I_{xi}(x)$ does not vanish at the edge as the boundary condition requires [5].

2.4 CUTOFF CONDITION FOR THE BOUND MODES IN COVERED AND OPEN MICROSTRIP

As explained in section 2.3, the complete spectrum of modes for covered and open microstrip includes a number of discrete guided modes as well as a continuum of radiation modes. The propagation coefficients for lossless, isotropic homogeneous media, for the guided as well as the radiation modes, are either pure real or pure imaginary [9].

The above modes should not be confused with the so called

complex 'leaky modes' of open microstrip, which correspond to energy transport away from the guide along the lateral direction [10-12]. Complex 'leaky modes', are in general, suitable for approximate field representation in the vicinity of the guiding and radiating structure but they do not belong to the complete set of modes [4].

It is noted that complex modes have also been reported for boxed microstrip [13]. However, in this instance, the modes occur as conjugate pairs so that the net energy gained by one mode balances the net energy lost by the second mode keeping the overall field real.

In order to establish the cutoff condition for bound modes and the radiation modes, the following conditions are imposed:

1) The fields must decay along the y-axis for open microstrip.

This conditions is met as follows. From (2.20) it is evident that the y-directed field components for open microstrip will decay exponentially along the y-axis if

$$[k_0(\rho)]^2<0 \qquad (2.55)$$

From (2.19) it can be seen that this condition is met

provided

$$\beta > K_0 \tag{2.56}$$

2) The dispersion relation (2.40) must not have any complex solutions.

This condition is met by considering the impedance operators in (2.38). Poles in the impedance operators occur where

$$\tilde{Y}'_1 = 0 \tag{2.57a}$$

or

$$\tilde{Y}''_1 = 0 \tag{2.57b}$$

The evaluation of the impedance operators (2.38) for the case where poles exist in the integral is achieved by a proper choice of integration path and by application of residue calculus techniques [11,14]. This would give rise to complex solutions of the dispersion relation. As explained previously, these modes are improper and are not allowed.

The poles occur at specific values $k_{1p}(\rho)$ of the y-directed wavenumber, where from (2.19)

$$\sqrt{\epsilon_i K_0^2 - \rho^2 - \beta^2} = k_{ip}(\rho) \qquad (\rho > 0) \tag{2.58}$$

In order to prevent the possible occurence of any complex solutions, we must have

$$\beta > \beta_c \tag{2.59}$$

where

$$\beta_c = \sqrt{\epsilon_i K_0^2 - k_{ic}(\rho)^2} \tag{2.60}$$

and $k_{ic}(\rho)$ is the value of the y-directed wavenumber for the i^{th} dielectric layer corresponding to the first pole.

Comparing (2.59) and (2.56) it will be found that the condition for equation (2.59) is the stronger one. That is provided condition (2.59) is obeyed then (2.56) will be automatically obeyed. Thus the cutoff condition for bound modes is established as that given by (2.59) and the spectrum for the guided modes lies in the region

$$\beta_c > \beta > K_0^2 \epsilon_{max} \tag{2.61}$$

where ϵ_{max} is the maximum value of relative permittivity among the dielectric layers.

It noted that an analysis of guiding and radiation characteristics of microstrip, in which the condition for the fields to decay along the lateral x-direction for open

and covered microstrip is considered [4], also establishes (2.59) as the condition for cutoff of the bound modes.

The continuous spectrum for the radiation modes will thus lie in the region

$$-\infty > \beta^2 > \beta_c^2 \tag{2.62}$$

The spectrum of radiation modes in (2.62) can then be divided into two regions [15, 16]. For

$$\beta_c > \beta > K_0 \tag{2.63}$$

the radiation modes decay along the y-direction (from (2.56)) but are unbound along the x-direction. This region is referred to as the "substrate leakage region" since the energy of these modes is concentrated in the vicinity of the guide. The second region of radiation is given by

$$-\infty > \beta^2 > K_0^2 \tag{2.64}$$

The radiation modes for this region are unbound along both the x and y- directions.

2.5 EXAMPLES OF DISPERSION CURVES

Figure 2.3 gives the dispersion curves obtained for a particular geometry of open microstrip. The radiation and substrate leakage regions are also indicated in the figure.

The continuum of radiation modes is excited at discontinuities in the circuit giving rise to radiation loss, and in addition, the excitation of the substrate modes is likely to give rise to stray coupling between isolated components in the circuit.

A solution to (2.58a) exists down to DC making substrate leakage unavoidable. From Figure 2.3 it can be seen that as the frequency increases, the phase velocity of the substrate modes approaches that of the fundamental mode. This is likely to increase the coupling between the guided modes and the substrate modes at discontinuities, due to phase matching

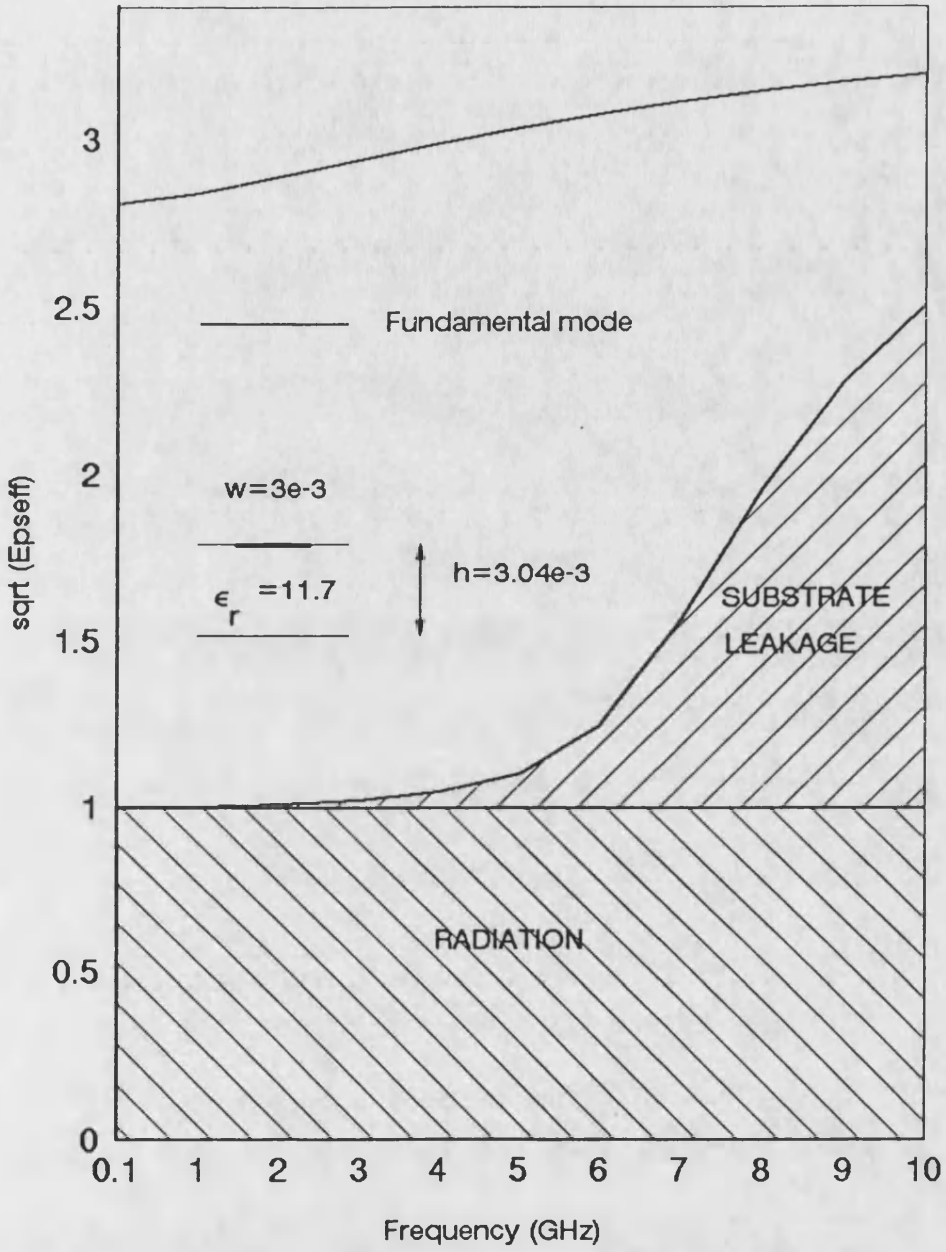

Figure 2.3 Dispersion characteristics of open microstrip (all dimensions in metres)

The dispersion curves for a cross-sectional geometry were the thickness of the dielectric layer is decreased significantly is given in Figure 2.4. By comparison with Figure 2.3, it can be seen that the substrate modes now propagate very close to cutoff, with a phase velocity that is very different from that of the fundamental mode.

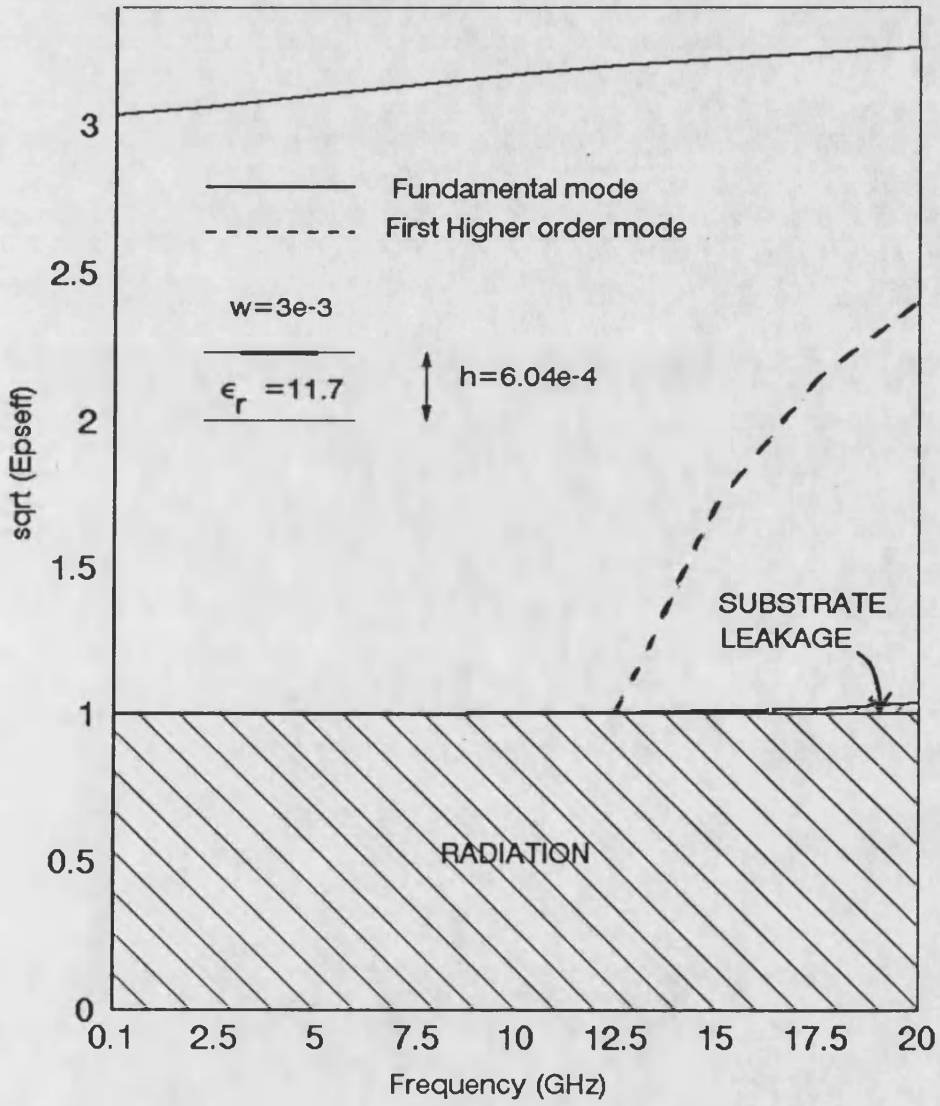

Figure 2.4 Dispersion characteristics of open microstrip (all dimensions in metres)

Comparing the results obtained in Figure 2.3 with those obtained in Figures 2.4, were the thickness of the dielectric substrate has been decreased, we would expect that the effect of stray coupling in microstrip circuits, due to the excitation of substrate modes at discontinuities is likely to be less significant for thinner substrate.

Experiments conducted on a comb line array antenna (Figure 2.5) and reported in [17] confirm this result. In these experiments sidelobe levels of -17 dB were initially obtained for a substrate thickness of 1.59 mm (ϵ_r=2.32). By shielding the substrate with absorbing material, it was found that the sidelobe levels were reduced to -20 dB. The experiment was then repeated for a substrate thickness of 0.793 mm and in this case it was found that shielding the substrate with absorbing material had a negligible effect on the radiation pattern of the antenna.

Although substrate leakage may be reduced by thinning down the thickness of the substrate, it can be seen from Figure 2.4, that higher order modes have emerged. In Figure 2.6, the cross-sectional geometry of Figure 2.4 has been modified by adding a thin layer of relatively low permittivity (ϵ_r=2.33) as shown in the figure. It can be seen from the figures, that a separation of phase velocities between the fundamental mode and the substrate modes is maintained. However, in the multilayered geometry

of Figure 2.6, no higher order modes exist up to a frequency of 20 GHz. Thus it may be concluded that substrate leakage control together with control of the higher order modes can be achieved in multilayered microstrip.

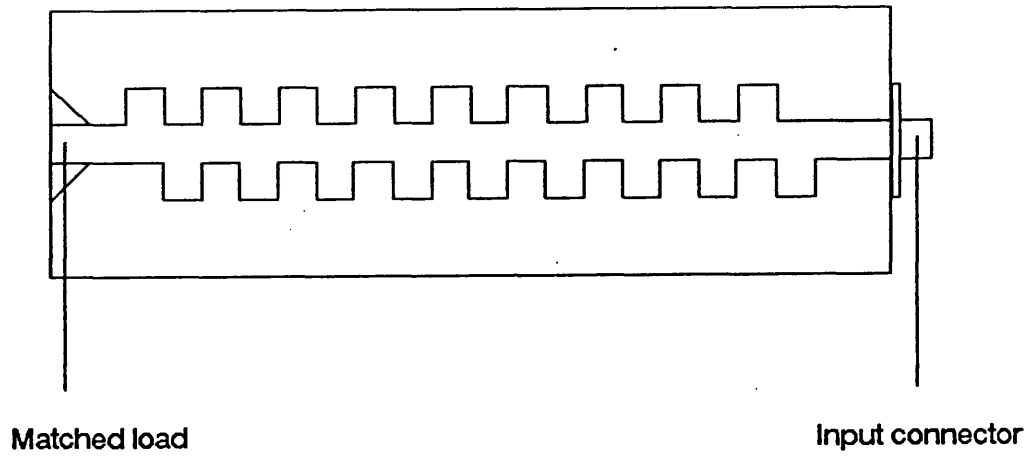

Figure 2.5 Example of a comb line array antenna

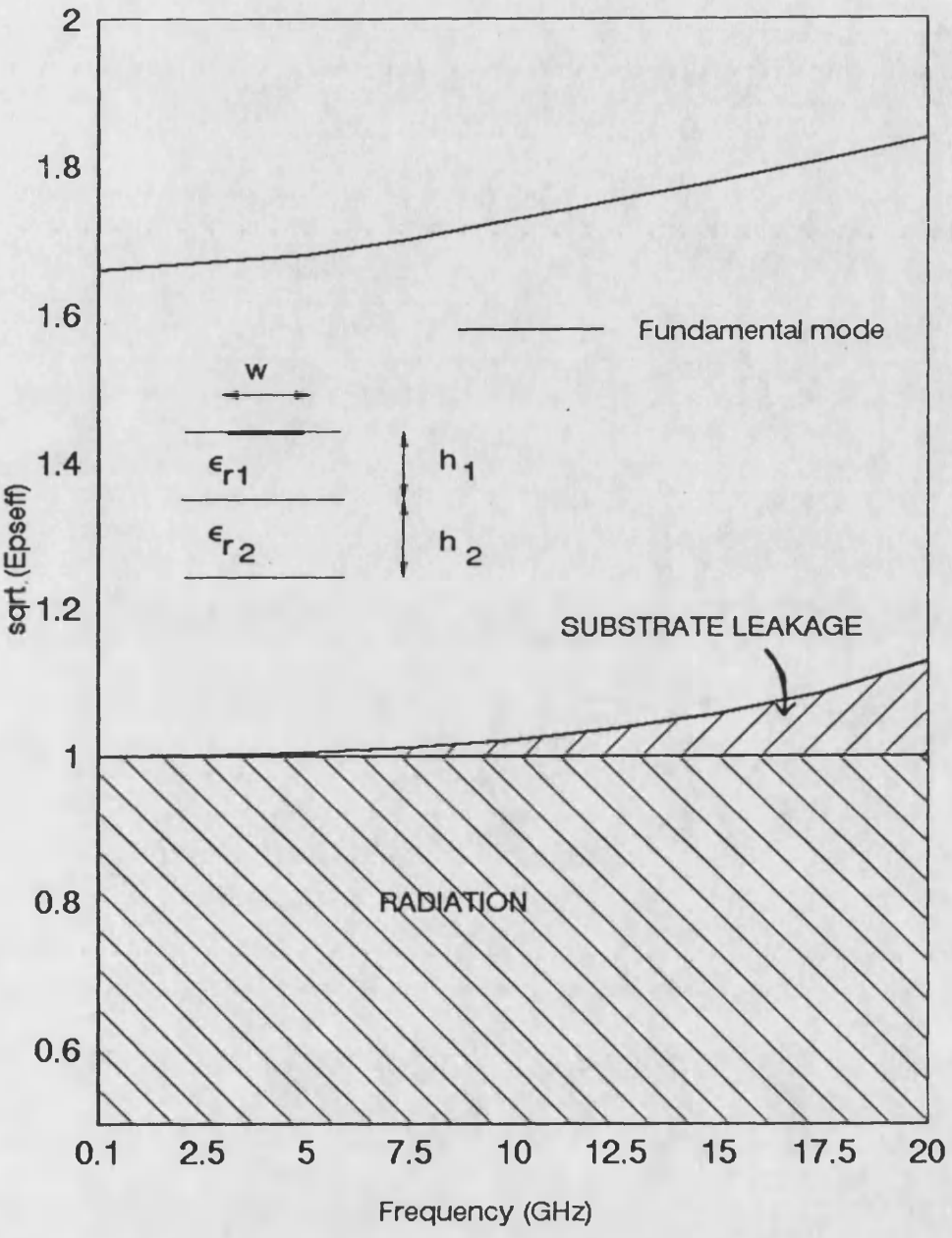

Figure 2.6 Dispersion characteristics in two-layer microstrip. ϵ_{r1}=2.04, ϵ_{r2}=11.7, h_1=6.35e-4, h_2=6.35e-4, w=3e-3 (all dimensions in metres).

2.5.1 CONVERGENCE OF SOLUTIONS FOR THE FUNDAMENTAL MODE

Table 2.1, below shows the convergence of the solutions obtained for the fundamental mode of an example geometry as a function of the number of basis functions used in (2.39).

It can be seen from the table that convergence to 4 significant figures is achieved using just 2 sets of basis functions for each of the current components. This highlights the importance of making the right choice of basis functions in order to achieve rapid convergence (as discussed in section 2.3.5)

	number of basis functions		
Frequency (GHz)	1 by 1	2 by 2	3 by 3
0.1	3.0524	2.9380	2.9377
2	3.0872	2.9590	2.9588
4	-	2.9845	2.9843
6	-	3.0052	3.0052
8	-	3.0217	3.0217
10	-	3.0350	3.0350

Table 2.1 Convergence of solutions for fundamental mode of open microstrip (h=0.635e-3, w=9.35e-3, ϵ_r=10.2 - all dimensions in metres)

CONCLUSION

A method of analysis has been presented for multilayered microstrip circuits taking into account the presence or absence of side walls and the top cover. It is noted that although the analysis was presented for the case were several dielectric layers are present underneath the strip, the presence of dielectric layers above the strip can easily be taken into account.

It is recognized that covered and open microstrip are open structures capable of supporting radiation and as well as bound modes. The spectrum of radiation modes has been separated into two regions where for one region, referred to as the "substrate leakage" region, the radiation modes decay along the transverse direction but are unbound along the lateral direction, while in the other region, the radiation modes are unbound along both the transverse and lateral directions. These modes may be excited at discontinuities in the circuit giving rise to stray coupling between components and contributing to the loss in the circuits. An estimate of these latter effects would require a full-wave analysis of microstrip including radiation as well as bound modes and this is beyond the scope of the thesis. However, it has been found that the substrate modes propagate at a range of phase velocities and the effect of substrate thickness on the propagation of these modes has been highlighted.

The effect of using multilayered microstrip as a means of controlling both substrate leakage and higher order modes has also been highlighted.

REFERENCES

1. Felsen and Marcuvitz, "Radiation and Scattering of Waves", Prentice-Hall, 1973.

2. R. E. Collin, "Field Theory of Guided Waves", McGraw-Hill, 1960.

3. S. Schelkunoff, "Generalised Telegraphists Equations for Waveguides", The Bell Syst. Tech. J., July 1952, pp. 784-801.

4. H. Ermert, "Guiding and Radiation Characteristics of Planar Waveguides", Microwaves, Optics and Acoustics, March 1979, Vol. 3., pp. 59-62.

5. Railton, "Analysis of Boxed Microstrip", Ph.D. thesis, University of Bath, Bath, 1987.

6. Mathews and Walker, "Mathematical Methods for Physicists", Benjamin, 1964.

7. L.W. Johnson and R.D. Riess, "Numerical Analysis", Addison-Wesley, 1982.

8. I.S. Gradshteyn and I.M. Ryshik, "Tables of Integrals,

series and products", New York, Academic Press, 1965, p.827.

9. T. Amir and A.A. Oliner, "Guided Complex Waves", Proceedings IEE, Vol. 110, No. 2, February 1963, pp. 310-334.

10. J. Boukamp and R. H. Jansen, "The High-frequency behaviour of microstrip open ends in microwave integrated circuits including energy leakage", 14th Eur. Mic. Conf., 1984, pp. 142-147.

11. N. K. Das and D. M. Pozar, "Full-Wave Spectral-Domain Computation of Material, Radiation, and Guided Wave Losses in Infinite Multilayered Printed Transmission Lines", IEEE Trans. Microwave Theory Tech., Vol. MTT-39, January 1991, pp. 54-60.

12. R. H. Jansen, "The Spectral-Domain Approach for Microwave Integrated Circuits", IEEE Trans. Microwave Theory Tech., Vol. MTT-33, Octobre 1985, pp. 1043-1055.

13. C.J. Railton and T. Rozzi, "Complex Modes in Boxed Microstrip", IEEE Trans. Microwave Theory Tech., Vol. MTT-36, May 1988, pp. 865-874.

14. G.B. Arfken, "Mathematical Methods for Physicists", New York, Academic Press, 1970.

15. L.J. Van Der Pauw, "The Radiation of Electromagnetic Power by Microstrip Configurations", IEEE Trans. Microwave Theory Tech., Vol. MTT-25, September 1977, pp. 719-729.

16. R.W. Jackson, "Full-Wave Finite Element Analysis of Irregular Microstrip Discontinuities", IEEE. Trans. Microwave Theory Tech., Vol. MTT-37, January 1989, pp. 81-87.

17. J.R. James, P.S. Hall, and C. Wood, "Microstrip Antenna Theory and Design", IEE Electromagnetic Wave Series 12, Peter Pereguins Ltd. 1981.

APPENDIX 2A

FORMULATION OF ADMITTANCE OPERATORS

The formulation of the admittance operators follows the same procedure given in [1]. Consider the fields at $y=0^-$. Substituting the expressions for the potential functions (2.17), with $\phi_e(\rho,x)$, $\phi_h(\rho,x)$ given by (2.14) for example, into (2.4), gives for the electric fields in the first dielectric layer ($0<y<-h_1$) :

$$E_x(x,y)=\int_0^\infty d\rho E'^1_x(\rho)\phi_h(\rho,x)\frac{Y'_1\cos k_{1n}(y+h_1)+jY'^D_2\sin k_{1n}(y+h_1)}{Y'_1\cos k_{1n}h_1+jY'^D_2\sin k_{1n}h_1} + E''^1_x(\rho)\phi_h(\rho,x)\frac{Y''_1\cos k_{1n}(y+h_1)+jY''^D_2\sin k_{1n}(y+h_1)}{Y''_1\cos k_{1n}h_1+jY''^D_2\sin k_{1n}h_1} \tag{2A.1}$$

where

$$E'^1_x(\rho)=\rho I'_1(\rho)Z'^D_1(\rho)\frac{1}{\sqrt{\rho^2+\beta^2}} \tag{2A.2a}$$

$$E''^1_x(\rho)=-j\beta V''_1(\rho)\frac{1}{\sqrt{\rho^2+\beta^2}} \tag{2A.2b}$$

Thus E_x at $y=0^-$ is given by

$$E_x(x,0^-)=\int_0^\infty E^1_x(\rho)\phi_h(\rho,x)\,d\rho \tag{2A.3}$$

where

$$E^1_x(\rho)=\left(\rho I'_1(\rho)Z'^D_1(\rho)-j\beta V''_1(\rho)\right)\frac{1}{\sqrt{\rho^2+\beta^2}} \tag{2A.4}$$

Similarly for the E_z, the field within the first dielectric layer is given by

$$E_z(x,y)=\int_0^{\infty} d\rho E'^1_z(\rho)\phi_e(\rho,x)\frac{Y'_1\cos k_{1n}(y+h_1)+jY'^D_2\sin k_{1n}(y+h_1)}{Y'_1\cos k_{1n}h_1+jY'^D_2\sin k_{1n}h_1} + E''^1_z(\rho)\phi_e(\rho,x)\frac{Y''_1\cos k_{1n}(y+h_1)+jY''^D_2\sin k_{1n}(y+h_1)}{Y''_1\cos k_{1n}h_1+jY''^D_2\sin k_{1n}h_1} \qquad (2A.5)$$

where

$$E'^1_z(\rho)=j\beta I'_1(\rho)Z'^D_1(\rho)\frac{1}{\sqrt{\rho^2+\beta^2}} \qquad (2A6.a)$$

$$E''^1_z(\rho)=-V''_1(\rho)\rho\frac{1}{\sqrt{\rho^2+\beta^2}} \qquad (2A.6b)$$

Thus $E_z(x,0^-)$ is given by

$$E_z(x,0^-)=\int_0^{\infty} E^1_z(\rho)\phi_e(\rho,x)\,d\rho \qquad (2A.7)$$

where

$$E^1_z(\rho)=\left(j\beta I'_1(\rho)Z'^D_1-V''_1(\rho)\rho\right)\frac{1}{\sqrt{\rho^2+\beta^2}} \qquad (2A.8)$$

rearranging (2A.8, 2A.4) then gives:

$$\begin{bmatrix} E^1_x(\rho) \\ -E^1_z(\rho) \end{bmatrix} = T(\rho) \begin{bmatrix} Z'^D_1(\rho) & 0 \\ 0 & 1 \end{bmatrix} \begin{bmatrix} -I'_1(\rho) \\ V''_1(\rho) \end{bmatrix}$$

The tangential magnetic fields within the first dielectric layer $(0<y<h_1)$ are given by:

$$H_x(x,y)=\int_0^{\infty} d\rho H'^1_x(\rho)\phi_e(\rho,x)\frac{Y'^D_2\cos k_{1n}(y+h_1)+jY'_2\sin k_{1n}(y+h_1)}{Y'^D_2\cos k_{1n}h_1+jY'_1\sin k_{1n}h_1} + H''^1_x(\rho)\phi_e(\rho,x)\frac{Y''^D_2\cos k_{1n}(y+h_1)+jY''_1\sin k_{1n}(y+h_1)}{Y''^D_2\cos k_{1n}h_1+jY''_1\sin k_{1n}h_1} \tag{2A.10}$$

where

$$H'^1_x(\rho)=j\beta I'_1(\rho)\frac{1}{\sqrt{\rho^2+\beta^2}} \tag{2A.11a}$$

$$H''^1_x(\rho)=V''_1(\rho)\frac{1}{\sqrt{\rho^2+\beta^2}}\rho Y''^D_1(\rho) \tag{2A.11b}$$

$$H_z(x,y)=\int_0^{\infty} d\rho H'^1_z(\rho)\phi_h(\rho,x)\frac{Y'^D_2\cos k_{1n}(y+h_1)+jY'_2\sin k_{1n}(y+h_1)}{Y'^D_2\cos k_{1n}h_1+jY'_1\sin k_{1n}h_1} + H''^1_z(\rho)\phi_h(\rho,x)\frac{Y''^D_2\cos k_{1n}(y+h_1)+jY''_1\sin k_{1n}(y+h_1)}{Y''^D_2\cos k_{1n}h_1+jY''_1\sin k_{1n}h_1} \tag{2A.12}$$

where

$$H'^1_z(\rho)=-I'_1(\rho)\rho\frac{1}{\sqrt{\rho^2+\beta^2}} \tag{2A.13a}$$

$$H''_z(\rho)=-j\beta V''_1(\rho)\frac{1}{\sqrt{\rho^2+\beta^2}}Y''^D_1(\rho) \tag{2A.13b}$$

Thus the expressions for the magnetic fields at $y=0^-$ are given by

$$H_x(x,0^-)=\int_0^{\infty} H^1_x(\rho)\phi_e(\rho,x)\,d\rho \tag{2A.14}$$

where

$$H_x^1(\rho) = \left(j\beta I'_1(\rho) + \rho V''_1(\rho)\, Y''^{D}_1(\rho)\right)\frac{1}{\sqrt{\rho^2+\beta^2}} \qquad (2A.15)$$

and

$$H_x(x, 0^-) = \int_0^{\infty} H_x^1(\rho)\,\phi_e(\rho, x)\, d\rho \qquad (2A.16)$$

where

$$H_z^1(\rho) = \left(-j\rho I'_1(\rho) - j\beta V''_1(\rho)\, Y''^{D}_1(\rho)\right)\frac{1}{\sqrt{\rho^2+\beta^2}} \qquad (2A.17)$$

Expressions (2A.17, 2A.15) can then be rearranged in matrix form to give:

$$\begin{bmatrix} H_z^1(\rho) \\ H_x^1(\rho) \end{bmatrix} = T(\rho) \begin{bmatrix} 1 & 0 \\ 0 & Y''^{D}_1(\rho) \end{bmatrix} \begin{bmatrix} -I'_1(\rho) \\ V''_2(\rho) \end{bmatrix} \qquad (2A.18)$$

The fields at $y=0^+$ can be treated in a similar manner.

References

[1] T. Rozzi and S. Hedges, "Rigorous Analysis and Network Modelling of the Inset Dielectric Guide", IEEE Trans. Microwave Theory Tech., Vol. MTT-35, 1987, pp. 823-833.

CHAPTER 3

ANALYSIS OF THE INSET DIELECTRIC GUIDE

3.1 INTRODUCTION

Inset Dielectric Guide (IDG) has shown promise as a low loss transmission line media at microwave and millimetric applications. Its advantages over other dielectric guides such as image line or insular line are its ability to negotiate bends with minimal loss and ease of manufacture [1].

In addition, IDG, has shown promise as an antenna media with low cross polarisation and good input match [2,3,4]. Both vertical and horizontal polarisation antennas have been designed in IDG [2,3].

IDG has been rigorously analyzed by Transverse Resonance Diffraction, where the case of a single dielectric layer in the slot has been considered [5]. In this chapter a rigorous hybrid method of analysis is presented for the case where multiple dielectric layers may exist in the slot.

A new feature of IDG is revealed, which is the large degree of control of the monomode bandwidth achievable by suitable

choice of cross sectional dimensions and the use of two dielectric layers of different permittivities in the slot. It is shown that by suitable choice of cross sectional dimensions and dielectric filling, a monomode bandwidth that is comparable to that of the ridge waveguide [6] can be achieved. Bandwidth control in a single-layered IDG is also investigated.

Experimental measurements of the fundamental and higher order modes, for several different geometries, are presented and these show good agreement with the computed results.

Convergence tests are carried out for a particular geometry and the rapid convergence that is achieved highlights the efficiency of the method of analysis.

3.2 ANALYSIS OF MULTILAYERED IDG

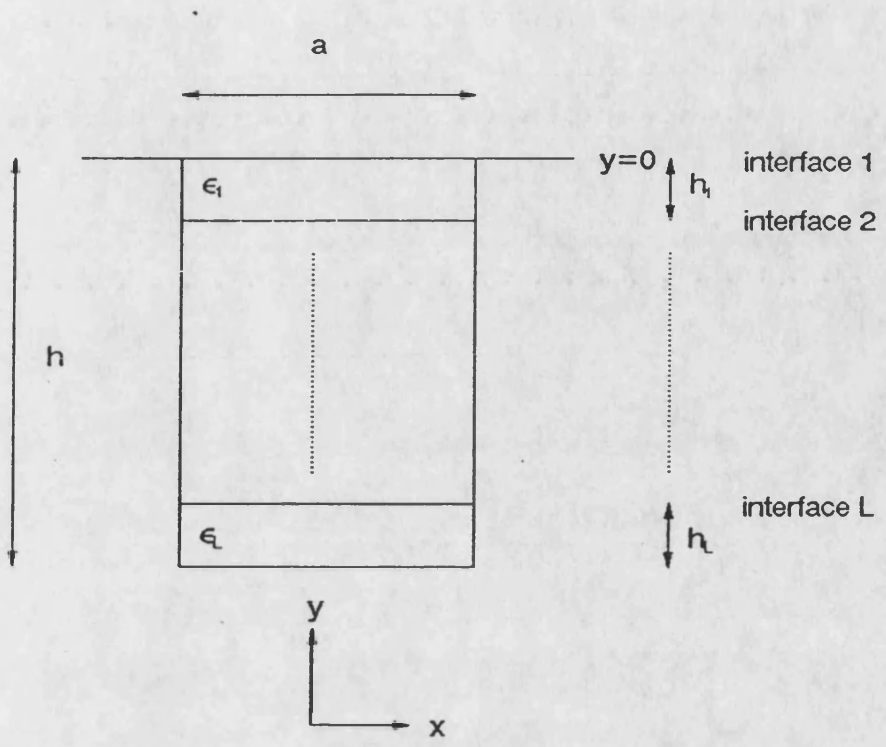

Figure 3.1 Cross section of multilayered IDG

Figure 3.1 above gives the cross section of a multilayered IDG structure. The analysis for IDG follows an analogous procedure to that used for microstrip in Chapter 2. The fields in the air region and each of the dielectric layers in the slot are expressed in terms of complete sets of y-directed electric and magnetic Hertzian potential functions as in section 2.2.1.

Considering the potential functions at either side of the discontinuiuty at $y=0$, the following choice of potential functions is made: for the uppermost dielectric layer the

potential functions (2.10) are chosen whereas for the air region, the potential functions (2.20) are chosen. Thus for $0<y<-h_1$, the potential functions are chosen as:

$$\psi_e(x,y)=\sum_{n=}^{\infty}\frac{I'_{1n}}{j\omega\epsilon_1}\frac{1}{\sqrt{((n\pi/a)^2+\beta^2)}}\phi_{en}(x)\qquad(3.1a)$$
$$\frac{jY'_1(n)\sin k_{1n}(y+h_1)+Y'^{D}_2(n)\cos k_{1n}(y+h_1)}{jY'_1(n)\sin k_{1n}h_1+Y'^{D}_2(n)\cos k_{1n}h_1}$$

$$\psi_h(x,y)=\sum_{n}^{\infty}\frac{V''_{1n}}{j\omega\mu_0}\frac{1}{\sqrt{((n\pi/a)^2+\beta^2)}}\phi_{hn}(x)\qquad(3.1b)$$
$$\frac{Y''_1(n)\cos k_{1n}(y+h_1)+jY''(n)^{D}_2\sin k_{1n}(y+h_1)}{Y''_1(n)\cos k_{1n}h_1+jY''^{D}_2(n)\sin k_{1n}h_1}$$

where the x- and y-dependence of the potential functions is given by the expressions (2.6, 2.7, 2.11 - 2.13).

For the air region, $y>0$, the potential functions are chosen as:

$$\psi_e(x,y)=\int_0^{\infty}\frac{I'_0(\rho)}{j\omega\epsilon_0}\frac{1}{\sqrt{(\rho^2+\beta^2)}}\phi_e(\rho,x)\,e^{jk_0(\rho)y}d\rho\qquad(3.2a)$$

$$\psi_h(x,y)=\int_0^{\infty}\frac{V''_0(\rho)}{j\omega\mu_0}\frac{1}{\sqrt{(\rho^2+\beta^2)}}\phi_h(\rho,x)\,e^{jk_0(\rho)y}d\rho\qquad(3.2b)$$

where the x- dependence of the potential functions is given by the expressions (2.14, 2.15).

The choice of potential functions (3.1) insures that the boundary conditions at the conducting walls of the slot are

obeyed. Since bound modes are considered, the fields in air must decay exponentially with increasing y. This condition is obeyed by the fields in air provided

$$\beta > k_0 \tag{3.3}$$

Condition (3.3) then defines the cutoff condition for the bound modes of the guide.

3.3 FORMULATION OF ADMITTANCE OPERATORS

In order to enforce the boundary conditions at the interface, y=0, admittance operators can be formulated for the air region and the slot region that express the tangential magnetic fields in terms of the tangential electric fields.

(i) Admittance operators for the slot

Consider modes with odd-E_z symmetry for example: by substituting the expressions for the potential functions into the expressions for the fields (2.4), the following expressions are obtained for the fields at $y=0^-$:

$$E_x(x,0^-) = \sum_{n=0,2,..}^{\infty} E_{xn}^1 \phi_{hn}(x) \tag{3.4a}$$

where

$$E^1_{xn}=\left(I'_{1n}\frac{n\pi}{a}Z'^{D}_{1}(n)-V''_{1n}j\beta\right)\frac{1}{\sqrt{\left(\frac{n\pi}{a}\right)^2+\beta^2}} \tag{3.4b}$$

$$E_z(x,0^-)=\sum_{n=2,4,..}^{\infty}E^1_{zn}\phi_{en}(x) \tag{3.5a}$$

where

$$E^1_{zn}=\left(j\beta I'_{1n}Z'^{D}_{1}(n)-V''_{1n}\frac{(n\pi)}{a}\right)\frac{1}{\sqrt{\left(\frac{n\pi}{a}\right)^2+\beta^2}} \tag{3.5b}$$

$Z'^{D}_{1}(n)$ is the input impedance looking down from interface 1, for the TM modes. Expressions (3.4b) and (3.5b) can be rearranged in matrix form to give

$$\begin{bmatrix}E^1_{xn}\\E^1_{zn}\end{bmatrix}=\begin{bmatrix}\cos\theta & -j\sin\theta\\-j\sin\theta & \cos\theta\end{bmatrix}\begin{bmatrix}Z'^{D}_{1}(n) & 0\\0 & 1\end{bmatrix}\begin{bmatrix}I'_{1n}\\V''_{1n}\end{bmatrix} \tag{3.6a}$$

$$= T_n \begin{bmatrix}Z'^{D}_{1}(n) & 0\\0 & 1\end{bmatrix}\begin{bmatrix}I'_{1n}\\V''_{1n}\end{bmatrix}$$

where T_n is a coordinate transformation with

$$\cos\theta=\frac{n\pi/a}{\sqrt{(n\pi/a)^2+\beta^2}} \qquad \sin\theta=\frac{\beta}{\sqrt{(n\pi/a)^2+\beta^2}} \tag{3.6b}$$

Similarly for the magnetic fields

$$H_x(x,0^-)=\sum_{n=2,4,..}^{\infty}H^1_{xn}\phi_{en}(x) \tag{3.7a}$$

$$H_z(x,0^-) = \sum_{n=0,2,..}^{\infty} H_{zn}^1 \phi_{hn}(x) \qquad (3.7b)$$

where

$$\begin{bmatrix} H_{zn}^1 \\ -H_{xn}^1 \end{bmatrix} = T_n \begin{bmatrix} 1 & 0 \\ 0 & Y''^D_1(n) \end{bmatrix} \begin{bmatrix} I'_{1n} \\ V'_{1n} \end{bmatrix} \qquad (3.8)$$

Finally, from (3.8) and (3.6a), by eliminating the coefficients I'_{1n}, V''_{1n}, the magnetic field components and the electric field components can be related to each other as

$$\begin{bmatrix} H_{zn}^1 \\ -H_{xn}^1 \end{bmatrix} = T_n \begin{bmatrix} Y'^D_1(n) & 0 \\ 0 & Y''^D_1(n) \end{bmatrix} T_n^{-1} \begin{bmatrix} E_{xn}^1 \\ E_{zn}^1 \end{bmatrix} \qquad (3.9)$$

(ii) Admittance operators for the air region

Following a similar operation for the air region, the following expressions are obtained

$$E_x(x,0^+) = \int_0^{\infty} E_x^0(\rho)\,\phi_h(\rho,x)\,d\rho \qquad (3.10a)$$

$$E_z(x,0^+) = \int_0^{\infty} E_z^0(\rho)\,\phi_e(\rho,x)\,d\rho \qquad (3.10b)$$

$$H_x(x,0^+) = \int_0^{\infty} H_x^0(\rho)\,\phi_e(\rho,x)\,d\rho \qquad (3.10c)$$

$$H_z(x,0^+)=\int_0^{\infty} H_z^0(\rho)\,\phi_h(\rho,x)\,d\rho \tag{3.10d}$$

where

$$\begin{bmatrix} -H_z^0(\rho) \\ H_x^0(\rho) \end{bmatrix} = T(\rho) \begin{bmatrix} Y_1'^U(\rho) & 0 \\ 0 & Y_1''^U(\rho) \end{bmatrix} T(\rho)^{-1} \begin{bmatrix} E_x^0(\rho) \\ E_z^0(\rho) \end{bmatrix} \tag{3.11}$$

with

$$T(\rho)=\begin{bmatrix} \cos\alpha & -j\sin\alpha \\ -j\sin\alpha & \cos\alpha \end{bmatrix} \tag{3.12a}$$

$$\cos\alpha=\frac{\rho}{\sqrt{\rho^2+\beta^2}} \qquad \sin\alpha \ \frac{\beta}{\sqrt{\rho^2+\beta^2}} \tag{3.12b}$$

3.4 SETUP OF DISPERSION RELATION

The fields at $y=0$ obey the following boundary conditions.

1. The tangential electric fields must be continuous at the interface. Thus

$$E_z(x,0^+)=E_z(x,0^-)=E_z(x,0)$$
$$E_x(x,0^+)=E_x(x,0^-)=E_x(x,0) \tag{3.13}$$

2. The tangential magnetic fields must be continuous at the interface over the width of the slot. Thus

$$H_z(x,0^+)=H_z(x,0^-)$$

$$(|x|<a/2) \tag{3.14}$$

$$H_x(x,0^+)=H_x(x,0^-)$$

From (3.9) and (3.11) the following expressions are obtained for the magnetic fields at either side of the interface at $y=0$:

$$\begin{bmatrix} H_z(x,0^-) \\ H_x(x,0^-) \end{bmatrix} = \begin{bmatrix} \tilde{Y}^s_{11} & \tilde{Y}^s_{12} \\ \tilde{Y}^s_{21} & \tilde{Y}^s_{22} \end{bmatrix} \begin{bmatrix} E_x(x,0) \\ E_z(x,0) \end{bmatrix} \tag{3.15}$$

Where the operators $\tilde{Y}^s_{11}$ are defined by

$$\tilde{Y}^s_{11}E_x(x,0)=\sum_n^{\infty}\left(\cos^2\theta Y_1'^D(n)+\sin^2\theta Y_1''^D(n)\right)\phi_{hn}(x)\int_0^{\infty}E_x(x,0)\,\phi_{hn}(x)\,dx \tag{3.16a}$$

$$\tilde{Y}^s_{12}E_z(x,0)=\sum_n^{\infty}j\cos\theta\sin\theta\left(Y_1'^D(n)-Y_1''^D(n)\right)\phi_{hn}(x)\int_0^{\infty}E_z(x,0)\,\phi_{en}(x)\,dx \tag{3.16b}$$

$$\tilde{Y}^s_{21}E_x(x,0)=\sum_n^{\infty}-j\cos\theta\sin\theta\left(Y_1'^D(n)-Y_1''^D(n)\right)\phi_{en}(x)\int_0^{\infty}E_x(x,0)\,\phi_{hn}(x)\,dx \tag{3.16c}$$

$$\tilde{Y}^s_{22}E_z(x,0)=\sum_n^{\infty}\left(\sin^2\theta Y_1'^D(n)+\cos^2\theta Y_1''^D(n)\right)\phi_{en}(x)\int_0^{\infty}E_x(x,0)\,\phi_{en}(x)\,dx \tag{3.16d}$$

While for the magnetic fields at $y=0^+$:

$$-\begin{bmatrix} H_z(x,0^+) \\ H_x(x,0^+) \end{bmatrix} = \begin{bmatrix} \tilde{Y}^a_{11} & \tilde{Y}^a_{12} \\ \tilde{Y}^a_{21} & \tilde{Y}^a_{22} \end{bmatrix} \begin{bmatrix} E_x(x,0) \\ E_z(x,0) \end{bmatrix} \tag{3.17}$$

Where the operators for the air region are given by

$$\tilde{Y}^a_{11}E_x(x,0)=\int_0^\infty\left(\cos^2\alpha\, Y'^U_1(\rho)+\sin^2\alpha\, Y''^U_1(\rho)\right)\phi_h(x,\rho)\int_0^\infty E_x(x,0)\,\phi_h(x,\rho)\,dx\;d\rho \tag{3.18a}$$

$$\tilde{Y}^a_{12}E_z(x,0)=\int_0^\infty j\cos\alpha\sin\alpha\left(Y'^U_1(\rho)-Y''^U_1(\rho)\right)\phi_h(x,\rho)\int_0^\infty E_z(x,0)\,\phi_e(x,\rho)\,dx\;d\rho \tag{3.18b}$$

$$\tilde{Y}^a_{12}E_x(x,0)=\int_0^\infty -j\cos\alpha\sin\alpha\left(Y'^U_1(\rho)-Y''^U_1(\rho)\right)\phi_e(x,\rho)\int_0^\infty E_x(x,0)\,\phi_h(x,\rho)\,dx\;d\rho \tag{3.18c}$$

$$\tilde{Y}^a_{22}E_z(x,0)=\int_0^\infty\left(\sin^2\alpha\, Y'^U_1(\rho)+\cos^2\alpha\, Y''^U_1(\rho)\right)\phi_e(x,\rho)\int_0^\infty E_x(x,0)\,\phi_e(x,\rho)\,dx\;d\rho \tag{3.18d}$$

Applying the boundary condition (3.14) to the magnetic fields gives:

$$\begin{bmatrix}\tilde{Y}_{11} & \tilde{Y}_{12}\\ \tilde{Y}_{21} & \tilde{Y}_{22}\end{bmatrix}\begin{bmatrix}E_x(x,0)\\ E_z(x,0)\end{bmatrix}=\underline{0} \tag{3.19}$$

where

$$\tilde{Y}_{11}=\tilde{Y}^s_{11}+\tilde{Y}^a_{11} \tag{3.20}$$

For the case of a single-layered IDG, the TM and TE admittances for the slot modes looking down from interface 1 (y=0) are those of a section of transmission line terminated with a short circuit at y=-h. These admittances

are given by:

$$Y^{I1}_{1}(n) = \frac{\omega \epsilon_0 \epsilon_{1r}}{k_{1n}} \frac{1}{j\tan k_{1n} h_1} \tag{3.21a}$$

$$Y^{II\,D}_{1}(n) = \frac{k_{1n}}{\omega \mu_0} \frac{1}{j\tan k_{1n} h_1} \tag{3.21b}$$

In this case the admittance operators (3.16, 3.18) are the same as those given in [5].

For a multilayered IDG, however, the TM and TE admittances for the slot mode looking down at interface 1 are those of cascaded sections of transmissions lines terminated by a short circuit at $y=-h$, and are given by the expressions (2.11-2.13).

3.5 APPLICATION OF GALERKIN PROCEDURE

In order to solve the dispersion relation (3.19), the Galerkin procedure is applied whereby the tangential electric fields are represented in terms of a basis of functions (see section 2.3.4) where

$$E_x(x,0) = \sum_{i=0}^{\infty} X_i E_{xi}(x) \tag{3.22a}$$

$$E_z(x,0)=\sum_{i=0}^{\infty} Z_i E_{zi}(x) \qquad (3.22b)$$

Substituting (3.22) into (3.19) gives

$$\begin{bmatrix} \tilde{Y}_{11}E_{x0} & \cdots & \tilde{Y}_{11}E_{xn} & \tilde{Y}_{12}E_{z0} & \cdots & \tilde{Y}_{12}E_{zm} \\ \tilde{Y}_{21}E_{x0} & \cdots & \tilde{Y}_{21}E_{xn} & \tilde{Y}_{22}E_{z0} & \cdots & \tilde{Y}_{22}E_{zm} \end{bmatrix} \begin{bmatrix} X_0 \\ \vdots \\ X_n \\ Z_0 \\ \vdots \\ Z_m \end{bmatrix} = 0 \qquad (3.23)$$

In order to determine the unknown weight coefficients in (3.22), the Galerkin procedure is completed by taking the inner product of the basis functions with (3.23) to give

$$\begin{bmatrix} \langle E_{x0}, \tilde{Y}_{11}E_{x0}\rangle & \cdots & \langle E_{x0}, \tilde{Y}_{11}E_{xn}\rangle & \langle E_{x0}, \tilde{Y}_{12}E_{z0}\rangle & \cdots & \langle E_{x0}, \tilde{Y}_{12}E_{zm}\rangle \\ \vdots & & \vdots & \vdots & & \vdots \\ \langle E_{xn}, \tilde{Y}_{11}E_{x0}\rangle & \cdots & \langle E_{xn}, \tilde{Y}_{11}E_{xn}\rangle & \langle E_{xn}, \tilde{Y}_{12}E_{z0}\rangle & \cdots & \langle E_{xn}, \tilde{Y}_{12}E_{zn}\rangle \\ \langle E_{z0}, \tilde{Y}_{21}E_{x0}\rangle & \cdots & \langle E_{z0}, \tilde{Y}_{21}E_{xn}\rangle & \langle E_{z0}, \tilde{Y}_{22}E_{z0}\rangle & \cdots & \langle E_{z0}, \tilde{Y}_{22}E_{zm}\rangle \\ \vdots & & \vdots & \vdots & & \vdots \\ \langle E_{zn}, \tilde{Y}_{21}E_{x0}\rangle & \cdots & \langle E_{zn}, \tilde{Y}_{21}E_{xn}\rangle & \langle E_{zn}, \tilde{Y}_{22}E_{z0}\rangle & \cdots & \langle E_{zn}, \tilde{Y}_{22}E_{z0}\rangle \end{bmatrix} \begin{bmatrix} X_0 \\ \vdots \\ X_n \\ Z_0 \\ \vdots \\ Z_m \end{bmatrix} = \underline{0} \qquad (3.24)$$

Solutions for (3.24) can be obtained by searching for the zeros of the determinant of (3.24), thus yielding the required propagation wavenumbers for the discrete modes (as in section 2.3.4).

3.5.1 CHOICE OF BASIS FUNCTIONS

As explained in section (2.3.5), the basis functions in (3.22) must be chosen carefully in order to achieve rapid convergence to the solution of (3.24). This can be achieved by choosing the basis functions that will closely model the actual field distribution of the tangential electric fields at the slot-air interface. The presence of the metallic corner causes a concentration of the fields at the interface and introduces a singularity in the field distribution. The order of the singularity in the field distribution is $r^{-1/3}$ where r is the radial distance away from the corner [7]. In order to include this behaviour in the basis functions, the following weight function is introduced into the latter:

$$W(2x/a) = (1-(2x/a)^2)^{-1/3} \tag{3.25}$$

A choice of functions which are orthogonal to the weight function (3.25) are the Gegenbauer polynomials [8] $C_m^{\nu}(x)$, with $\nu=1/6$. Thus the basis functions are chosen as

$$f_m(2x/a) = \frac{1}{N_m}\frac{C_m^{\nu}(2x/a)}{W(2x/a)} \qquad 0 \geq |x| \geq a/2$$
$$= 0 \qquad |x| > a/2 \tag{3.26}$$

where N_m is a normalization factor.

From (3.24), and considering the odd-parity modes for example, it evident that the following integrals must be

evaluated:

$$\prec E_{zi}, \phi_{en}(x) \succ = \frac{2}{\sqrt{a}} \int_0^{a/2} E_{zi} \sin\left(\frac{n\pi}{a}x\right) dx \qquad (3.27a)$$

$$\prec E_{xi}, \phi_{hn}(x) \succ = \frac{2\delta_n}{\sqrt{a}} \int_0^{a/2} E_{xi} \cos\left(\frac{n\pi}{a}x\right) dx \qquad (3.27b)$$

$$\prec E_{xi}, \phi_h(\rho, x) \succ = \frac{2}{\sqrt{\pi}} \int_0^{a/2} E_{xi} \cos(\rho x) dx \qquad (3.28a)$$

$$\prec E_{zi}, \phi_e(\rho, x) \succ = \frac{2}{\sqrt{\pi}} \int_0^{a/2} E_{zi} \sin(\rho x) dx \qquad (3.28b)$$

Consider the inner products (3.27). Integrating (3.27a) by parts:

$$\begin{aligned} \prec E_{zi}(x), \phi_{en}(x) \succ &= -\frac{2}{\sqrt{a}}\left[\frac{a}{n\pi} E_{zi}(x) \sin\left(\frac{n\pi}{a}x\right)\right] + \frac{2}{\sqrt{a}} \int_0^{a/2} \frac{a}{n\pi} \partial_x E_{zi}(x) \sin\left(\frac{n\pi}{a}x\right) dx \\ &= \frac{2}{\sqrt{a}} \frac{a}{n\pi} \int_0^{a/2} \partial_x E_{zi}(x) \sin\left(\frac{n\pi}{a}x\right) dx \end{aligned} \qquad (3.29)$$

The first term on the RHS of (3.29) reduces to zero since $E_{zi}(x)$ must be zero at the conducting edge as the boundary conditions require. Since $E_x(x)$ and $\partial_x E_z(x)$ have the same singular behaviour at the edge, the basis functions in (3.27b) and (3.29) are chosen as

$$E_{xi}(x) = f_{2i}(2x/a) \qquad (i=0,1,2,..) \qquad (3.30a)$$

$$\partial_x E_{zi}(x) = f_{2i}(2x/a) \qquad (i=1,2,..) \qquad (3.30b)$$

Note that in (3.30b) the series starts from i=1 since for the zeroth term E_{z1} is not zero at the conducting edge as the boundary condition requires [5].

The evalutation of the the normalisation factor N_m, and the inner products (3.27, 3.28) is given in Appendix 3A.

3.6 BANDWITH CONTROL IN SINGLE-LAYERED IDG

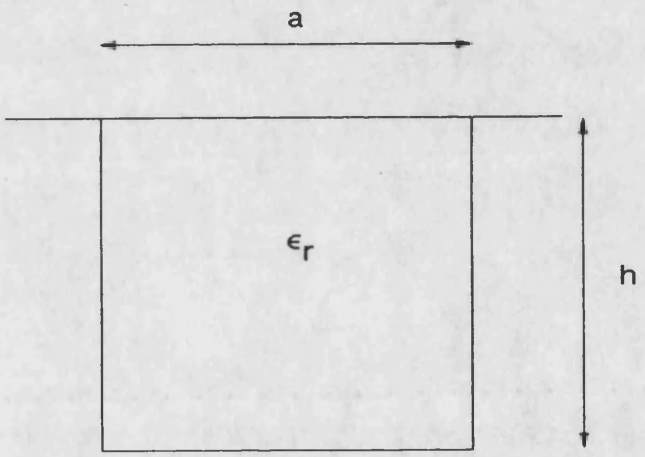

Figure 3.2 Cross section of single-layered IDG

Figure 3.2 above gives the cross section of an IDG guide with a single layer of dielectric material in the slot. In Figure 3.3 (a-d), dispersion curves are presented for the first two modes in the IDG keeping h fixed and varying the aperture of the slot a. In order to give a measure

of the bandwidth of the guide as the aspect ratio (a/h) is changed, we define the monomode bandwidth in terms of the cutoff frequencies of the fundamental and first higher order modes, f_0 and f_1 respectively as:

$$monomode\ bandwidth = \frac{f_1 - f_0}{f_1 + f_0} \times 100\% \qquad (3.31)$$

where the monomode bandwidth is expressed as a percentage.

As the aspect ratio (a/h) is increased, the behaviour of the guide is expected to approach that of a dielectric slab, and in Figure 3.3a, the first two modes of the dielectric slab are included for comparison with the dispersion curves of IDG with a relatively large aspect ratio. Thus as the aspect ratio increases the monomode bandwidth would tend to 100%. Although a large monomode bandwidth is achievable by increasing the aspect ratio, this is not considered to be of any practical use since the increase in aspect ratio will result in a lack of field confinement which is one of the advantages of IDG. As the aspect ratio is decreased, the cutoff frequency of the fundamental even mode increases until an aspect ratio of 2 is reached (Figure 3.3b) where the first even mode and the first odd mode propagate with nearly equal phase velocities. Below an aspect ratio of 2, the fundamental mode becomes odd in parity. Thus at an aspect ratio of around 2, the monomode bandwidth would drop down to 0%, and would begin to increase again as the aspect ratio is further decreased as can be seen in Figures 3.3c,3.3d. At

an aspect ratio of 0.6 , the cutoff of the second odd mode becomes even larger than that of the first even mode.

By comparing the Figures 3.3a -3.3d, it can be seen that the cutoff of the odd parity mode is not affected very much by the change in slotwidth, however, the cutoff of the even parity mode increases rapidly as the side walls are brought in. A possible explanation for this behaviour might be seen if the original TM and TE modes of the slab waveguide (IDG with side walls removed to infinity) are considered. The TM-to-y mode has the following field components H_x, E_z, E_y, while the TE-to-y mode has the field components E_x, H_y, H_z. Bringing in the side walls in the slot introduces singular behaviour in some of the field components. In addition, however, the three TM components are forced to zero at the side walls, whereas the TE components do not have this boundary condition imposed upon them. Thus it can be argued that the TM mode is perturbed strongly by the presence of the conducting walls with its cutoff frequency increasing as the slot aperture decreases.

Figures (3.3 a-d) however reveal an important mechanism of bandwidth control, namely that the relative cutoff between odd parity modes and even parity modes can be controlled through changing the width of the slot.

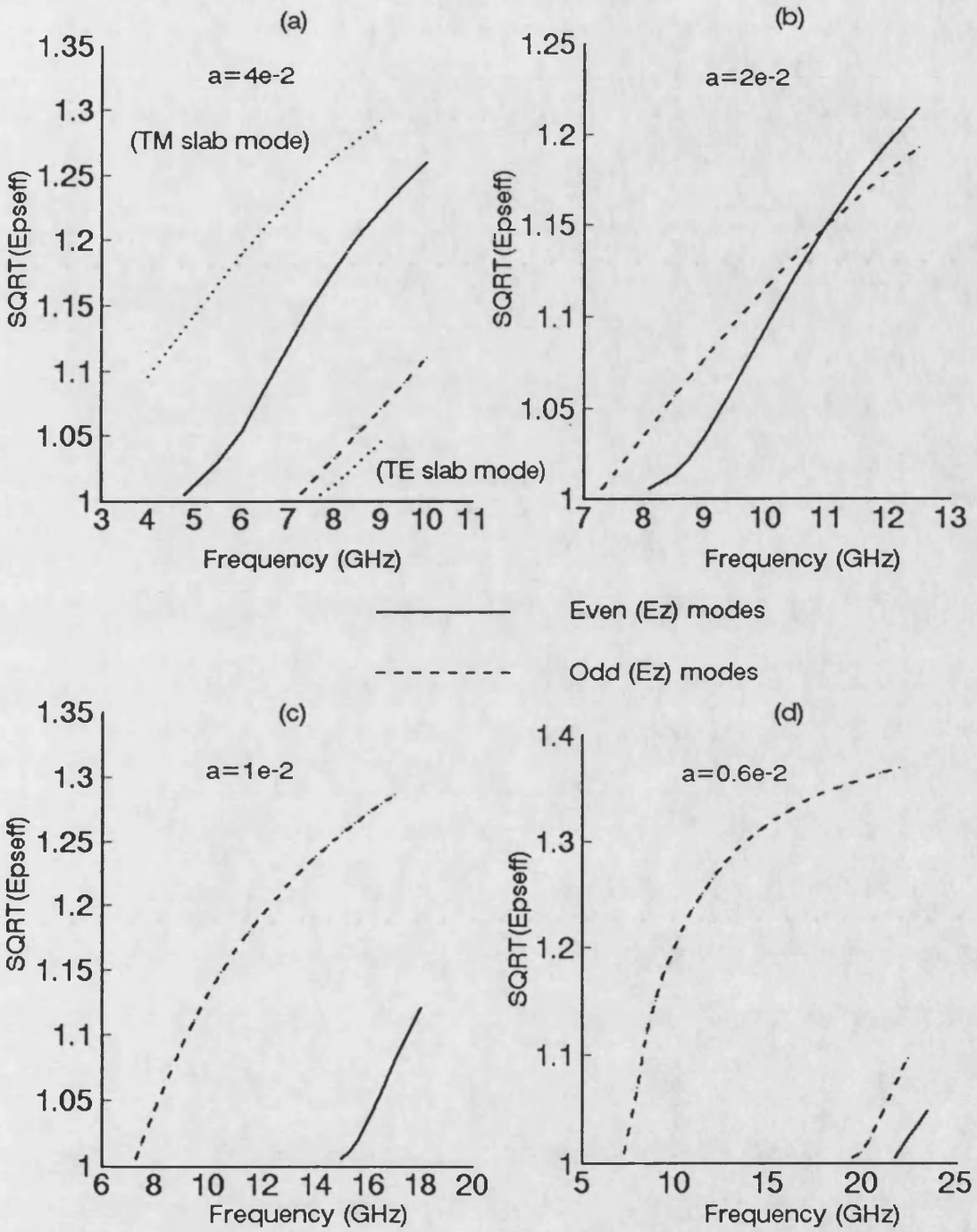

Figure 3.3 Dispersion curves for single-layered IDG keeping the slot depth constant and varying the slotwidth. h=1e-2, ϵ_r=2.04. All dimensions in metres.

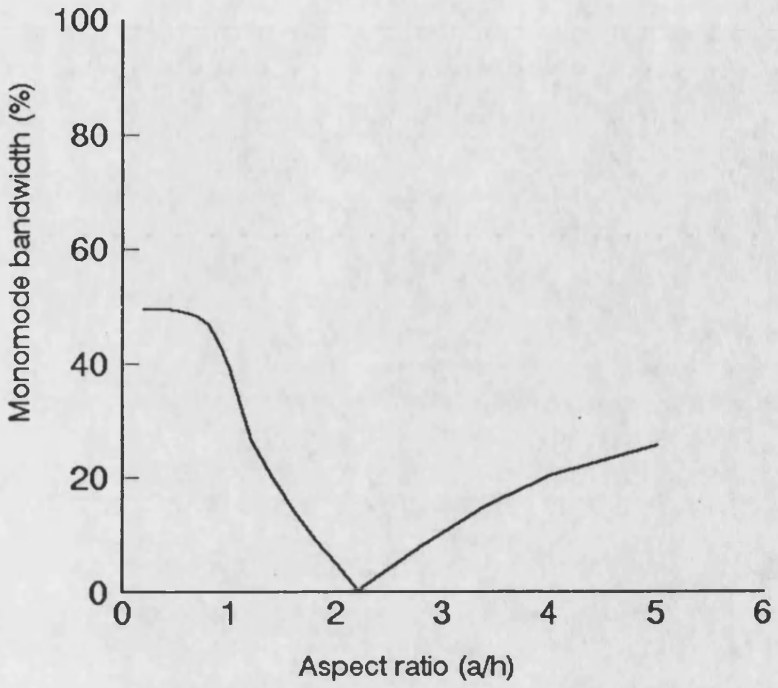

Figure 3.4 Monomode bandwidth versus aspect ratio for IDG. h=1e-2m,

Figure 3.4, above, gives a plot of monomode bandwidth versus aspect ratio (keeping h fixed). From the figure it can be seen that in a deep slot the bandwidth optimises at 49% at an aspect ratio of 0.66. It is noted that below this aspect ratio the first higher order mode is also of odd parity (see Figure 3.3d) and thus the control mechanism mentioned above is no longer of any use below an aspect ratio of 0.66.

The magnitude of the E_x field component over the cross section of the guide is plotted in Figure 3.5 for the three modes of Figure 3.3d. The three plots illustrate that as the frequency is increased in IDG, and higher order modes begin to propagate, the higher order mode patterns may be setup either across the IDG slot aperture (the first even mode) or along the depth of the IDG (the second odd mode).

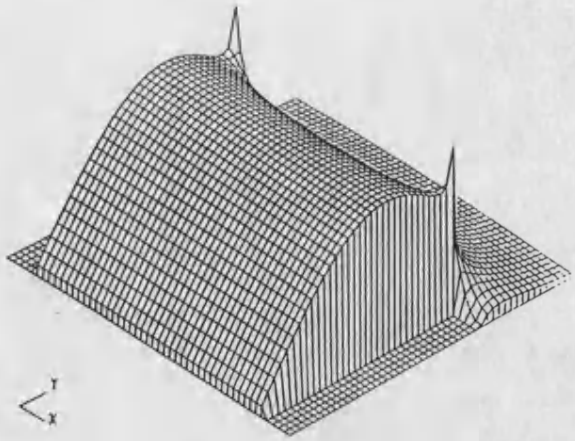

Fundamental (odd) mode

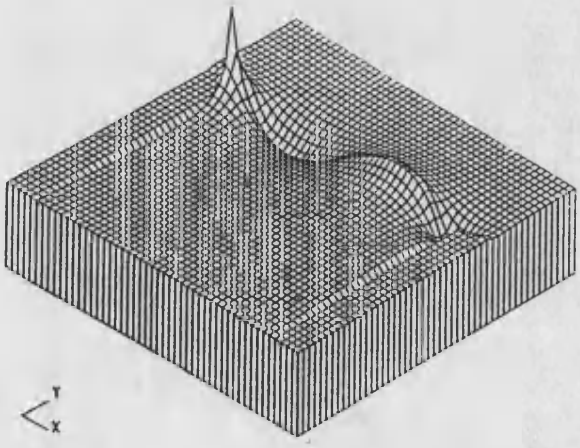

First even mode

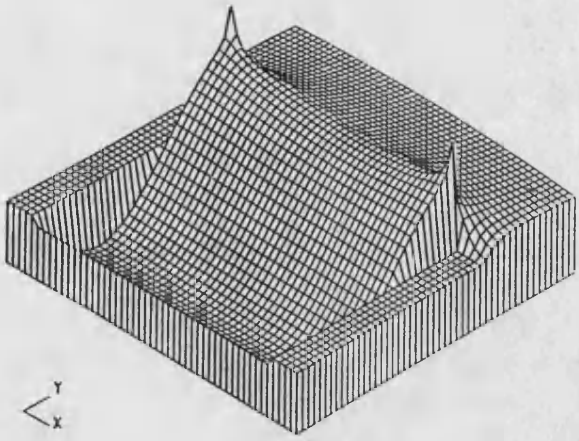

Second odd mode

Figure 3.5 Magnitude of the E_x component of the three modes of Figure 3.3d, plotted over the cross section of the guide (Frequency = 22 GHz).

3.6 BANDWIDTH CONTROL IN TWO-LAYER IDG

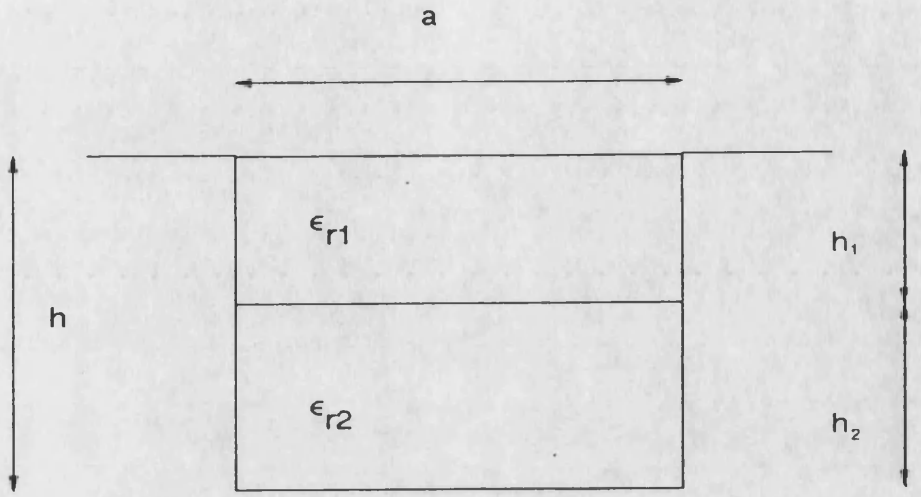

Figure 3.6 Cross section of twin-layered IDG

Figure 3.6 above gives the cross section of an IDG with two dielectric layers in the slot. The cutoff of the first three modes as a function of dielectric filling for such a guide is shown in Figure 3.7. An aspect ratio of 0.66 was chosen which is the aspect ratio where optimum bandwidth (of 50%) is obtained for a single-layered IDG. A relatively high permittivity material (ϵ_r=10.2) was used for the top dielectric layer. It can be seen that the effect of introducing the higher permittivity layer is to lower the cutoff of the modes and as the thickness of the top layer is increased, the cutoff decreases further, as expected. However, it can be seen that whereas the variation of cutoff for the first odd and even modes follows a similar pattern, the cutoff of the second odd mode remains relatively unchanged until the top dielectric layer

penetrates into the bulk of the guide. The field patterns given in Figure 3.5 above may offer an explanation for this behaviour since for the second odd mode, a higher order mode pattern is setup along the depth of the slot, and thus the mode remains relatively unperturbed if a thin dielectric layer is introduced at the top of slot.

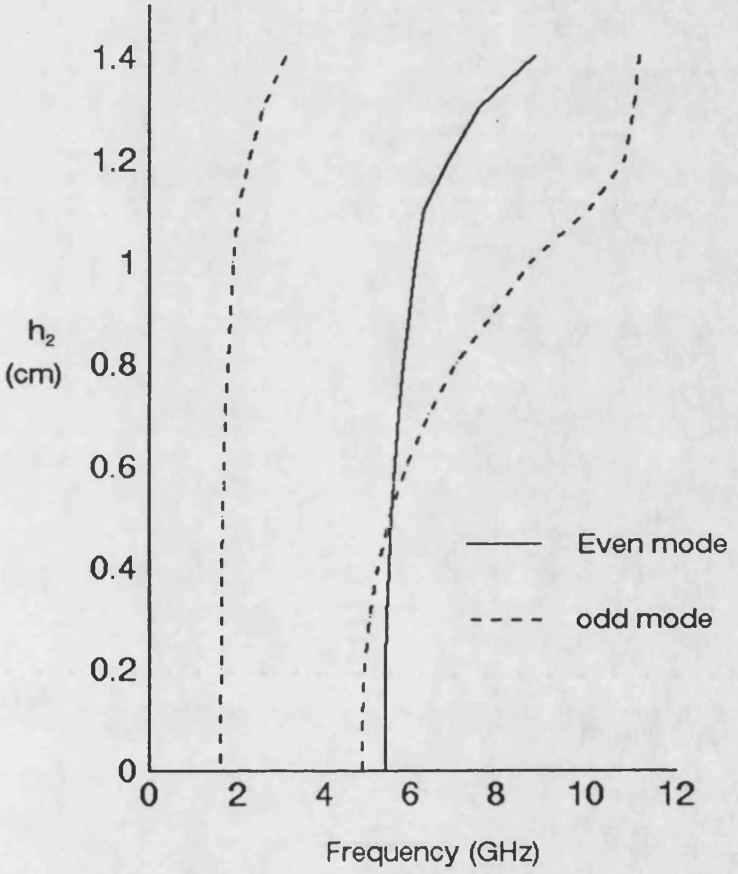

Figure 3.7 Cutoff of first three modes in two-layer IDG. a=1.016e-2, h=1.524e-2, ϵ_{r1}=2.04 ϵ_{r2}=10.2. (all dimensions in metres unless otherwise specified).

No gain in monomode bandwidth is achieved for the guide of Figure 3.7. However, a significant gain in bandwidth is obtained, if the width of the slot is controlled along with the dielectric filling as can be seen in Figure 3.8, where for a particular dielectric filling the width of the slot is decreased in order to increase the cutoff of the even mode (as was done for a single-layer IDG).

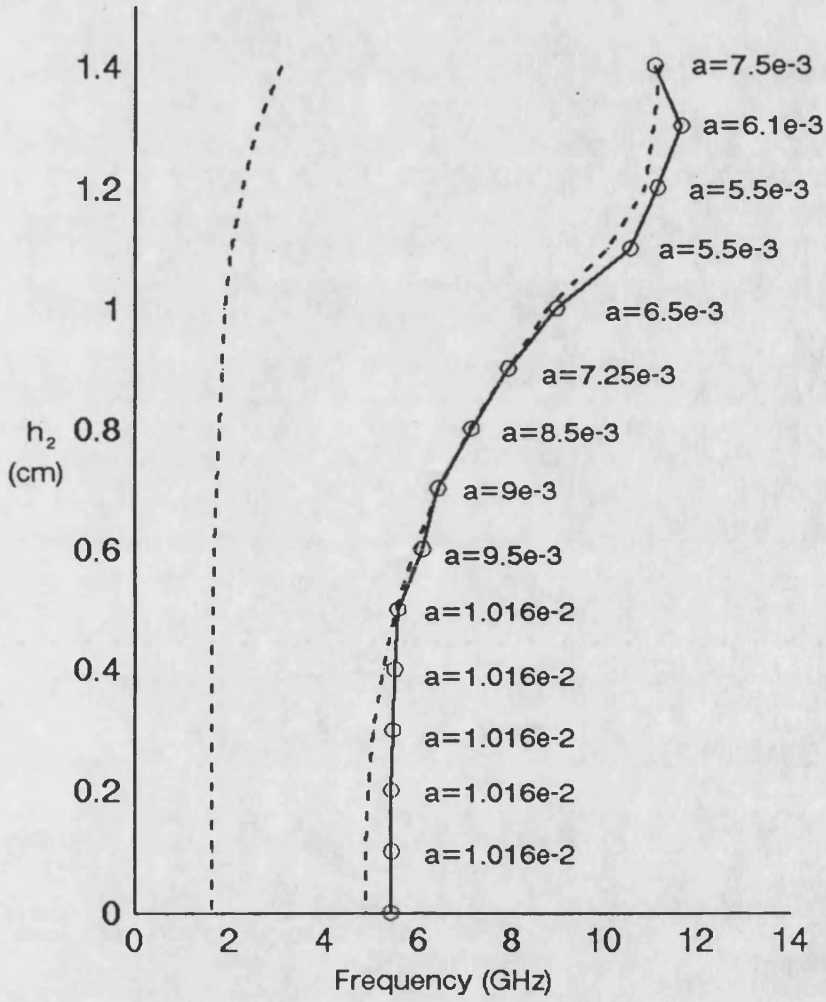

Figure 3.8 Cutoff of first three modes in two-layer IDG. Same dimensions as Figure 3.7 but slot width is varied in order to optimise bandwidth. (All dimensions in metres unless otherwise specified).

In Figure 3.9, the monomode bandwidth is plotted as a function of dielectric filling for the IDG dimensions of Figure of 3.8 and it can be seen that the optimum monomode bandwidth increases significantly from 50% in a single layer/ IDG to 66% in a two-layer IDG. Figure 3.9 thus shows that significant improvement in monomode bandwidth is achievable by choosing an appropriate dielectric filling and cross sectional dimensions in a two-layer IDG.

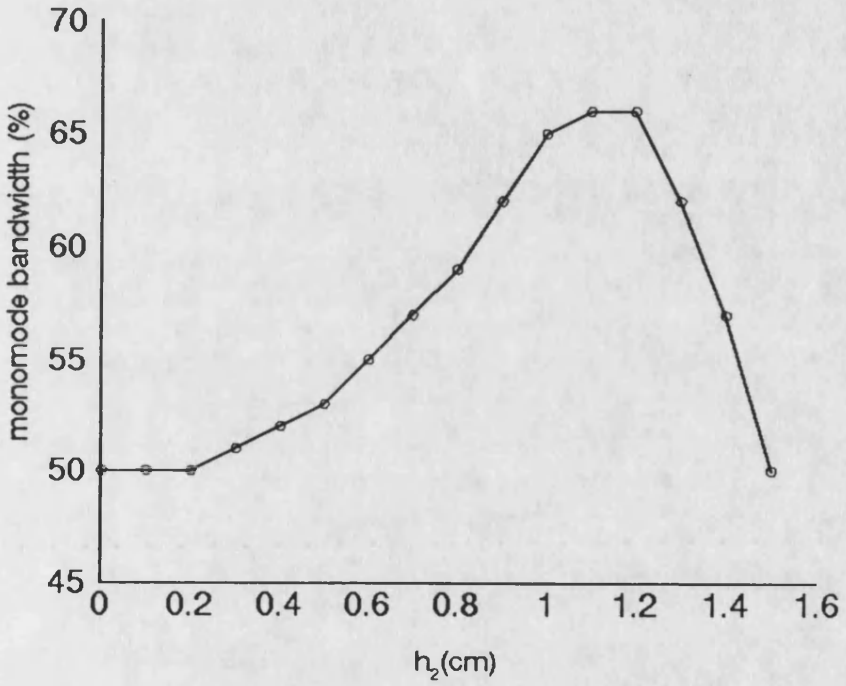

Figure 3.9 Monomode bandwidth calculated from Figure 3.8

The dispersion characteristics for one of the optimal dimensions given in Figure 3.8 are presented in Figure 3.10. We expect dispersion in IDG to vary linearly with the scaling of dimensions and in Figure 3.11, the

dimensions of Figure 3.10 are scaled down by a factor of 2 in order to achieve a cutoff frequency of 5 GHz for the fundamental mode.

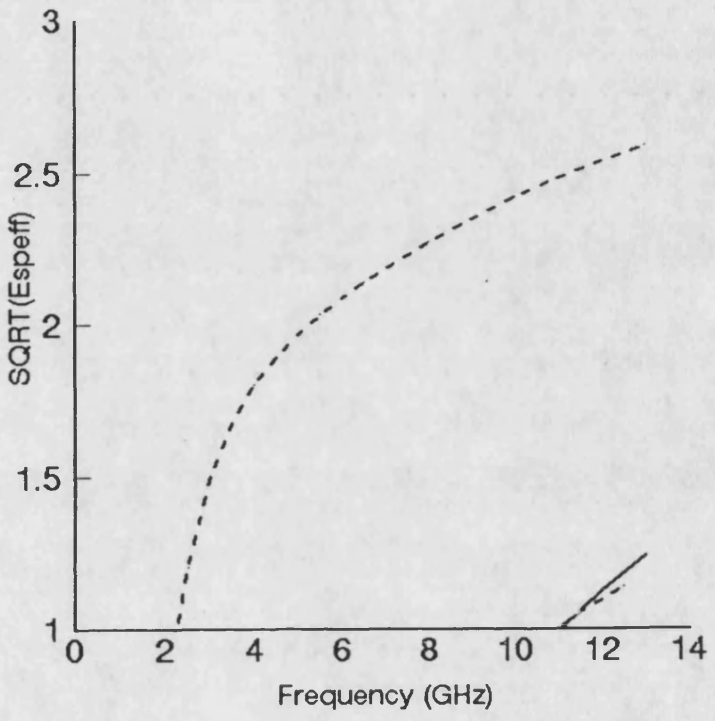

Figure 3.10 Dispersion characteristics of two-layer IDG with the dimensions chosen to give optimum bandwidth. a=5.5e-2, h=1.524e-2, h2=1.2e-2, ϵ_{r1}=2.04 ϵ_{r2}=10.2 (all dimensions in metres).

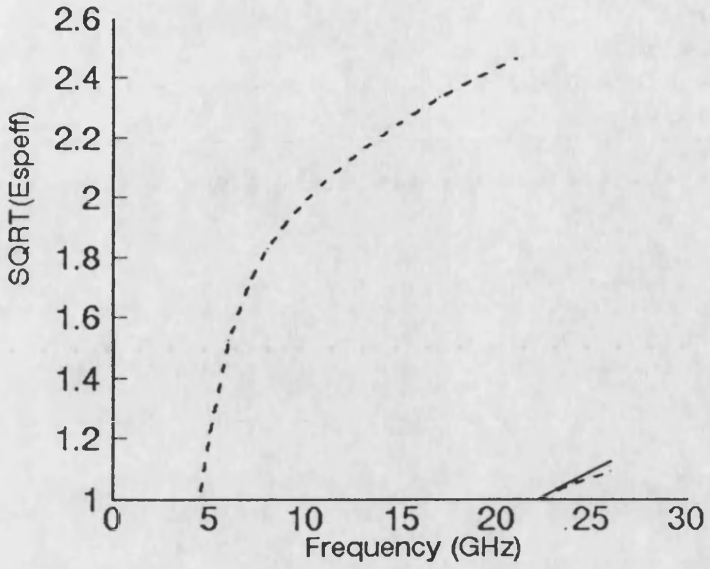

Figure 3.11 Dispersion characteristics of two-layer IDG. Dimensions of Figure 3.10 scaled down by a factor of 2.

FIGURE 3.7 COMPARISON WITH MEASURED RESULTS

Experimental measurement of dispersion was carried out for a number of different cross sections of IDG, including partially filled and two-layer IDG in order to assess the accuracy of the analysis presented in the previous sections.

The experiment was designed using the resonant section technique. A section of the IDG was terminated with short circuits at both ends (Figure 3.12). Energy was then coupled into the structure by inserting magnetic probes

through the short circuits resulting in a weakly coupling mechanism (transmission loss < 25 dB). Thus the section would be virtually short-circuited at both ends. This imposes the condition that the electric field components tangential to the short circuits and the magnetic field components normal to the short circuits be zero This is only satisfied for specific waveguide wavelengths such that

$$\frac{n\lambda_g}{2}=L \tag{3.31}$$

where λ_g is the wavelength of the guided wave,
L is the length of the section,
n is an integer,

Thus energy will couple into the section at specific frequencies corresponding to the wavelengths that satisfy (3.31). The transmission response over a range of frequencies was obtained using a HP8510A analyzer allowing the resonant frequencies to be measured.

The parity of the excited fields can be controlled by changing the orientation of the magnetic probes, provided the latter are placed over the centre of the guide (x=0). For the odd parity modes H_x is zero at the centre of the IDG line, while H_y is finite. Therefore, vertically oriented probes placed at the line centre will only excite even parity modes. Similarly, for the even parity modes, H_y is zero at the guide centre and H_x is finite, and

horizontally orientated probes will only excite odd parity modes. It is important, however, that the probes be positioned at the centre of the guide as accurately as possible and that the orientation of the probe be kept either horizontal or vertical. Otherwise, both parities would be excited at the same time making isolation of the resonances for each parity difficult. The insertion loss for a resonant section of IDG for horizontal and vertical orientation of the magnetic probes is shown in Figure 3.13 illustrating the ability to separately excite either even or odd parity modes.

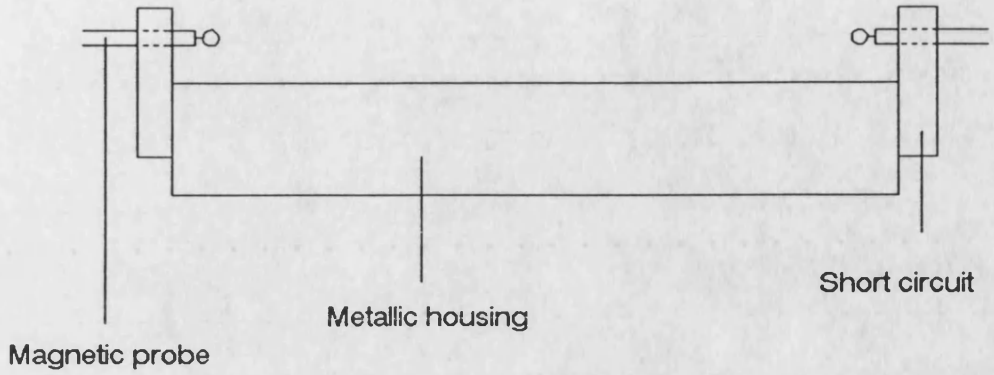

(Side view)

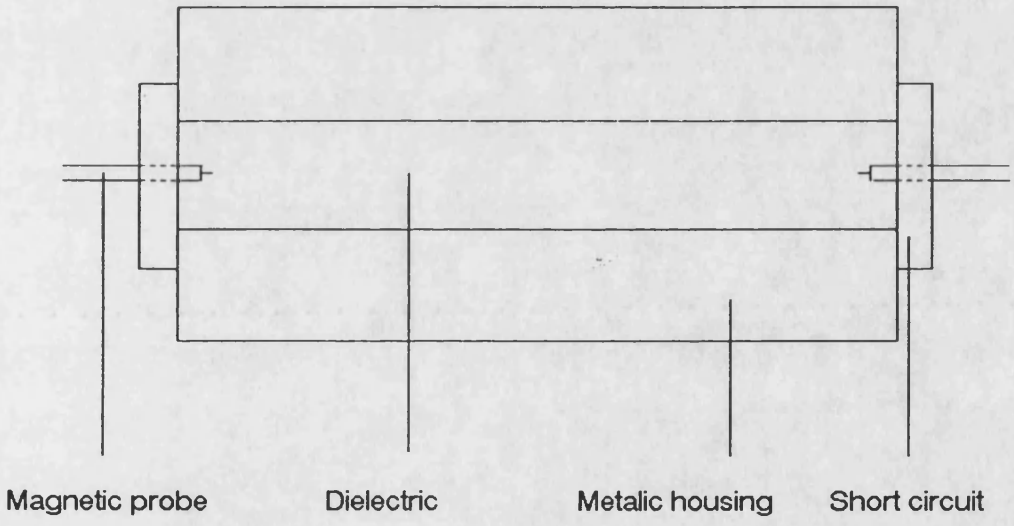

(Top view)

Figure 3.12 A view of experimental setup for measuring dispersion characteristics of IDG

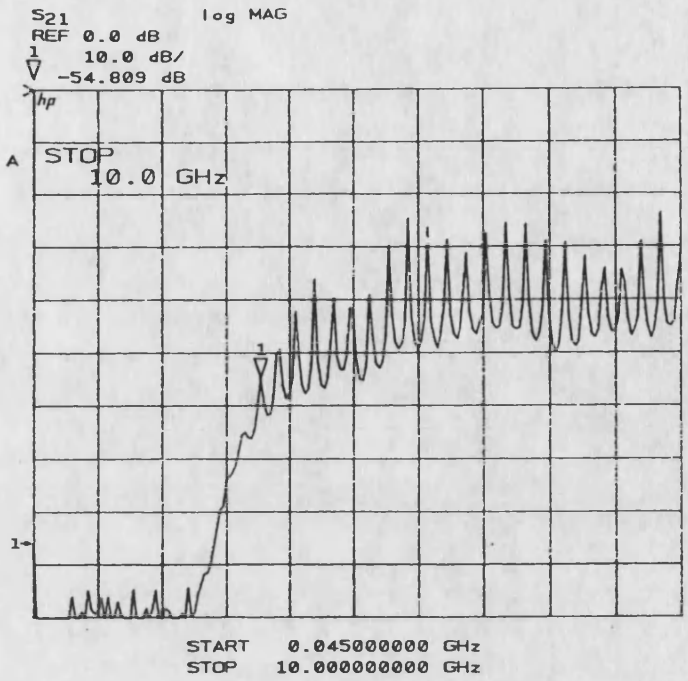

Fundamental (odd mode)

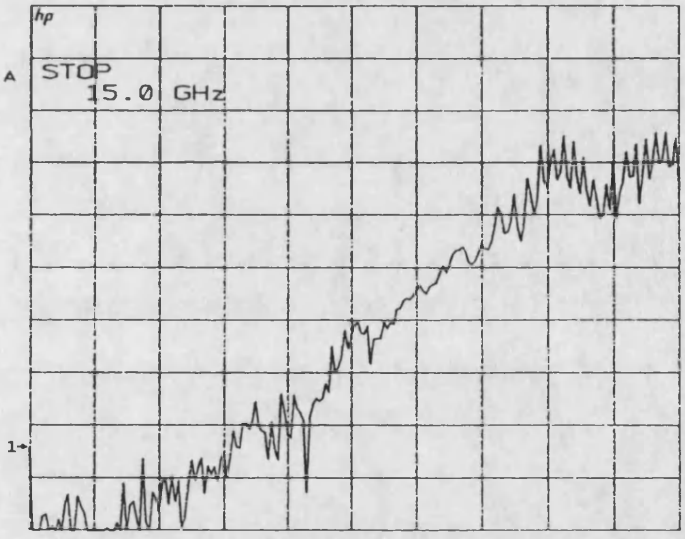

First higher order (even mode)

Figure 3.13 Measured Insertion loss of a resonant section of two-layer IDG (h=1.524e-2, a=1.016e-2, h_2=1.426e-2, ϵ_{r1}=10.2, ϵ_{r1}=2.04) - measured on a HP8510A network analyzer.

In order to determine the wavelength of the guided wave, it is important to know the integer n in (3.31). This was done as follows, the source was tuned to a specific resonant frequency. The wavelength of the guided wave, λ_g, ,as well as n , for that resonant frequency where then measured with a field probe. Several values of the guided wavelength were measured along the section.

Table 3.1 gives, values of λ_g that were measured with a field probe, at a resonant frequency of the fundamental (odd) mode, and a resonant frequency of the first higher order (even) mode (Cross sectional geometry of Figure 3.13).

Successive resonances correspond to successive values of n. Thus, having accurately determined λ_g and n for one resonant frequency, the dispersion curve was calculated as λ_0/λ_g for the rest of the resonant frequencies. The dispersion characteristics for the cross sectional geometry of Figure 3.13 are given in Figure 3.16.

Fundamental (Odd) mode		First higher order (Even mode)	
i^{th} value	λ_g (cm)	i^{th} value	λ_g (cm)
1	1.36	1	1.14
2	1.40	2	1.15
3	1.41	3	1.12
4	1.34	4	1.10
5	1.37	5	1.17
6	1.35	6	1.15
7	1.36	7	1.12
8	1.39	8	1.14
9	1.38	9	1.15
10	1.33	10	1.13
λ_g	1.37 ± 0.03	λ_g	1.14 ± 0.02
λ_0/λ_g:	1.37 ± 0.03	λ_0/λ_g:	1.07 ± 0.02

Table 3.1 Values of λ_g measured with a field probe, for the fundamental (odd) mode (at the resonant frequency of 7.95 GHz) and the first higher order (even) mode (at the resonant frequency of 12.24 GHz) - (cross sectional geometry of Figure 3.13).

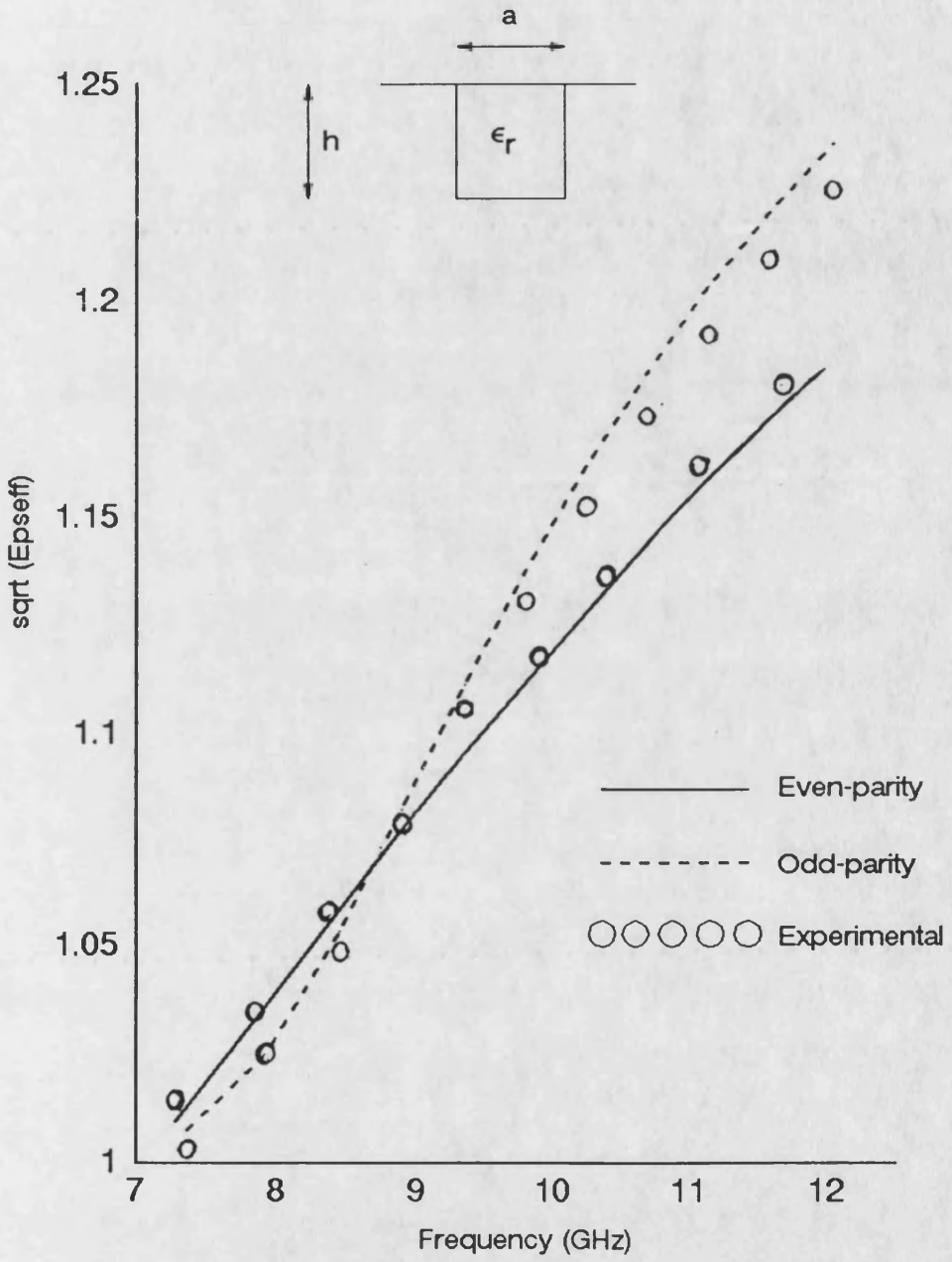

Figure 3.14 Dispersion characteristics of IDG. a=2.286e-2, h=1.016e-2, ϵ_r=2.04 (All dimensions in metres).

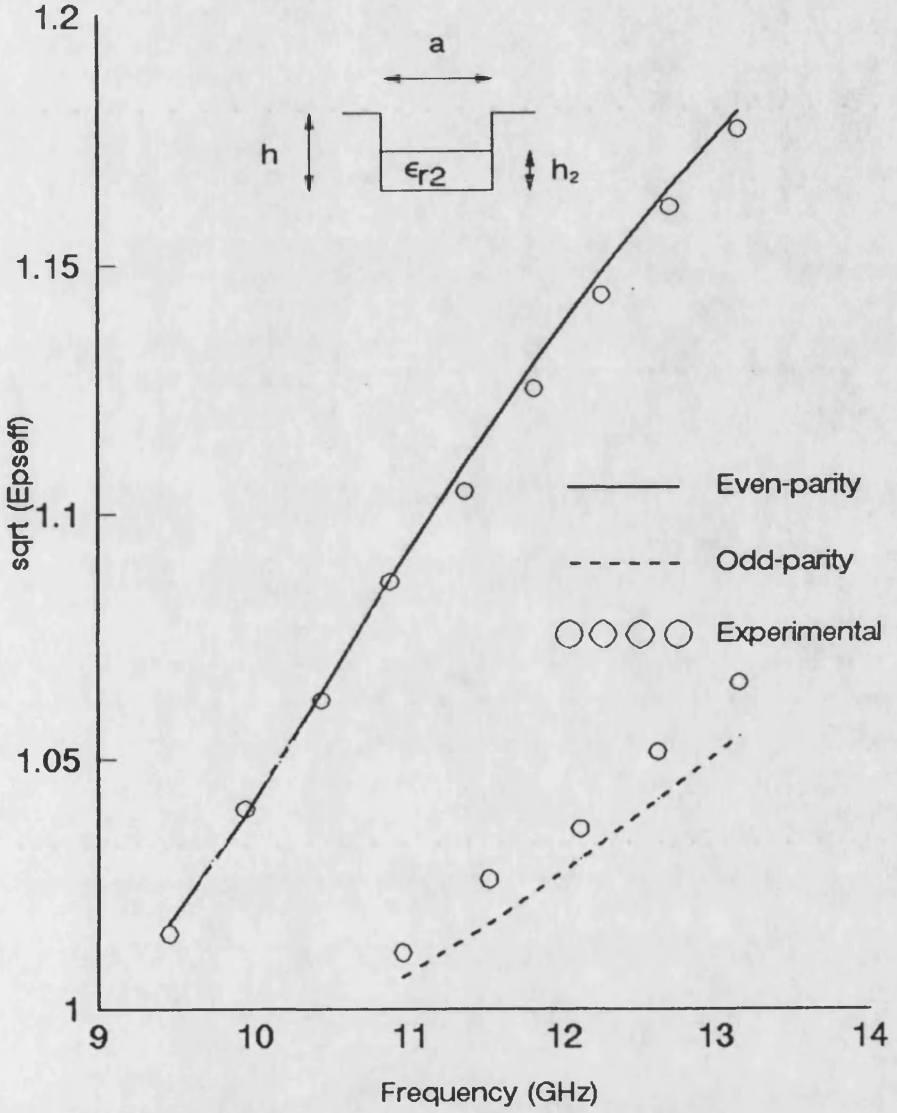

Figure 3.15 Dispersion characteristics of partially filled IDG. a=2.286e-2, h=1.016e-2, h2=7e-3, ϵ_{r2}=2.04 (all dimensions in metres).

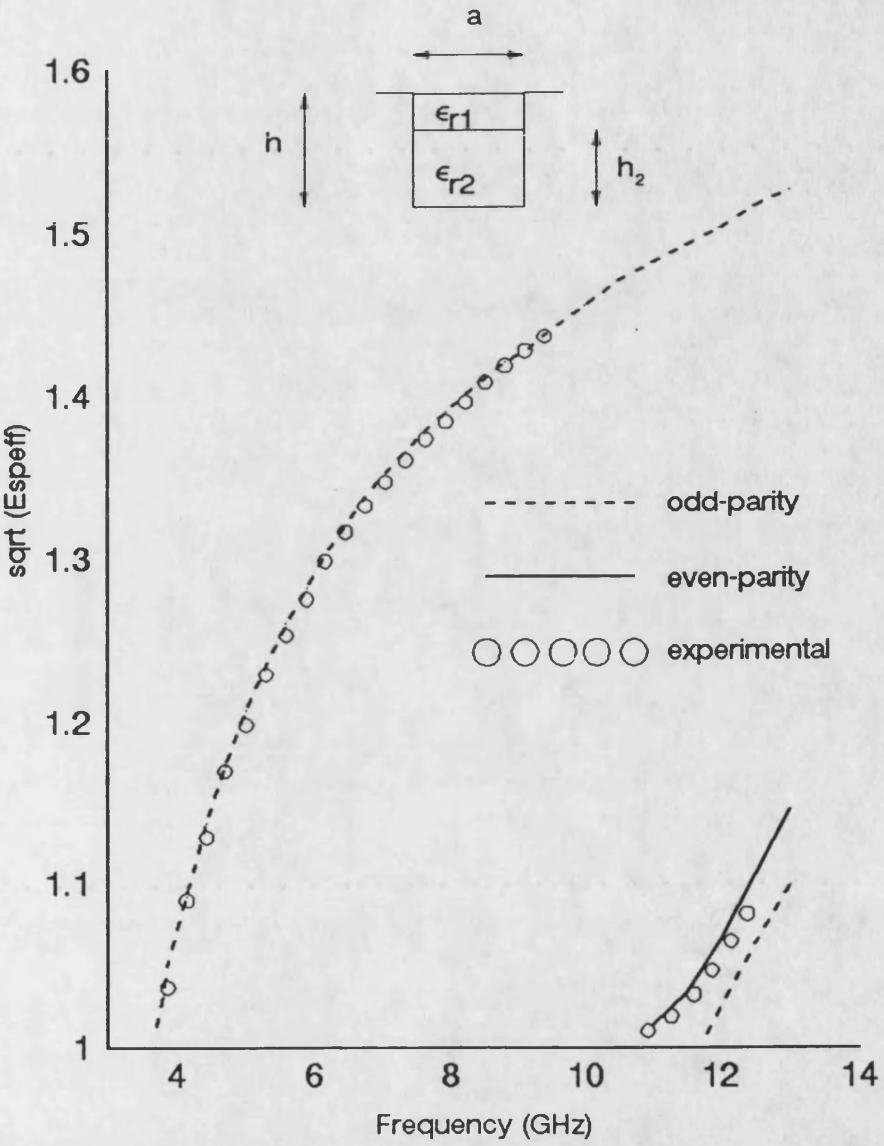

Figure 3.16 Dispersion characteristics of two-layer IDG. a=1.016e-2, h=1.524e-2, h_2=1.46e-2, ϵ_{r1}=10.2, ϵ_{r2}=2.04 (All dimensions in metres).

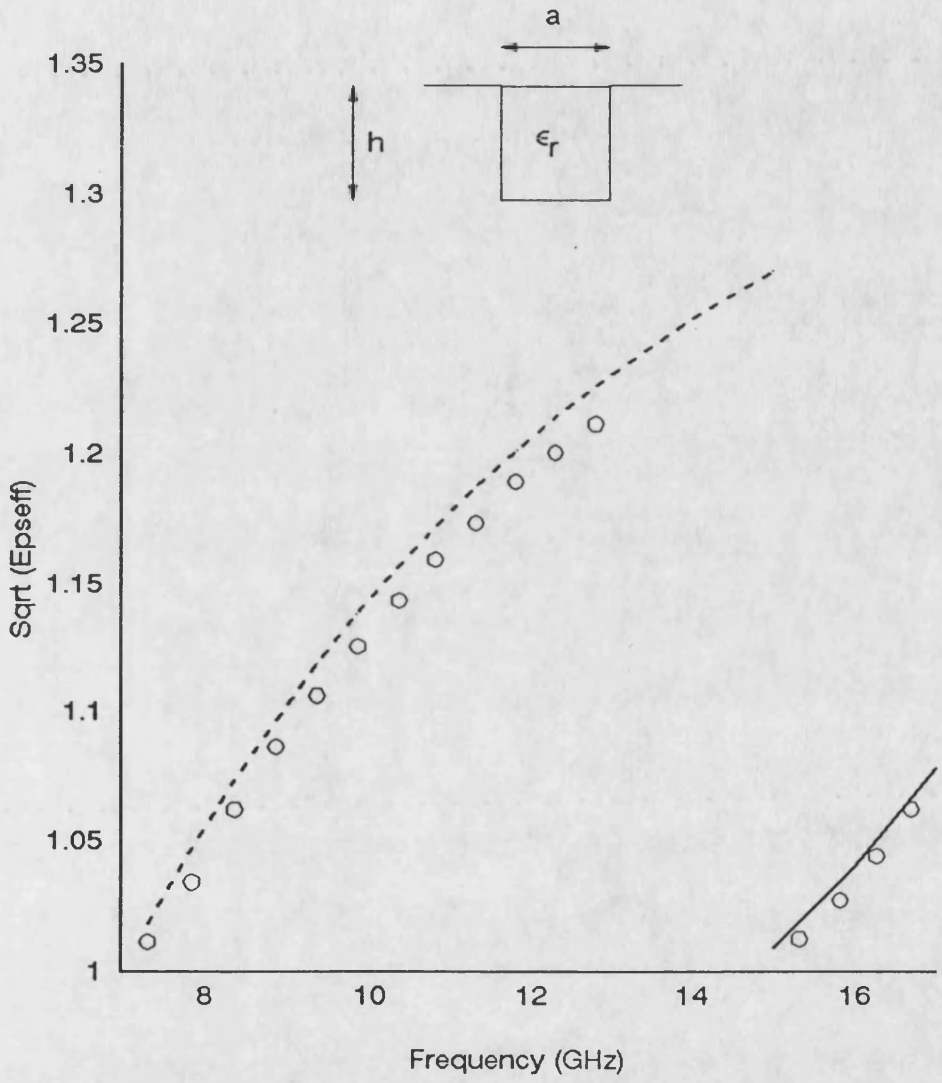

Figure 3.17 Dispersion characteristics of single-layer IDG. a=1.016e-2, h=1.016e-2, ϵ_r=2.04 (all dimensions in metres)

The results given in Figures (3.14-3.17) clearly show very good agreement between the theoretical and experimental values of dispersion that were obtained for the various cross sectional geometries.

The magnitude of the field components over the guide cross section, are plotted in Figures 3.18 and 3.19. The isometric plots presented are those of the odd mode and the even mode of the cross sectional geometry of Figure 3.14. It is noted from the field plots that, as mentioned in section 3.7, H_y is zero at the guide centre for the even mode and H_x is zero for the odd mode. It is noted that each plot has been individually scaled by the computer plotting routine and so there is no amplitude correlation between the various plots.

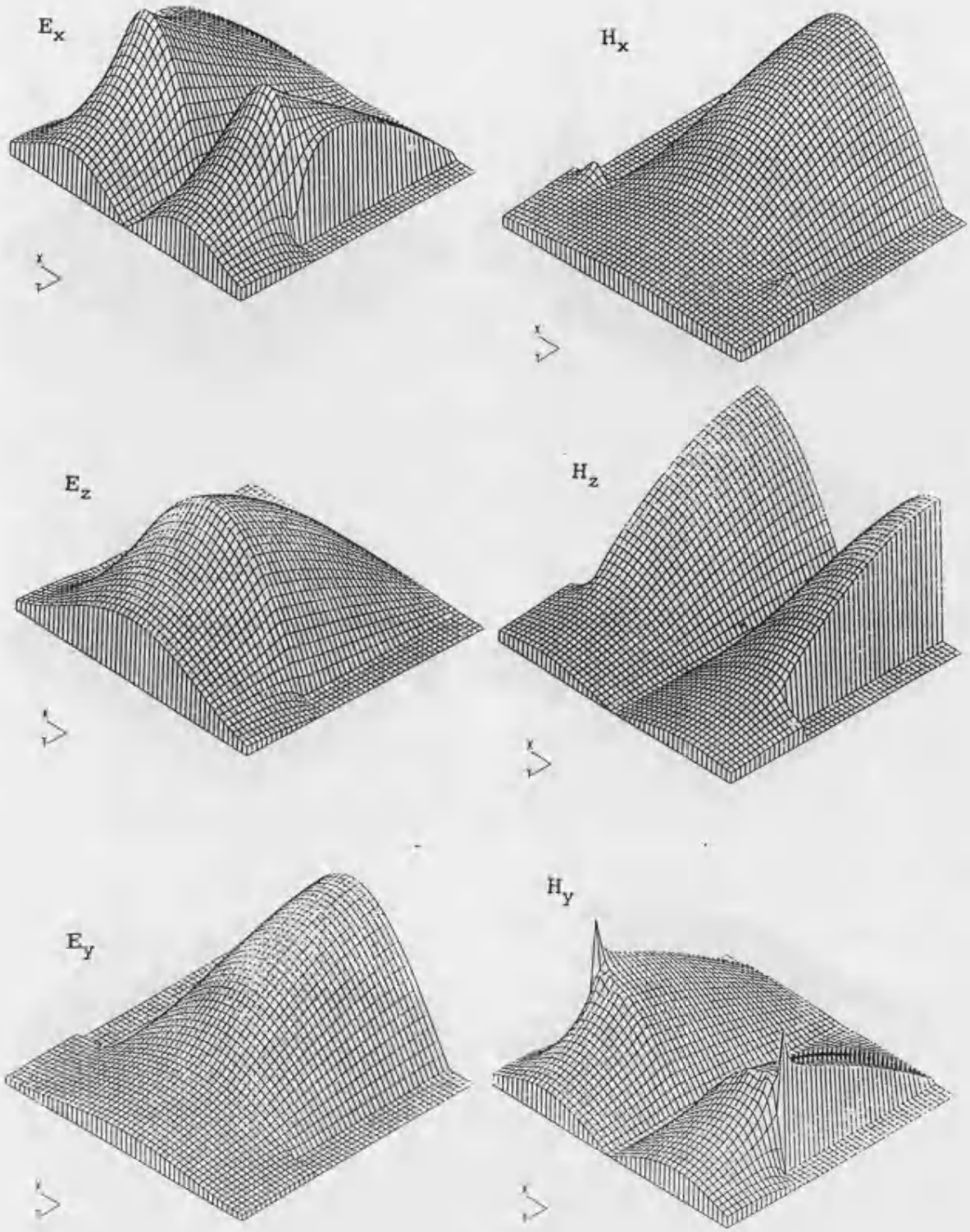

Figure 3.18 Magnitude of the field components for the even mode of Figure 3.14 plotted over the cross section of the guide (Frequency=10 GHz).

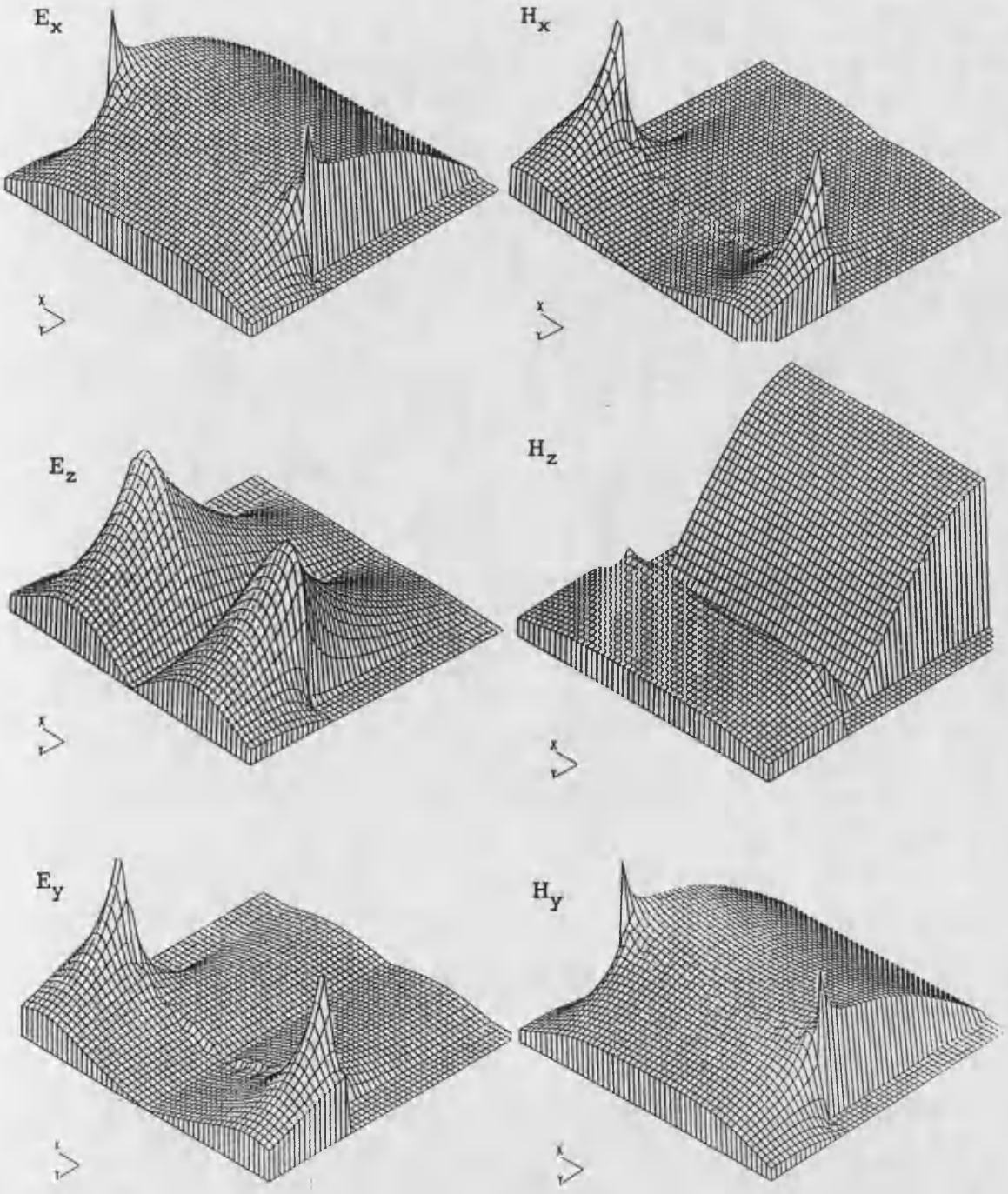

Figure 3.19 Magnitude of the field components for the even mode of Figure 3.14 plotted over the cross section of the guide (Frequency=10 GHz).

3.8 CONVERGENCE OF SOLUTIONS FOR THE FUNDAMENTAL MODE

The convergence of solutions for the fundamental mode, as a function of the number of basis functions used in (3.22), for a multilayered IDG is given in Table 3.2.

It can be seen from the table that convergence to 3 significant figures is achieved using just two sets of basis functions for each of the tangential electric field components at the slot-air interface.

	λ_0/λ_g as a function of the number of basis functions		
Frequency (GHz)	1 by 1	2 by 2	3 by 3
4	1.0947	1.0701	1.0686
6	1.3213	1.2930	1.2913
8	1.4274	1.3939	1.3913
10	1.5010	1.4569	1.4544
12	1.5746	1.5068	1.5034

Table 3.2 Convergence of solutions for fundamental mode of IDG with two dielectric layers in the slot, a=1.016e-2 (m), h=1.524e-2 (m), h_2=1.46e-2 (m), ϵ_{r1}=10.2, ϵ_{r2}=2.04.

CONCLUSION

The Inset Dielectric Guide has been rigorously analyzed, for the case where several dielectric layers may exist in the slot. Experimental measurements of dispersion have been presented for several geometries and these show very good agreement with the theoretical results. Convergence to the solutions of the dispersion relation is fast, thus highlighting the efficiency of the method.

Bandwidth control in IDG has been investigated. It has been shown that wide monomode bandwidth can be achieved in IDG through the use of two dielectric layers in the slot and by suitable choice of cross-sectional dimensions and dielectric filling. This wide monomode bandwidth, however, is achieved at the cost of a more complicated manufacturing process.

REFERENCES

1. S. J. Hedges, "The Analysis of the Inset Dielectric Guide by Transverse Resonance Diffraction", PhD Thesis, Bath University, Bath, 1987.

2. T. Rozzi, R. De Leo, L. Ma and A. Morini, "Equivalent Network of Transverse Dipoles on Inset Dielectric Guide : Application to Linear Arrays", IEEE Trans. Antenna Prop., 1989.

3. T. Rozzi, R. De Leo, and A. Morini, "Analysis of the Microstrip-Loaded Inset Dielectric Waveguide", IEEE MTT-S, 1989, pp. 923-925.

4. L. Ma, S.R. Pennock and T. Rozzi, "Linear Arrays Realised in IDG", Paper 6, IEE Colloquium "Components for Novel Transmission Lines", London 26th March 1990 (Digest No. 1990/048).

5. T. Rozzi and S.J. Hedges, "Rigorous Analysis and Network Modelling of the Inset Dielectric Guide", IEEE Trans. Microwave Theory Tech., Vol. MTT-35, 1987, pp. 823-833.

6. S. B. Cohn, "Properties of the Ridge Waveguide", Proc. IRE, Vol 35, 1947, pp. 783-788.

7. R. E. Collin, "Field Theory of Guided Waves", McGraw-Hill, 1960.

8. I.S. Gradshteyn and I.M. Ryshik, "Tables of Integrals, series and products", New York, Academic Press, 1965, p.827.

APPENDIX 3A

1. Normalisation of basis function

The basis functions (3.26) must be normalised so that

$$\int_0^{a/2} f_m(2x/a)\, f_n(2x/a)\, dx=\delta_{nm} \qquad \text{(A3.1)}$$

This is achieved provided that

$$N_m^2=\int_0^{a/2} w(2x/a)\, (C_m^{1/6}(2x/a))\, dx \qquad \text{(A3.2)}$$

From the mathematical tables [1]:

$$\int_{-1}^{1} (1-t^2)^{(\nu-1/2)}\, (C_m^{\nu}(t))^2 dt=\frac{\pi 2^{(1-2\nu)}\Gamma(2\nu+m)}{m!\,(m+\nu)\,(\Gamma(\nu))^2} \qquad \text{(A3.3)}$$

Substituting $x=\frac{a}{2}t$ in (3A.3) gives:

$$2\int_0^{a/2} (1-(2x/a)^2)^{-1/3}\, (C_m^{-1/6}(2x/a))^2 \frac{2}{a}\, dx=\frac{\pi 2^{2/3}\Gamma(m+1/3)}{m!\,(m+1/6)\,(\Gamma(1/6))^2} \qquad \text{(3A.4)}$$

from which the normalisation factor N_m is recovered as

$$N_m^2=\frac{a\pi 2^{-4/3}\Gamma(m+1/3)}{m!\,(m+1/6)\,((\Gamma(1/6))^2} \qquad \text{(3A.5)}$$

2. Evalution of inner products of basis functions

In order to evaluate the inner products (3.27a, 3.29), the

following coefficients must be evaluated

$$I_m(n) = \int_0^{a/2} f_{2m}(2x/a)\cos\left(\frac{n\pi}{a}\right) dx \qquad (m=0,1,2) \tag{3A.6}$$

From the tables [1]:

$$\int_0^1 (1-t)^{(\nu-1/2)} C_{2m}^{\nu} \cos(bt)\ dt = \frac{(-1)^m \pi\Gamma(2m+2\nu)}{(2m)!\Gamma(\nu)(2b)^{\nu}} J_{(\nu+2m)}(b) \tag{3A.7}$$

Substituting $x=\frac{a}{2}t$, and $\nu=1/6$ into (3A.7) gives:

$$\int_0^{a/2} (1-(2x/a)^2)^{-1/3} C_{2m}^{1/6} \cos(2b/a)\, x\frac{2}{a}\, dx = \frac{(-1)^m\pi\ \Gamma(2m+1/3) J_{2m+1/6}(b)}{(2m)!\ \Gamma(1/6)(2b)^{1/6}} \tag{3A.8}$$

Comparing (3A.6) with (3A.8) gives:

$$\begin{aligned} I_m(n) &= \frac{1}{N_{2m}}\frac{a}{2}\frac{(-1)^m\pi\Gamma(2m+1/2)}{(2m)!\Gamma(1/6)(n\pi)^{1/6}} J_{2m+1/6}\left(\frac{n\pi}{2}\right) && (n>0) \\ &= \frac{1}{N_0}\frac{a}{2}\frac{\pi\Gamma(1/3)}{\Gamma(1/6)2^{5/6}\Gamma(1+1/6)} && (n=0, m=0) \\ &= 0 && (n=0, m=1,2) \end{aligned} \tag{3A.9}$$

References

1. I.S. Gradshteyn and I.M. Ryshik, "Tables of Integrals, series and products", New York, Academic Press, 1965.

CHAPTER 4

ANALYSIS OF THE MICROSTRIP LOADED INSET DIELECTRIC GUIDE

4.1 INTRODUCTION

Microstrip loaded inset dielectric guide (MLIDG) (Figure 4.1) is a transmission media which has found useful application in the design of leaky wave dipole arrays where longitudinal dipoles are placed on an IDG operating under LSM polarization [1,2]. MLIDG may also be useful as a transmission line media alternative to microstrip, where the presence of the slot walls may be used to control coupling in a multiconductor circuit (Figure 4.2).

In the present chapter a rigorous analysis of MLIDG is presented for the case where a single dielectric layer or multiple dielectric layers may be present in the slot.

In order to realise complete MLIDG array antennas or MLIDG circuits, it is necessary to determine the characteristic impedance of MLIDG. Results for the characteristic impedance of single-layered MLIDG are presented, where the latter was computed using the commonly adopted power-current definition.

Experimental measurements of dispersion are presented for the fundamental and first higher order mode for some example geometries, showing good agreement with the computed results. Experimental measurements of the characteristic impedance are presented, also showing good agreement with computed results.

The variation of monomode bandwidth and characteristic impedance with circuit dimensions and strip width is investigated.

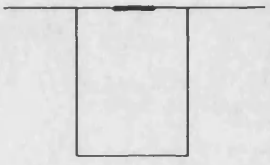

Figure 4.1 Cross section of MLIDG

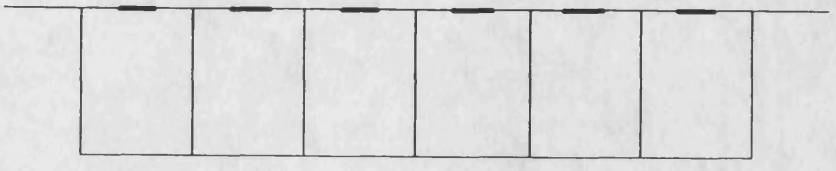

Figure 4.2 MLIDG in a multiconductor circuit

4.2 ANALYSIS OF MULTILAYERED MLIDG

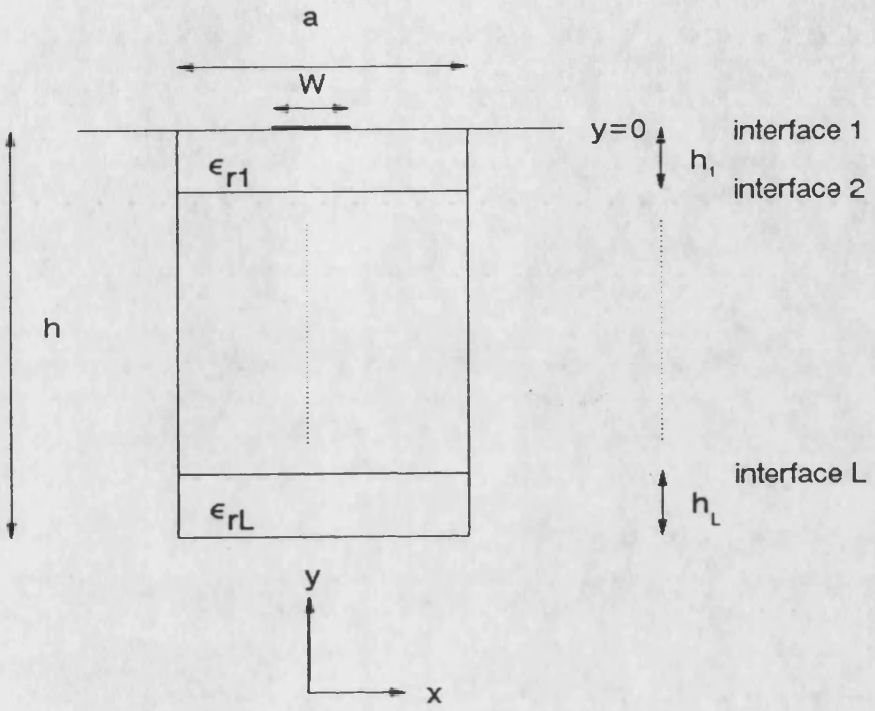

Figure 4.3 Cross section of multilayered MLIDG

Figure 4.3 gives the cross section of a multilayered MLIDG structure. The choice of potential functions for the air region and for the dielectric layers within the slot is identical to that used for the IDG (section 3.1) and thus the formulation of the admittance operators is unchanged and will not be repeated here.

The presence of the conducting strip, however, modifies the boundary conditions at the interface $y=0$.

For the case of MLIDG, the boundary conditions for the tangential electric and magnetic fields at $y=0$ are:

1. The tangential electric fields are continuous at the interface, giving:

$$E_z(x,0^+)=E_z(x,0^-)=E_z(x,0)$$
$$E_x(x,0^+)=E_x(x,0^-)=E_x(x,0) \qquad (4.1)$$

2. The tangential electric fields are zero over the conducting strip:

$$E_x(x,0)=E_z(x,0)=0 \qquad (|x|<w/2) \qquad (4.2)$$

3. While for the magnetic fields

$$H_z(x,0^+)-H_z(x,0^-)=I_x(x)$$
$$H_x(x,0^+)-H_x(x,0^-)=-I_z(x) \qquad (4.4)$$

where $I_x(x)$, $I_z(x)$ are the x-directed and z-directed current components on the strip respectively.

Applying the boundary conditions on the tangential magnetic fields and expressing the latter in terms of the tangential electric fields then gives the dispersion relation

$$\begin{bmatrix} \tilde{Y}_{11} & \tilde{Y}_{12} \\ \tilde{Y}_{21} & \tilde{Y}_{22} \end{bmatrix} \begin{bmatrix} E_x(x,0) \\ E_z(x,0) \end{bmatrix} = \begin{bmatrix} I_x(x) \\ I_z(x) \end{bmatrix} \qquad (4.4)$$

where the admittance operators are given by the expressions (3.16 - 3.20).

4.3 APPLICATION OF THE GALERKIN PROCEDURE

The dispersion relation (4.4) is solved by following the same procedure that was applied for solving the dispersion relation of IDG (section 3.4). The tangential electric field in (4.4) are first represented in terms of a set of basis functions:

$$E_x(x,0)=\sum_{i=0}^{\infty} X_i E_{xi}(x) \tag{4.5a}$$

$$E_z(x,0)=\sum_{i=0}^{\infty} Z_i E_{zi}(x) \tag{4.5b}$$

The Galerkin procedure is then completed by taking the inner product of the basis functions with both sides of the dispersion relation giving:

$$\begin{bmatrix} \langle E_{x0}, \tilde{Y}_{11}E_{x0}\rangle & \cdots & \langle E_{x0}, \tilde{Y}_{11}E_{xn}\rangle & \langle E_{x0}, \tilde{Y}_{12}E_{z0}\rangle & \cdots & \langle E_{x0}, \tilde{Y}_{12}E_{zm}\rangle \\ \vdots & & \vdots & \vdots & & \vdots \\ \langle E_{xn}, \tilde{Y}_{11}E_{x0}\rangle & \cdots & \langle E_{xn}, \tilde{Y}_{11}E_{xn}\rangle & \langle E_{xn}, \tilde{Y}_{12}E_{z0}\rangle & \cdots & \langle E_{xn}, \tilde{Y}_{12}E_{zn}\rangle \\ \langle E_{z0}, \tilde{Y}_{21}E_{x0}\rangle & \cdots & \langle E_{z0}, \tilde{Y}_{21}E_{xn}\rangle & \langle E_{z0}, \tilde{Y}_{22}E_{z0}\rangle & \cdots & \langle E_{z0}, \tilde{Y}_{22}E_{zm}\rangle \\ \vdots & & \vdots & \vdots & & \vdots \\ \langle E_{zn}, \tilde{Y}_{21}E_{x0}\rangle & \cdots & \langle E_{zn}, \tilde{Y}_{21}E_{xn}\rangle & \langle E_{zn}, \tilde{Y}_{22}E_{z0}\rangle & \cdots & \langle E_{zn}, \tilde{Y}_{22}E_{z0}\rangle \end{bmatrix} \begin{bmatrix} X_0 \\ \vdots \\ X_n \\ Z_0 \\ \vdots \\ Z_m \end{bmatrix} = \underline{0} \tag{4.6}$$

Note that the RHS of (4.6) is reduced to zero since the tangential electric fields are zero where the current in (4.4) is non-zero and vice-versa. A search for the zeros of the determinant of (4.6) then gives the required propagation coefficients. By comparing (4.6) with the dispersion relation obtained for IDG in (3.24), it can be seen that the two expressions are identical. However, the

basis function in (4.6) and (3.24) obey different boundary conditions where the former must be chosen to be zero over the conducting strip

4.3.1 CHOICE OF BASIS FUNCTIONS

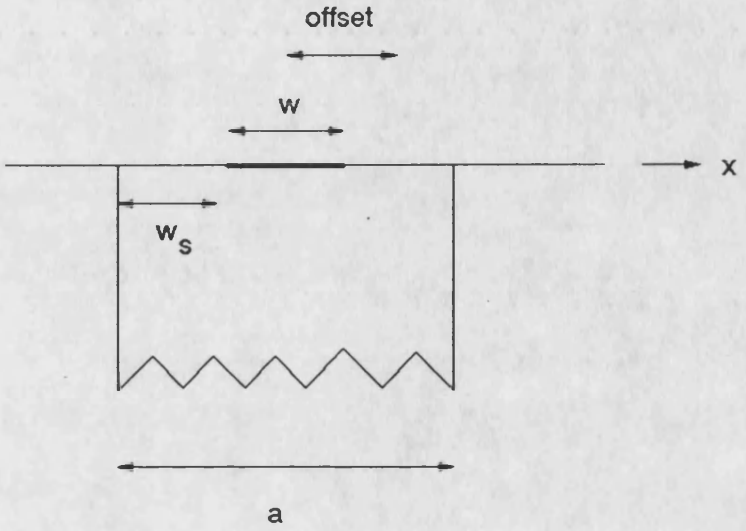

Figure 4.4 Cross section of MLIDG

In order to achieve rapid convergence to the solution of (4.6), using as few a number of basis functions as possible, it is important to introduce a set of basis functions that will closely model the actual distribution of the tangential electric fields at the interface. The metallic corner at $x=\pm a/2$ and the edges of the conducting strip at $x=\pm w/2$ introduce singularities in the field distribution. The singularities are of the type $r^{-1/3}$ at the metallic corners and $r^{-1/2}$ at the strip edges [3]. In order to model this behaviour, the following weight function is introduced into the basis functions:

$$W(2t/w_s)=\frac{1}{(1+2t/w_s)^{1/2}}\cdot\frac{1}{(1-2t/w_s)^{1/3}} \qquad (4.7)$$

where (see Figure 4.4)

$$w_s=a/2-w/2 \qquad (4.8a)$$

$$t=x-offset \qquad (4.8b)$$

and

$$offset=w/2+w_s/2 \qquad (4.8c)$$

The function (4.7) introduces into the basis functions a singularity of the order -1/2 at the edge of the strip and a singularity of the order -1/3 at the 90° corner of the slot.

A set of functions which are orthogonal with respect to the weight function (4.7) are the Jacobi polynomials $P_n^{(\alpha,\beta)}(t)$ with $\alpha=-1/2$ and $\beta=-1/3$ [4]. Thus the basis functions are defined as

$$f_m(2t/w_s)=\frac{1}{N_m}\frac{P_m^{-1/2,-1/3}(2t/w_s)}{W(2t/w_s)} \qquad |t|<w_s/2$$
$$=0 \qquad otherwise \qquad (4.9)$$

where t, w_s are given by (4.8). The basis functions (4.9) are used to represent $E_{xi}(x)$ and $\partial_x E_{zi}(x)$ which have the same singular bahaviour as the basis functions (see section 2.3.5 and 3.4.1).

The normalization factor N_m, together with the inner products of the basis functions (4.9) with $\phi_{en,hn}(x)$ and $\phi_{e,h}(\rho,x)$ which must be computed in (4.6) are given in Appendix 4A and Appendix 4B respectively.

4.4 CHARACTERISTIC IMPEDANCE FOR SINGLE-LAYER MLIDG

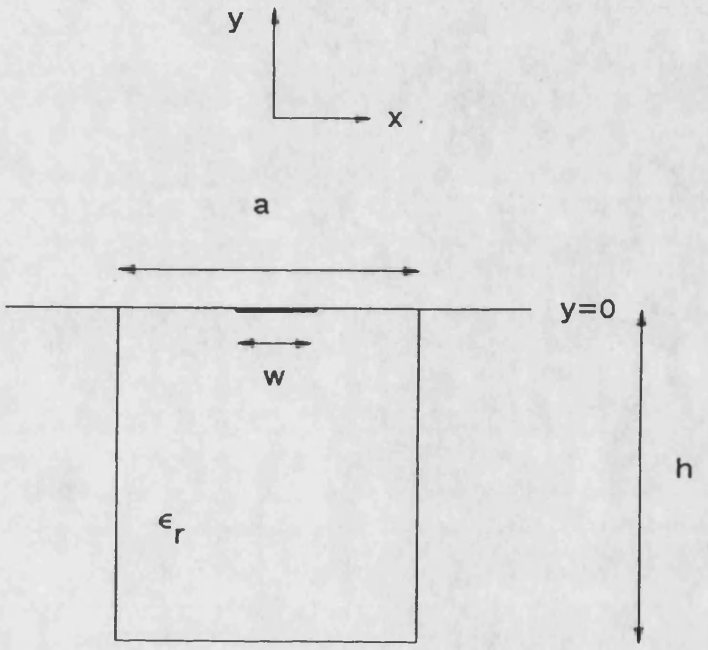

Figure 4.5 Cross section of single-layered MLIDG

Several different definitions of characteristic impedance have been used in the literature [5-7]. A commonly used definition of the characteristic impedance for microstrip, however, is the power-current definition where the characteristic impedance is defined as

$$Z_0 = \frac{P}{\left[\int_0^{w/2} I_z(x)\,dx\right]^2} \qquad (4.10)$$

Where P is the total power flow along the guide, and $I_z(x)$ is the longitudinal (z-directed) current on the strip. This definition was adopted as the definition of characteristic impedance for MLIDG.

The total power flow along the guide, P, can be evaluated as the time-averaged Poynting vector over the transverse guide cross section which is given by

$$P=\frac{1}{2}\int_{cross\text{-}section} RE(E \wedge H^*)\cdot\hat{z}\, da \qquad (4.11)$$

The integral in (4.11) can be split into two parts: an integral over the slot and an integral over the air region above the slot. Thus

$$\begin{aligned} P&=P_a+P_s \\ &=\frac{1}{2}\int_{-h}^{0}\int_{0}^{a/2} Re\left\{ E_x(x,y)\,H_y^*(x,y)-H_x^*(x,y)\,E_y(x,y)\right\} dxdy \\ &+\frac{1}{2}\int_{0}^{\infty}\int_{0}^{a/2} Re\left\{ E_x(x,y)\,H_y^*(x,y)-H_x^*(x,y)\,E_y(x,y)\right\} dxdy \end{aligned} \qquad (4.12)$$

Note that since, due to symmetry, the x-dependence of the potential functions: $\phi_{en,hn}(x)$ and $\phi_{e,h}(\rho,x)$ have been normalised over the half space $0>x>a/2$, the integrals in (4.11) and (4.12) were also evaluated between these limits for the x-dimension.

4.4.1 The Total Power Flow Along the Guide

Since there is only a single dielectric layer in the slot, the expressions for the fields within the slot simplify to:

$$E_x(x,y) = \sum_{n=1,3..}^{\infty} E_{xn}^1 \phi_{hn}(x) \frac{\sin k_{1n}(y+h)}{\sin k_{1n} h} \tag{4.13a}$$

$$E_y(x,y) = \sum_{n=1,3..}^{\infty} E_{yn}^1 \phi_{en}(x) \frac{\cos k_{1n}(y+h)}{\cos k_{1n} h} \tag{4.13b}$$

$$H_x(x,y) = \sum_{n=1,3..}^{\infty} H_{xn}^1 \phi_{en}(x) \frac{\cos k_{1n}(y+h)}{\cos k_{1n} h} \tag{4.13c}$$

$$H_y(x,y) = \sum_{n=1,3..}^{\infty} H_{yn}^1 \phi_{hn}(x) \frac{\sin k_{1n}(y+h)}{\sin k_{1n} h} \tag{4.13d}$$

Thus the total power flow within the slot region is given by

$$\begin{aligned} P_s = \frac{1}{2} re \{ & \sum_{n=1,3,..}^{\infty} E_{xn}^1 H_{yn}^{1*} \int_{-h}^{0} \frac{\sin k_{1n}(y+h)}{\sin k_{1n} h} \cdot \frac{\sin k_{1n}^*(y+h)}{\sin k_{1n}^* h} dy \\ & + H_{xn}^{1*} E_{yn}^1 \int_{-h}^{0} \frac{\cos k_{1n}(y+h)}{\cos k_{1n} h} \cdot \frac{\cos k_{1n}^*(y+h)}{\cos k_{1n}^* h} dy \} \\ = \frac{1}{4} re \{ & \sum_{n=1,3}^{\infty} \frac{E_{xn}^1 H_{yn}^{1*}}{\sin k_n h \sin k_n^* h} \left(\frac{\sin(k_n - k_n^*)h}{k_n - k_n^*} - \frac{\sin(k_n + k_n^*)h}{k_n + k_n^*} \right) \} \\ + \frac{1}{4} re \{ & \sum_{n=1,3}^{\infty} \frac{H_{xn}^{1*} E_{yn}^{1*}}{\cos k_n h \cos k_n^* h} \left(\frac{\sin(k_n - k_n^*)h}{k_n - k_n^*} + \frac{\sin(k_n + k_n^*)h}{k_n + k_n^*} \right) \} \end{aligned} \tag{4.14}$$

whereas the total power flow in the air region above the slot is given by

$$\begin{aligned} P_a &= \frac{1}{2} re \{ \int_0^{\infty} \left(E_x^0(\rho) \; H_y^{0*}(\rho) - H_x^{0*}(\rho) \; E_y^0(\rho) \right) \int_0^{\infty} e^{jk_0(\rho)y} e^{jk_0(\rho)y^*} dy d\rho \} \\ &= \frac{1}{4} re \{ \int_0^{\infty} \frac{\left(E_x^0(\rho) \; H_y^{0*}(\rho) - H_x^{0*}(\rho) \; E_y^0(\rho) \right)}{|k_0(\rho)|} d\rho \} \end{aligned} \tag{4.15}$$

4.4.2 The Longitudinal Current

Closed form expressions for the longitudinal current on the strip do not exist, since the latter was treated as a dependent variable in the dispersion relation (4.4). The longitudinal current can however, be computed from the boundary conditions (4.3) as:

$$\begin{aligned} I_z(x) &= H_x(x,0^-) - H_x(x,0^+) \qquad (x<w/2) \\ &= \sum_{n=1,3..}^{\infty} H_{xn}^1 \phi_{en}(x) + \int_0^{\infty} H_x^0(\rho)\,\phi_e(\rho,x)\,d\rho \end{aligned} \tag{4.16}$$

The integral of the current over the strip is then given by

$$\begin{aligned} I_z = \int_0^{w/2} I_z(x)\,dx &= \sum_{n=1,3..}^{\infty} \int_0^{w/2} H_{xn}^1 \phi_{en}(x)\,dx \\ &\quad + \int_0^{\infty}\int_0^{w/2} H_x^0(\rho)\,\phi_e(\rho,x)\,dx d\rho \\ &= -\frac{2}{\sqrt{a}} \sum_{n=1,3,..}^{\infty} H_{xn}^1 \frac{a}{n\pi} \sin\left(\frac{n\pi}{a}\frac{w}{2}\right) \\ &\quad - \frac{2}{\sqrt{\pi}} \int_0^{\infty} H_z^0(\rho)\,\frac{1}{\rho}\sin(\rho w/2)\,d\rho \end{aligned} \tag{4.17}$$

The characteristic impedance can finally be evaluated from (4.14,4.15,4.17) as

$$Z_0 = \frac{P_s + P_a}{I_z^2} \tag{4.18}$$

4.5 EXPERIMENTAL MEASUREMENT OF DISPERSION

Measurements of dispersion for example geometries of MLIDG were carried out using the resonant section technique which was described in Chapter 3 (section 3.7), and the dispersion in MLIDG is plotted as λ_0/λ_g as a function of frequency for two typical geometries (Figure 4.6 and 4.7). It can be seen from the figures that the experimental results show good agreement with the computed results. The convergence of the computed solutions for the cross sectional geometry of Figure 4.6 are shown in Table 4.1. It can been from the table that convergence to three significant figure is achieved using just 2 x 2 basis functions.

	λ_0/λ_g as a function of the number of basis functions		
Frequency (GHz)	1 by 1	2 by 2	3 by 3
0.1	1.2948	1.2510	1.2513
2	1.3019	1.2558	1.2561
4	1.3253	1.2697	1.2699
6	1.3629	1.2908	1.2908
8	1.4164	1.3150	1.3145

Table 4.1 Convergence of solutions to the fundamental mode of MLIDG. Dimensions as in Figure 4.6

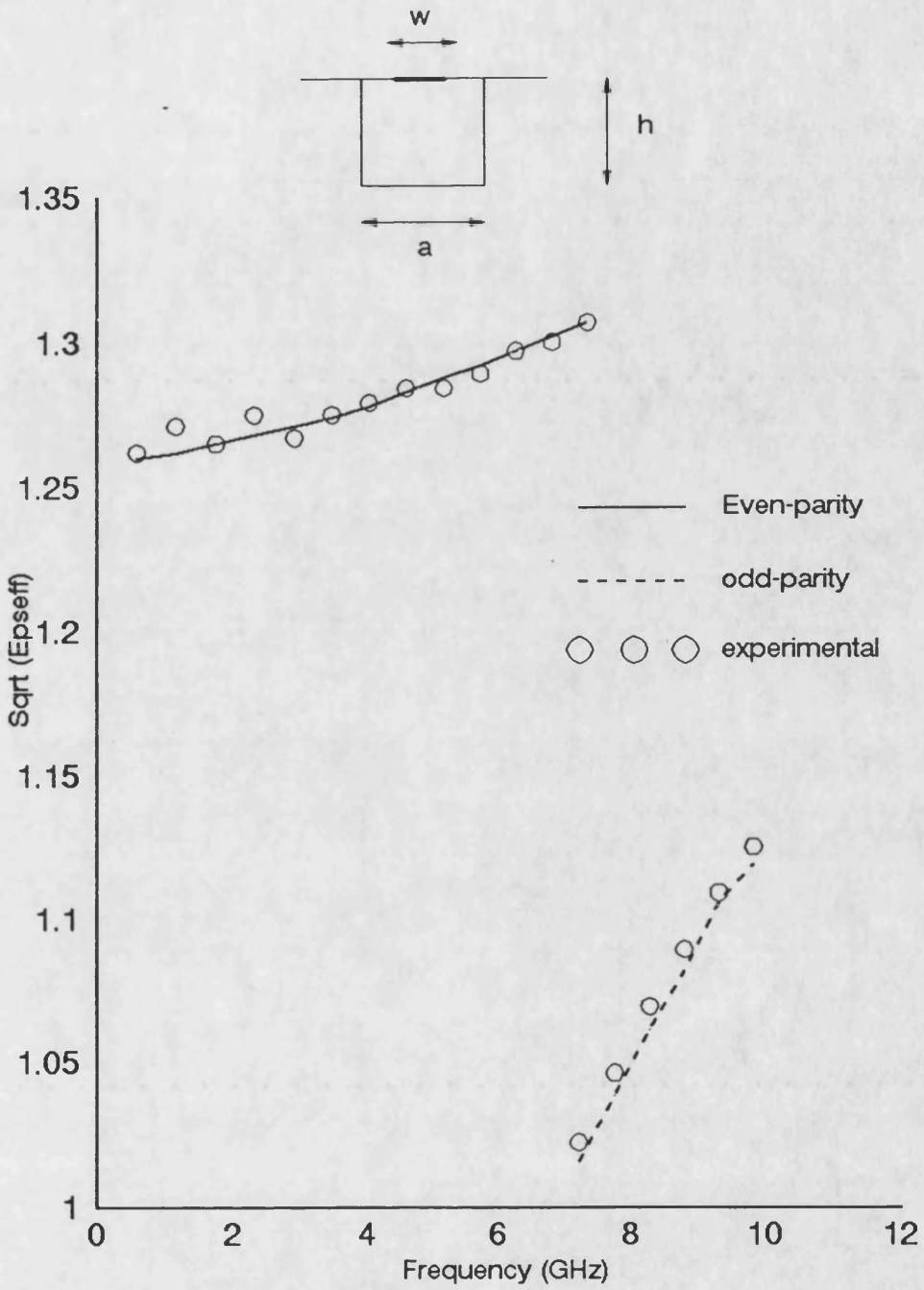

Figure 4.6 Dispersion in single-layer IDG. a=2.286e-2, h=1.016e-2, ϵ_r=2.04, w=5e-3 (all dimensions in metres).

The results obtained for a two-layer MLIDG are shown in Figure 4.7. Here it can be seen that a systematic error occurs between the measured and theoretical curves. The cause in the systematic error can be attributed to:

1) Variation in the relative permittivity of the material. Theoretical curves with a nominal variation of 2% in the relative permittivities of the dielectric material are included in the figure, and it can be seen that taking into account this variation, better agreement between the theoretical and experimental values is obtained.

2) The conducting plates placed at the ends of the resonant section, will not form complete short circuits. Thus the number n in (3.31) will not be an integer value but will either be slightly less or slightly greater than an integer value. This will give rise to an error in the measured value of λ_g.

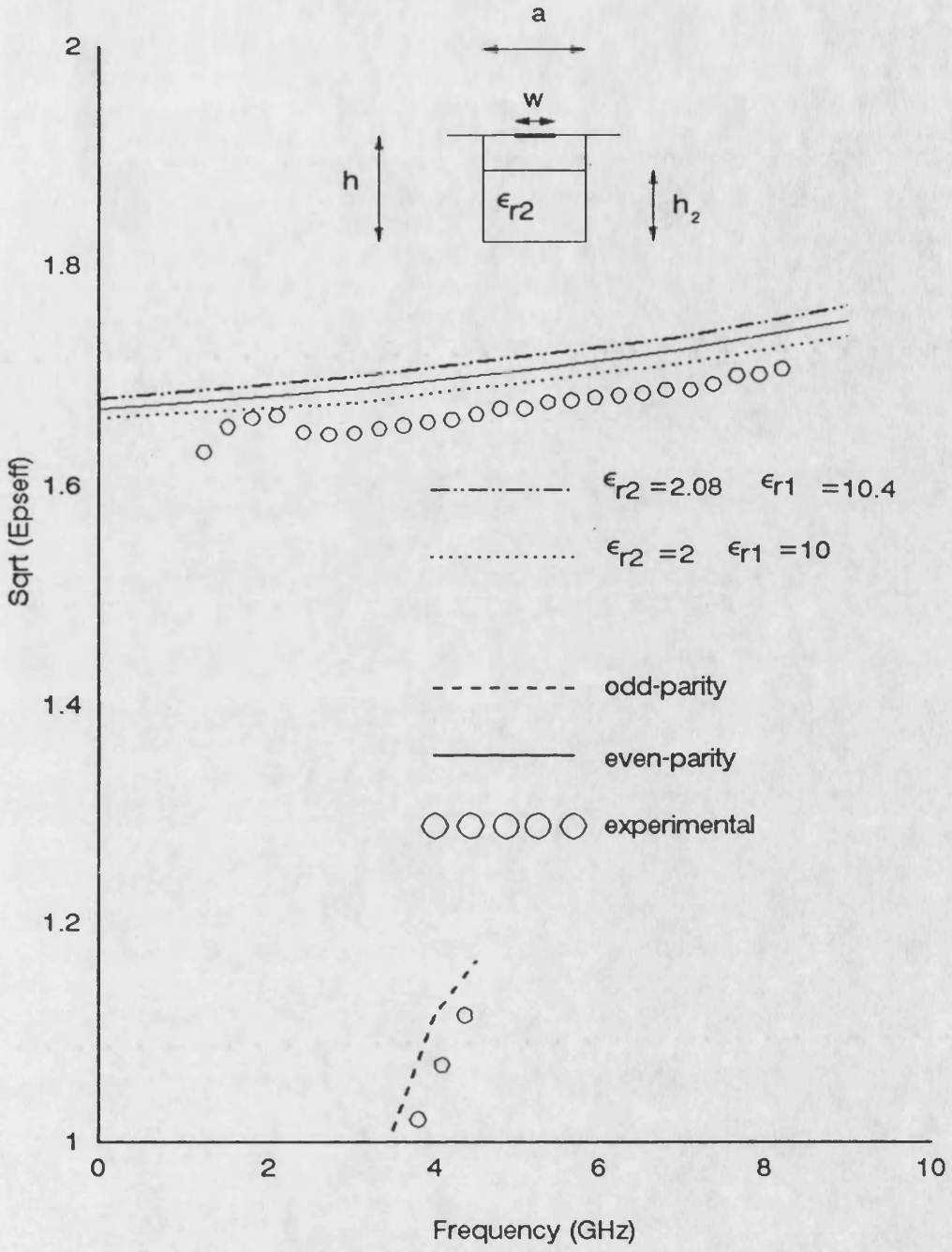

Figure 4.7 Dispersion in a two-layer MLIDG. a=1.016e-2, h=1.524e-2, h1=1.4605e-2, ϵ_{r1}=10.2, ϵ_{r2}=2.04 (all dimensions in metres).

4.6 VARIATION OF MONOMODE RANGE WITH STRIP WIDTH AND SLOT DEPTH

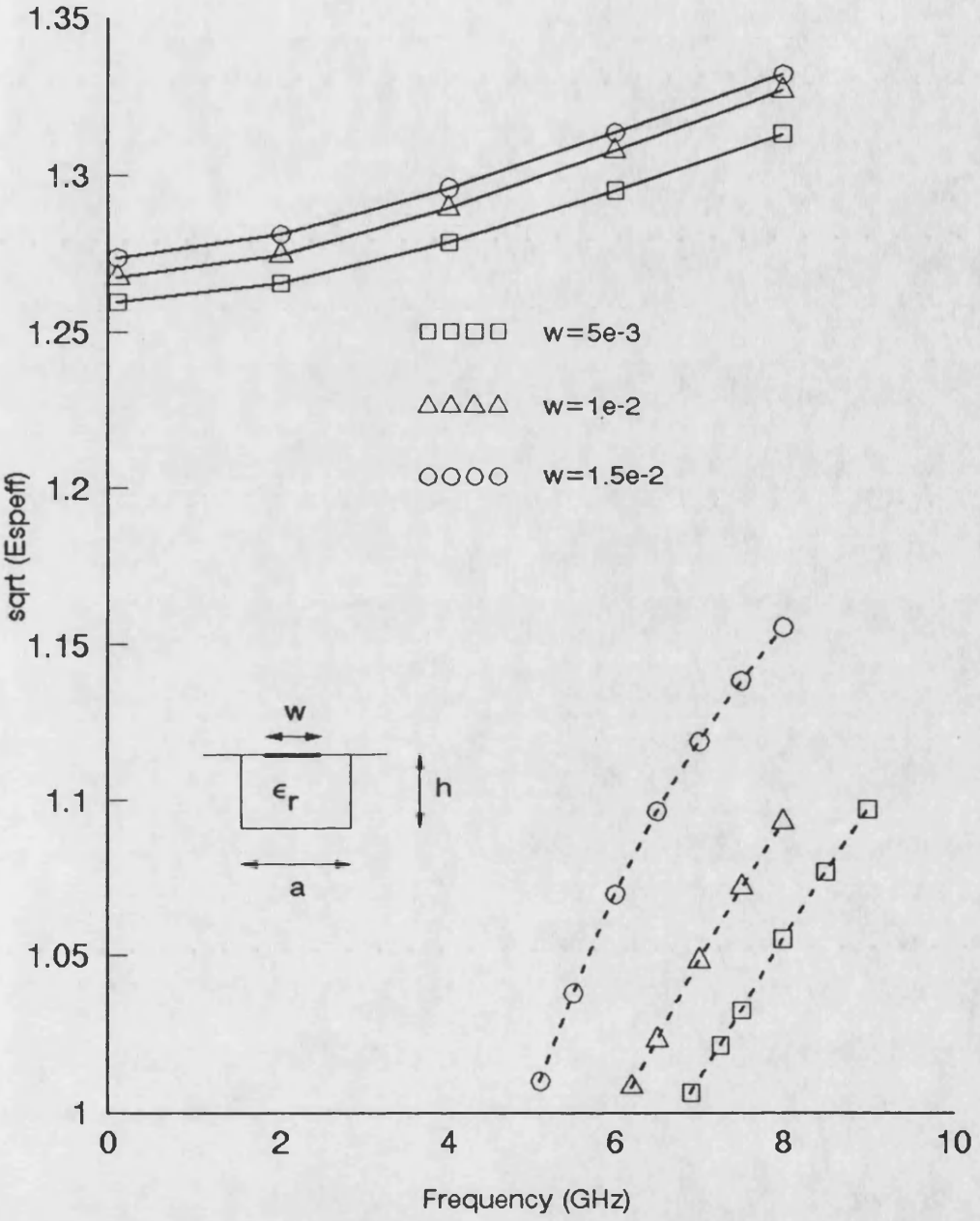

Figure 4.8 Dispersion characteristics of MLIDG as a function of strip width. a=2.286e-2, h=1.016e-2, ϵ_r =2.04 (all dimensions in metres)

The effect of changing the width of the conducting strip on

dispersion for the cross sectional geometry of Figure 4.6 is shown in Figure 4.8.

It can be seen from Figure 4.8 that as the width of the strip is increased, λ_0/λ_g changes slightly for the fundamental mode. However, the cutoff of the first higher order mode decreases as the width of the strip is increased. In Figure 4.9 the cutoff of the first higher order mode is plotted as a function of strip width and it can be seen from the figure that the monomode range is reduced significantly when the width of the strip approaches that of the slot

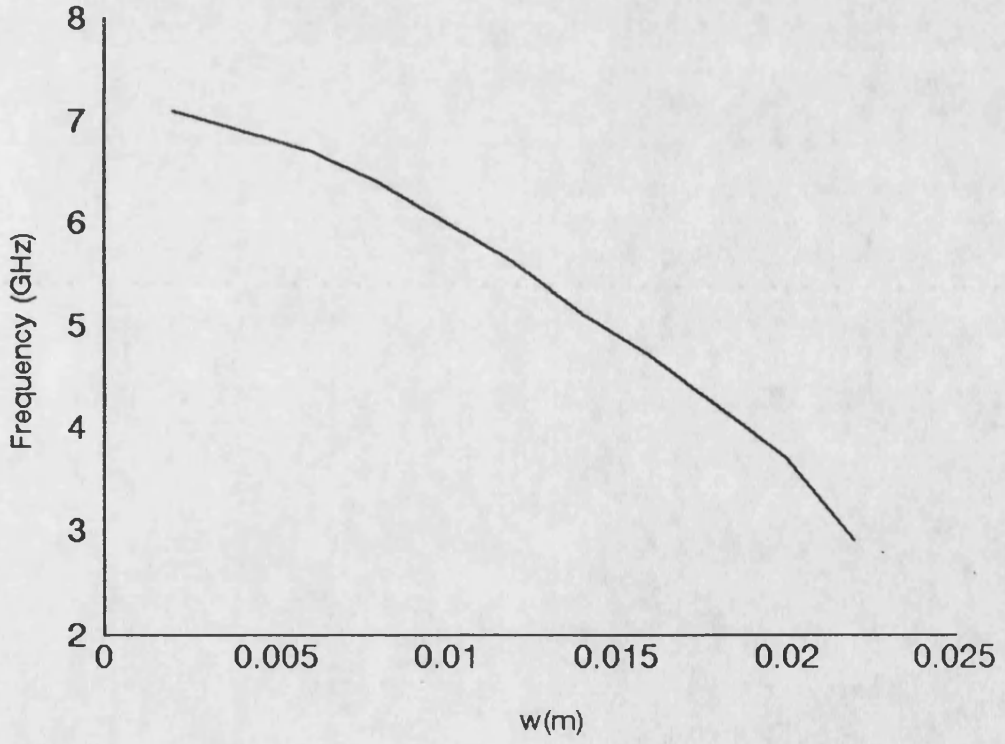

Figure 4.9 Cutoff of the first higher order mode as a function of stripwidth (Cross sectional geometry of Figure 4.8).

In Figure 4.10, the depth of the slot is decreased while keeping the stripwidth fixed. It can be seen from the figure that an improvement in monomode range is achieved by decreasing the depth of the slot.

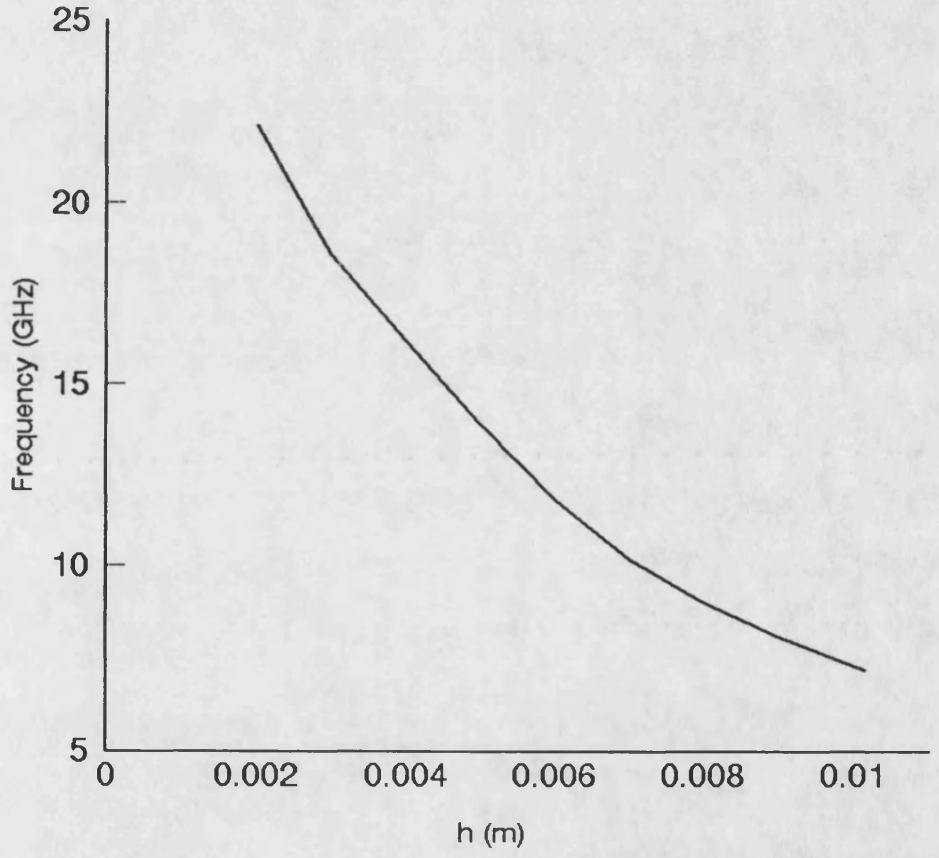

Figure 4.10 Cutoff of the first higher order mode as a function of the slot depth (Cross sectional geometry of Figure 4.6)

4.7 MEASUREMENT OF CHARACTERISTIC IMPEDANCE

The characteristic impedance of MLIDG was measured using the time-domain step response facility on the HP8510A network analyzer.

The feed probes from the analyzer were first calibrated to match a termination with a characteristic impedance of 50 Ω.

The probes were then fed into a section of MLIDG via coaxial connectors and the reflection at the inputs was measured. The characteristic impedance was then calculated from the measured reflection.

The results obtained are discussed in the following section.

4.8 VARIATION OF CHARACTERISTICS IMPEDANCE WITH FREQUENCY AND STRIP WIDTH

The variation of characteristic impedance with strip width for the geometry of Figure 4.8 is given in Figure 4.12. Experimental measurement of the characteristic impedance, by the method of section 4.7, is also included in the figure, where it can be seen that good agreement with the measured values was obtained.

From the figure it can be seen that the characteristic impedance varies from infinity (in the limit as the strip width tends to zero) down to zero (in the limit as the strip width tends towards the slot width).

The variation of characteristic impedance with frequency is given in Fig. 4.13 for different values of stripwidth. It can be seen from the figure that the characteristic impedance increases slightly with frequency, and that the change in characteristic impedance with frequency increases as the strip width is decreased, so that the characteristic impedance becomes more dispersive with a narrower stripwidth. Such behaviour is typical for the characteristics impedance of microstrip [8].

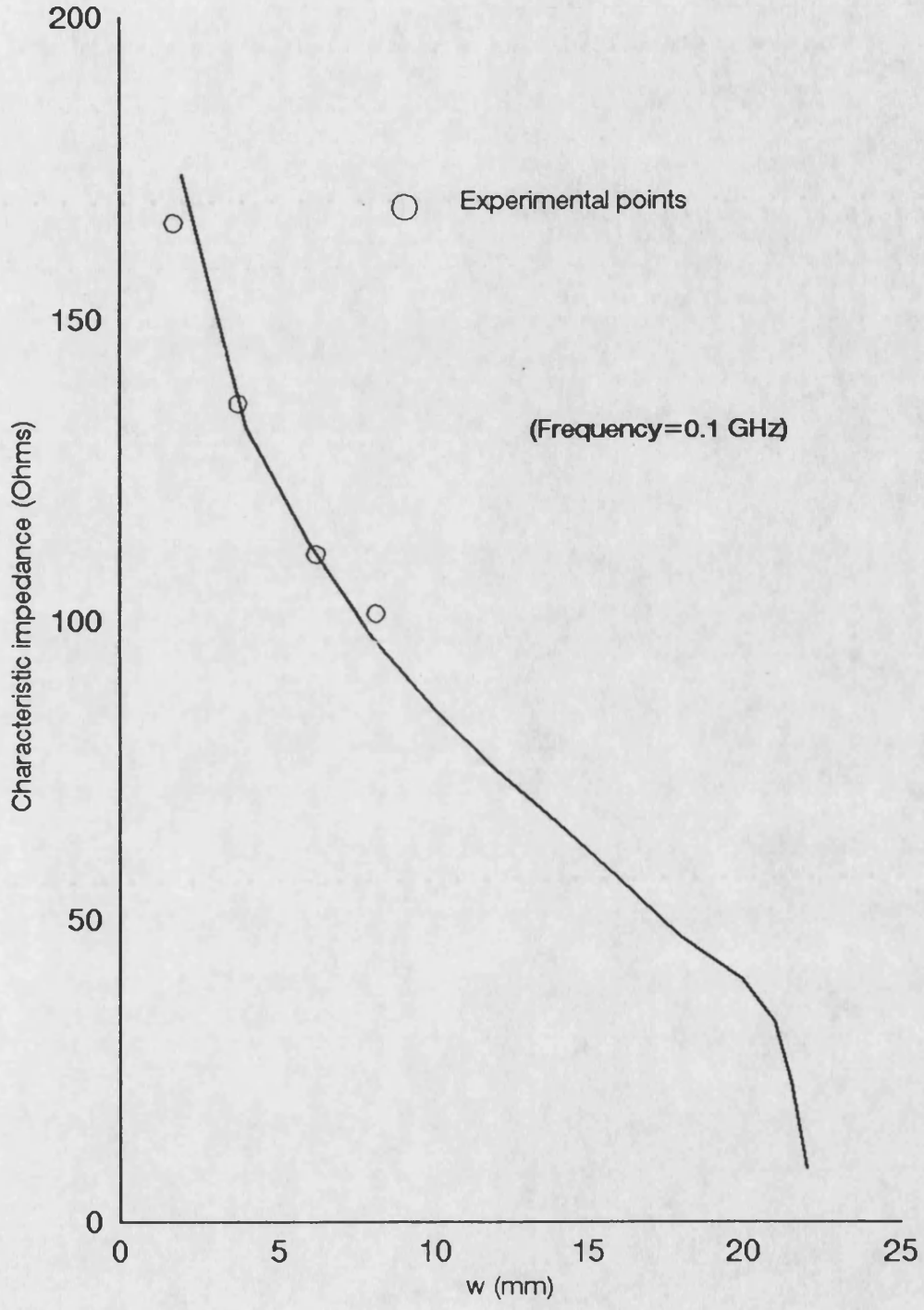

Figure 4.12 Characteristic impedance as a function of stripwidth (cross sectional geometry of Figure 4.8)

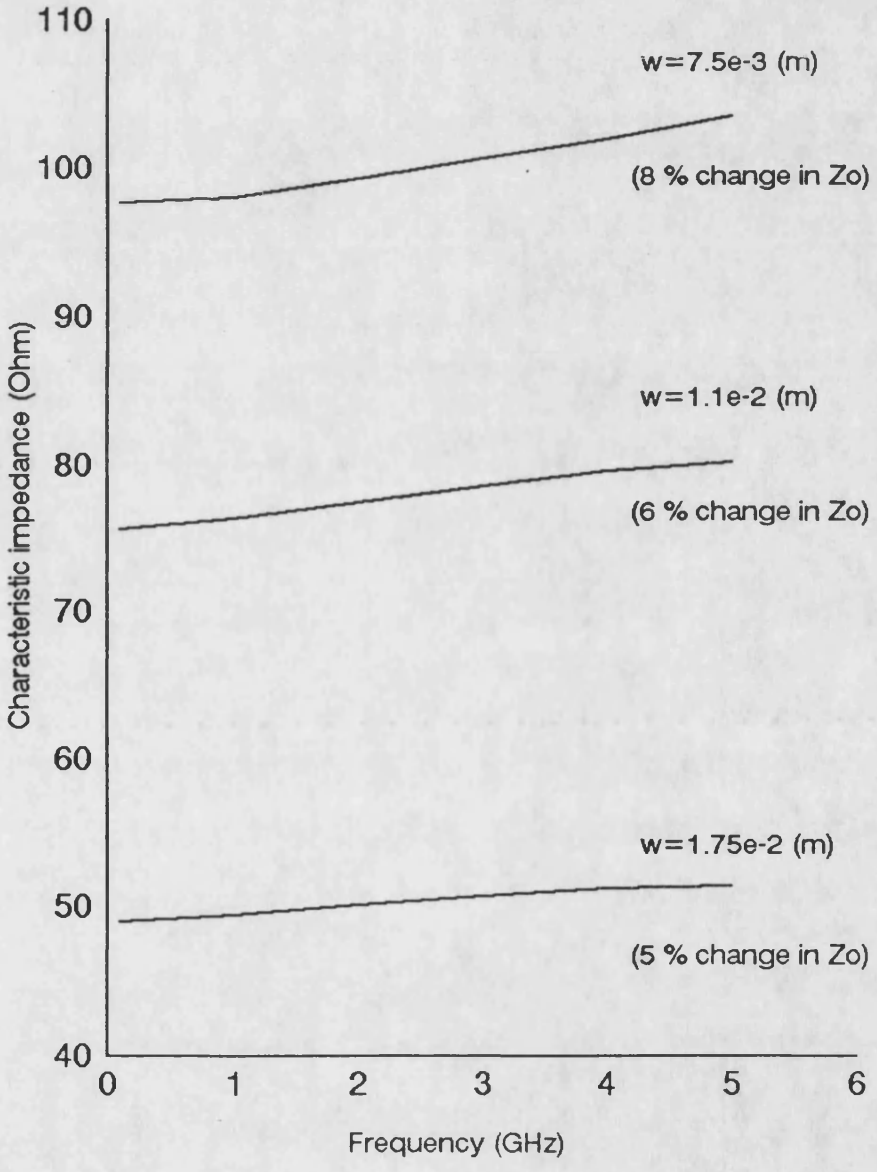

Figure 4.13 Characteristic impedance as a function of frequency for various values of stripwidth. Cross sectional geometry of Figure 4.8. The percentage change in characteristic impedance (between 0.1 GHz and 5 GHz) is given in the figure.

4.9 CONCLUSION

A rigorous analysis of the MLIDG has been presented. Dispersion results have been presented for the case of single-layered and twin-layered MLIDG showing good agreement with the measured results.

The characteristic impedance of MLIDG has been computed using the power-current formulation and comparison with measured results also shows good agreement.

The variation of monomode bandwidth and characteristic impedance with cross sectional dimensions has been investigated and it is noted that the monomode bandwidth deteriorates rapidly as the stripwidth approaches the width of the slot.

REFERENCES

1. T. Rozzi, I R. De Leo , and A. Morini, "Analysis of the Microstrip Loaded Inset Dielectric Guide", IEEE MTT-S, 1989, pp. 923-926.

2. L. Ma, T. Rozzi and A. Morini, "Linear Arrays Realized in IDG", Paper 6, IEE Collodium "Components for Novel Transmission Lines", London 26th March, 1990 (Digest No. 1990/048).

3. R.E. Collin, "Field Theory of Guided Waves", McGraw-Hill, 1960.

4. I.S. Gradshteyn and I.M. Ryslik, "Table of Integrals, Series and, Products", New York, Academic Press, 1965.

5. E.J. Jansen and M. Kirschnig, "Arguments and an Accurate Model for the Power-Current Formulation on Microstrip Characteristic Impedance", Arch. Elek. Ubertragung, 1983, Vol. 37, pp 108-112.

6. W.J. Getsinger, "Measurement and Modelling of the Apparent Characteristic Impedance of Microstrip", IEEE Trans. Microwave Theory Tech., Vol. MTT-31, Aug. 1983, pp. 624-632.

7. E.F. Keuster, "Frequency Dependent Definitions of

Microstrip Characteristic Impedance", Dig. Int. URSI Symp. Electromagnetic Waves (Munich), 1980, pp. 355B1-355B13.

8. R.H. Jansen, "High-Speed Computation of Single and Coupled Microstrip Parameters Including Dispersion, High-Order Modes, Loss and Finite Strip Thickness", IEEE Trans. Microwave Theory Tech., Vol. MTT-26, Feb. 1978, pp. 75-81.

APPENDIX 4A

NORMALIZATION OF BASIS FUNCTIONS

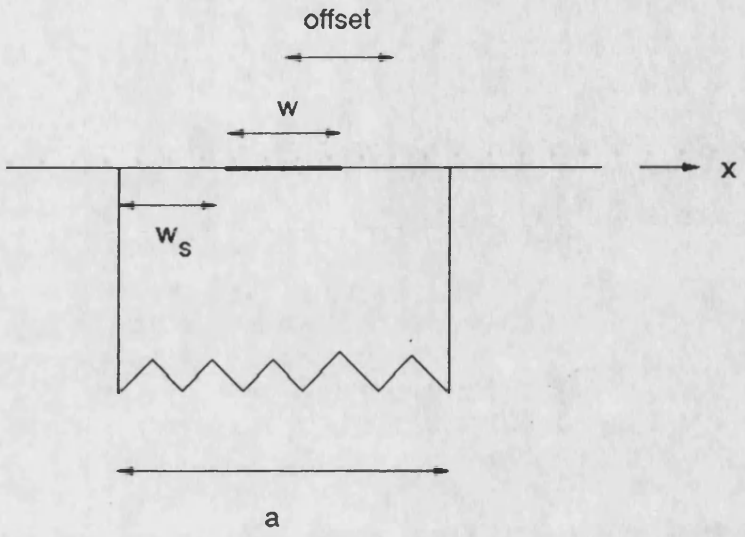

Figure 4A.1 Cross section of MLIDG

The basis functions $f_m(2t/w_s)$ in (4.9) must be normalized such that

$$\int_{-w_s/2}^{w_s/2} f_m(2t/w_s)\, f_n(2t/w_s)\, dt = \delta_{nm} \qquad (4A.1)$$

where (see figure above)

$$t = x - offset \qquad (4A.2a)$$

$$w_s = a/2 - w/2 \qquad (4A.2b)$$

From mathematical tables [1]:

$$\int_{-1}^{1}(1-v)^{\alpha}(1+v)^{\gamma}P_n^{\alpha,\gamma}(v)\,P_m^{\alpha,\gamma}(v)\,dv=\begin{cases}0 & m\neq n\\ \dfrac{2^{\alpha+\gamma+1}\Gamma(\alpha+n+1)\Gamma(\gamma+n+1)}{n!\,(\alpha+\gamma+1+2n)\Gamma(\alpha+\gamma+n+1)} & m=n\end{cases} \tag{4A.3}$$

substituting $t=w_s v/2$ in (4A.3) gives

$$\int_{-w_s/2}^{w_s/2}(1+2t/w_s)^{\gamma}(1-2t/w_s)^{\alpha}P_n^{\alpha,\gamma}(2t/w_s)\,P_m^{\alpha,\gamma}(2t/w_s)\,\frac{2}{w_s}\,dt \tag{4A.4}$$

$$=\frac{2^{\alpha+\gamma+1}\Gamma(\alpha+n+1)\Gamma(\gamma+n+1)}{n!\,(\alpha+\gamma+1+2n)\Gamma(\alpha+\gamma+n+1)}$$

From which the normalization factor is found as

$$N_m^2=\frac{w_s 2^{\alpha+\gamma}\Gamma(\alpha+n+1)\Gamma(\gamma+n+1)}{n!\,(\alpha+\gamma+1+2n)\Gamma(\alpha+\gamma+n+1)} \tag{4A.5}$$

APPENDIX 4B

EVALUATION OF THE INNER PRODUCTS OF THE BASIS FUNCTIONS

The following inner products must be evaluated for the basis functions in (4.9):

$$\langle E_{xi},\phi_{hn}(x)\rangle \tag{4B.1a}$$

$$\langle E_{xi},\phi_{h}(x,\rho)\rangle \tag{4B.1b}$$

$$\langle E_{zi},\phi_{en}(x)\rangle \tag{4B.2a}$$

$$\prec E_{zi}, \phi_e(x,\rho) \succ \qquad (4B.2b)$$

where the index n in (4B.1a. 4B.2a) takes on the values n=1,3,.. for the even modes and n=0,2,.. for the odd modes.

Consider the inner products (4B.1a, 4B.2a) for example. Since $E_x(x,0), \partial_x E_z(x,0)$ have the same singular behaviour at the strip edge and the corner, they can both be represented in terms of the basis functions (4.9). Therefore Intergrating (4B.2a) by parts, gives:

$$\prec E_{zi}, \phi_{en}(x) \succ = \frac{a}{n\pi} \prec \partial_x E_{zi}, \phi_{hn}(x) \succ \qquad (4B.3)$$

Integrating by parts has the added advantage of improving the convergence due to the 1/n term which is introduced in (4B.3).

Thus the basis functions are chosen as

$$E_{xm}(t) = f_m(2t/w) \qquad (m=0,1,2,..) \qquad (4B.4a)$$

$$\partial_x E_{zm}(t) = f_m(2t/a) \qquad (m=1,2,..) \qquad (4B.4b)$$

Note that for $\partial_x E_{zm}$ the series starts from m=1 since for the zeroth term $\partial_x E_{zm}$ would be constant in the gap. This would give rise to a ramp function in $E_z(x)$ which does not satisfy the boundary conditions.

Substituting the expression for the basis functions (4B.4) into (4B.1a) and (4B.3), it is evident that the following

identity must be computed:

$$I_m(n) = \int_{-w_s/2}^{w_s/2} f_m(2t/w)\,\phi_{hn}(t+offset)\,dt \qquad (m=0,1,2) \qquad (4B.5)$$

where for the even modes

$$I_m(n) = \frac{2}{\sqrt{a}} \int_{-w_s/2}^{w_s/2} f_m(2t/w_s)\cos\left(\frac{n\pi}{a}(t+offset)\right)dt$$

$$= \frac{2}{\sqrt{a}}\left\{\cos\left(\left(\frac{n\pi}{a}\right)offset\right)\int_{-w_s/2}^{w_s/2} f_m(2t/w_s)\cos\left(\frac{n\pi}{a}t\right)dt \right. \qquad (4B.6)$$

$$\left. -\sin\left(\left(\frac{n\pi}{a}\right)offset\right)\int_{-w_s/2}^{w_s/2} f_m(2t/w_s)\sin\left(\frac{n\pi}{a}t\right)dt\right\}$$

while for the odd modes

$$I_m(n) = \frac{2}{\sqrt{a}} \int_{-w_s/2}^{w_s/2} f_m(2t/w_s)\sin\left(\frac{n\pi}{a}(t+offset)\right)dt$$

$$= \frac{2}{\sqrt{a}}\left\{\cos\left(\left(\frac{n\pi}{a}\right)offset\right)\int_{-w_s/2}^{w_s/2} f_m(2t/w_s)\sin\left(\frac{n\pi}{a}t\right)dt \right. \qquad (4B.7)$$

$$\left. +\sin\left(\left(\frac{n\pi}{a}\right)offset\right)\int_{-w_s/2}^{w_s/2} f_m(2t/w_s)\cos\left(\frac{n\pi}{a}t\right)dt\right\}$$

The sine and cosine transforms in (4B.6-7) are evaluated as follows. From mathematical tables [2]:

$$\mathcal{F}(b) = \int_{-1}^{1} (1+v)^{\alpha}(1-v)^{\gamma} P_m^{\alpha,\gamma}(v)\, e^{-jvb} dv$$

$$= \int_{-1}^{1} (1+v)^{\alpha}(1-v)^{\gamma} P_m^{\alpha,\gamma}(v)\, (\cos vb - j\sin vb)\, dv \qquad (4B.8)$$

$$= \frac{(-1)^m\, i^m\, 2^{m+\alpha+\gamma+1}\, b^m}{m!} B(m+\alpha+1, m+\gamma+1)\, e^{ib}$$

$$ {}_1F_1(m+\alpha+1; 2m+\alpha+\gamma+2; -2ib)$$

where $B(a,b)$ is the beta function defined by [1]

$$B(a,b) = \frac{\Gamma(x)\Gamma(y)}{\Gamma(x+y)} \qquad (4B.9)$$

and ${}_1F_1(a,b,z)$ is the confluent hypergeometric function defined by [3]

$${}_1F_1(a,b,z) = 1 + \frac{az}{b} + \frac{(a)_2}{(b)_2}\frac{z^2}{2!} + \ldots + \frac{(a)_n}{(b)_n}\frac{z_n}{n!} + \ldots \qquad (4B.10a)$$

where

$$(a)_n = a(a+1)(a+2)\ldots(a+n-1), \qquad (a)_0 = 1 \qquad (4B.10b)$$

By substituting $t = w_s v/2$ the following expressions are recovered for the sin and cosine trasforms in (4B.6-7):

$$\int_{-w_s/2}^{w_s/2} f_m(2t/w_s)\cos\left(\frac{n\pi}{a}t\right) dt = \frac{1}{N_m}\frac{2}{w_s}\left(Re\left(\mathcal{F}_m\left(\frac{n\pi}{a}\frac{w_s}{2}\right)\right)\right) \qquad (4B.11a)$$

$$\int_{-w_s/2}^{w_s/2} f_m(2t/w_s)\sin\left(\frac{n\pi}{a}t\right) dt = \frac{1}{N_m}\frac{2}{w_s}\left(-Im\left(\mathcal{F}_m\left(\frac{n\pi}{a}\frac{w_s}{2}\right)\right)\right) \qquad (4B.11b)$$

If $|z| > 1$ in (4B.10a), the individual terms in the series can reach very large values. Thus in evaluating the confluent

hypergeometric function (4B.10a), the following sysmptotic approximation was introduced for $|z|>15$ [3]:

$$\frac{M(a,b,z)}{\Gamma(b)} = e^{\pm i\pi a}\frac{z^{-a}}{\Gamma(b-a)}\sum_{n=0}^{R-1}\frac{(a)_n(1+a-b)_n}{n!}(-z)^{-n} \qquad (4B.12)$$
$$e^{z}z^{a-b}\sum_{n=0}^{S-1}\frac{(b-a)_n(1-a)_n}{n!}z^{-n}$$

where the upper sign is taken in (4B.12) if $-1/2\pi < arg(z) < 3/2\pi$ and the lower sign is taken if $-3/2\pi < arg(z) \leq -1/2\pi$.

References

1. I.S. Gradshteyn and I.M. Ryshik, "Tables of Integrals, series and products", New York, Academic Press, 1965.

2. Harry Bateman, "Tables of Integral Transforms", McGraw-Hill Company Inc., 1954.

3. "Handbook of Mathematical Functions with Formulas, Graphs, and Mathematical Tables", National Bureau of Standards, Applied Mathematics, Series 55, 1964

CHAPTER 5

ANALYSIS OF PARTIALLY FILLED MLIDG, EMBEDDED STRIP IDG, AND MULTIPLE STRIP IDG

5.1 INTRODUCTION

In this chapter several novel waveguide structures are investigated including the Partially Filled Microstrip Loaded Inset Dielectric Guide (Partially Filled MLIDG), the Embedded Strip Inset Dielectric Guide, and the Multiple Strip Inset Dielectric Guide (Figure 5.1). The potential application of these guides as antenna feeds and antenna elements is discussed.

A rigorous hybrid method of analysis is presented for these structures. Experimental measurement of dispersion for the fundamental and first higher order mode are presented for different example geometries and compared with computed results in order to verify the validity of the method of analysis.

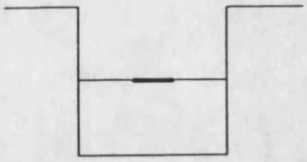

(a) Partially Filled MLIDG

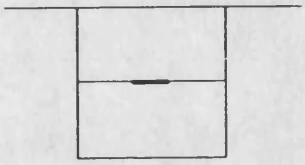

(b) Imbedded Strip IDG

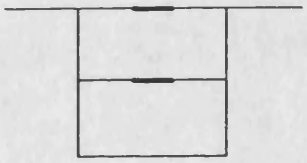

(c) Multiple Strip IDG

Figure 5.1 Cross sections of waveguides to be considered in this chapter

5.2 POTENTIAL APPLICATIONS AS ANTENNA MEDIA

As mentioned in Chapter 1, microstrip circuits in general and in particular microstrip antenna circuits are known to suffer from stray coupling, especially at higher frequencies. This is due to the excitation of surface waves which subsequently scatter of discontinuities in the

circuit. Stray coupling limits the optimum sidelobe levels that can be achieved, and in addition the power efficiency of the antennas will be reduced due to power loss in exciting these waves.

Two sources of these surface waves can be identified. The first source is the excitation of dielectric slab modes from open-circuit terminations, such as in the case of patch antennas for example. The fundamental TM-mode of the dielectric slab propagates down to DC and, as a result, the excitation of these modes is unavoidable.

In addition, any discontinuities in the microstrip transmission line will excite substrate modes, which have been discussed in Chapter 2. The excitation of these modes is also unavoidable.

The excitation of these surface waves can be controlled by housing the circuit within the IDG slot. Whereas the fundamental mode of the dielectric slab has a zero cutoff frequency, the corresponding surface modes of 'IDG do not propagate down to DC. Thus by placing the microstrip circuit in an IDG housing, and driving the circuit at a frequency below the cutoff frequency of the IDG modes, the excitation of surface waves at open circuit terminations is eliminated.

In addition whereas lateral-leakage due to the substrate

modes, occurs in open microstrip, the presence of side walls in IDG confines the fields and eliminates this leakage.

The excitation of surface waves in microstrip antenna circuits is generally controlled by decreasing the thickness of the substrate [1]. This however, results in a narrower bandwidth for the antenna [1]. Thus in microstrip antennas a trade-off exists between bandwidth and stray coupling, and the latter is controlled at the cost of a decrease in the bandwidth of the antenna [1].

To summarise, the potential advantages of placing generalised microstrip circuits within an IDG housing are the control of stray coupling and an increase in the bandwidth of microstrip antennas if relatively thicker substrates are used.

5.3 OVERVIEW OF THE METHOD OF ANALYSIS

In order to be able to analyze the waveguides structures of Figure 5.1, it is important to be able to develop a generalised method of analysis which would take into account the possible presence of multiple dielectric layers and multiple conductors between the various layers.

The spectral domain immitance approach [2], enables the rigorous and efficient analysis of generalised microstrip

circuits. However, this technique is only applicable to structures where the cross-sectional geometry is uniform.

A generalisation of the spectral domain immitance approach is presented in [3]. This technique, referred to as a "Mixed Spectral Domain Approach", has been applied to structures such as the pedestal-supported fin-line (Figure 5.2a).

In this approach the apertures in the original structure are shorted, and magnetic current sources are introduced in the circuit leading to an equivalent structure (Figure 5.2b). This resulting equivalent structure is composed of individual circuit elements, where each element has a uniform cross sectional geometry, and can therefore be analyzed using the spectral domain immitance approach (as can be seen in Figure 5.2b).

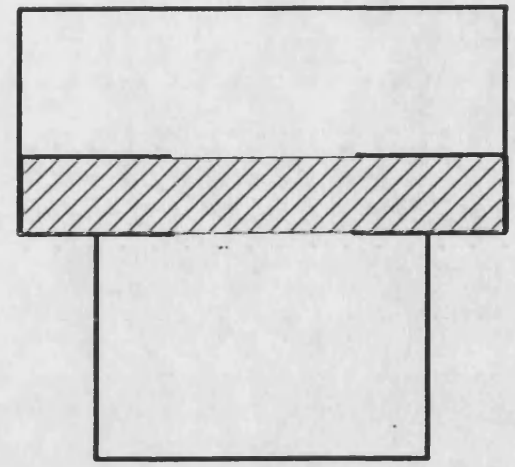

a) Pedestal Mounted Fin-line

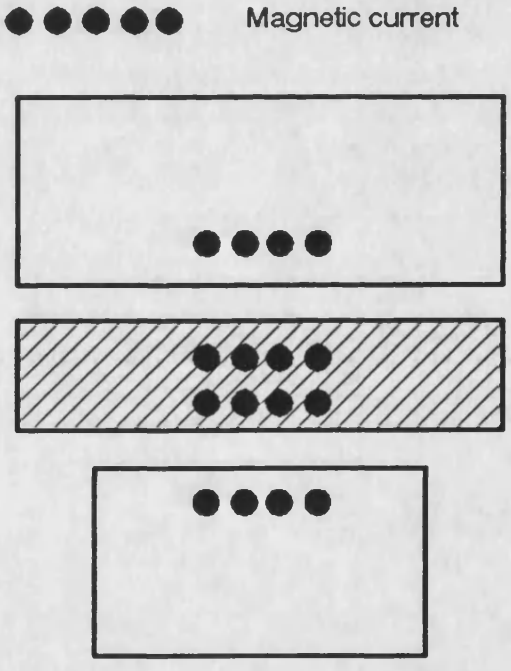

b) Equivalent structure

Figure 5.2 The pedestal-supported fin-line, and it equivalent structure.

An approach similar to that given in [3] may be applied to the structures of Figure 5.1 as will be detailed below.

Consider, for example, partially filled MLIDG (Figure 5.3). If the fields in the structure are considered to be generated from a current source at $y=-h_1$, then as propagation of the electromagnetic waves along the transverse direction is considered, on encountering the slot edge at $y=0$, the electromagnetic field generated from the current source, will be scattered with a proportion of the field penetrating into the air region, and the rest reflecting back into the slot.

The analysis of the electromagnetic penetration of fields through apertures has received a great deal of attention in the past [4, 5]. A possible approach for analyzing this problem [6, 7], is to reformulate the problem in terms of an equivalent structure. Applied to the partially filled MLIDG, for example, the procedure is as follows. The aperture at $y=0$ is initially closed by an infinitely thin conducting plane. The tangential electric fields at $y=0^-$ are then restored by introducing a magnetic current source at $y=0-$ over the shorted aperture. The fields in the air region, $y>0^+$, are also restored by introducing a second magnetic current source over the aperture at $y=0^+$. This would result in the equivalent structure of Figure 5.4.

Following this procedure, the total field in the structure

is then expressed as the sum of the fields generated from the current source at $y=-h_1$ in the presence of the short circuit - the so called "short circuited" field, and the fields generated from the magnetic current sources. As in [2] and [3], initially, we consider each source individually, and then express the total field as the superposition of the fields from these sources and impose on the total fields, the various boundary conditions that must be obeyed at all the interfaces of the structure. This would lead to the equivalent structure of Figure 5.5.

Finally it is noted that the fields in circuit 1 and 2 of Figure 5.5 can equally well be generated from electric field sources rather than magnetic field sources. Thus the equivalent structure of Figure 5.6 is finally adopted as an equivalent structure for the partially filled MLIDG of Figure 5.3.

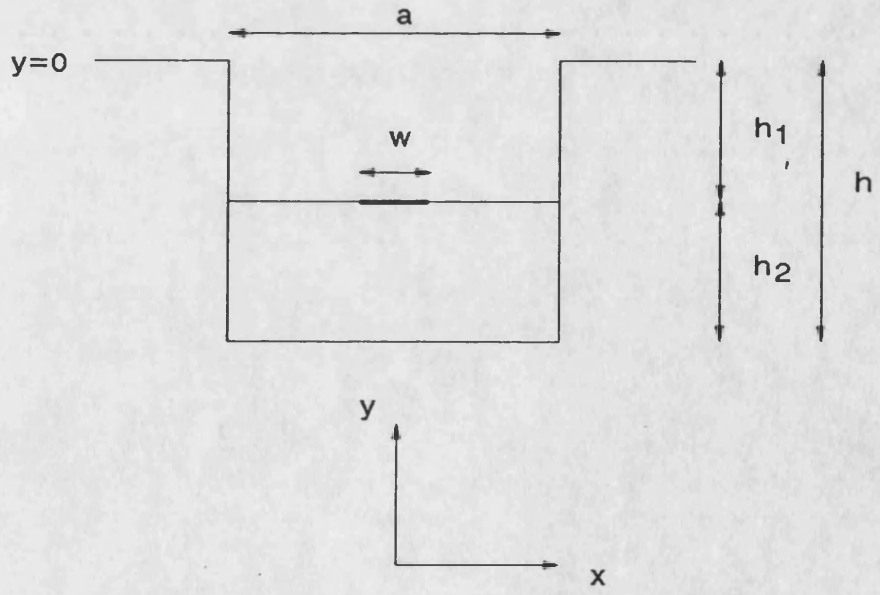

Figure 5.3 Cross section of Partially Filled MLIDG

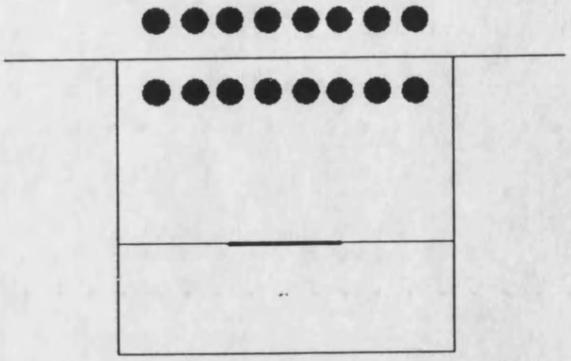

Figure 5.4 Equivalent structure for partially filled MLIDG. Aperture is shorted with a conducting plane and electric fields at aperture are restored by introducing magnetic surface currents

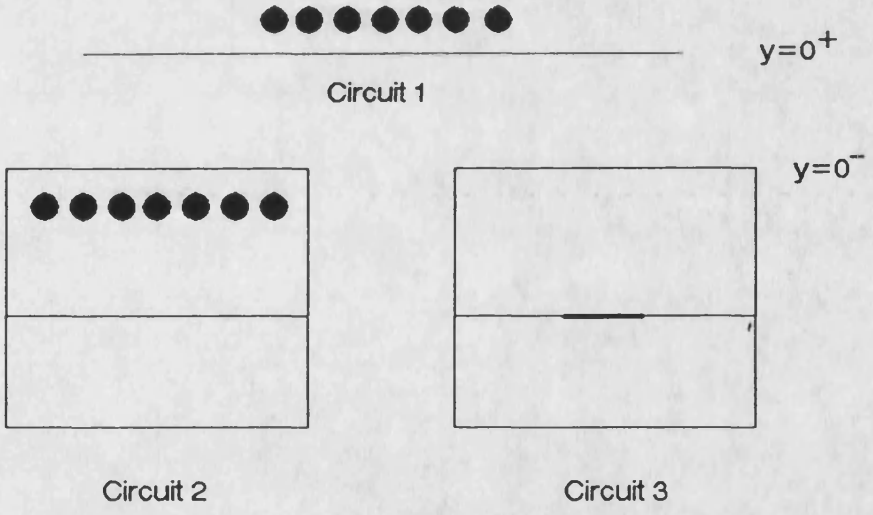

Figure 5.5 Equivalent structure for partially filled MLIDG. Total fields are expressed as the superposition of fields from the individual sources

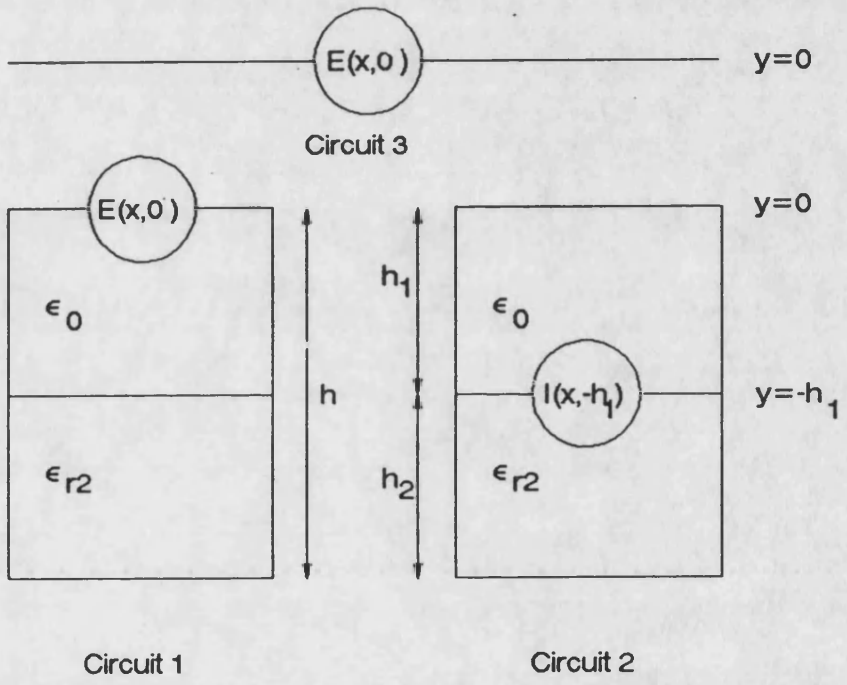

Figure 5.6 Equivalent model for partially filled MLIDG. Magnetic sources in Figure 5.5 are replaced by electric field sources

5.4 FORMULATION OF OPERATORS

As discussed in the previous section, the fields in Partially filled MLIDG are given by the total field generated by the equivalent circuit of Figure 5.6. The total field must obey the boundary conditions at the interface $y=0$ and $y=-h_1$, which include

1. At interface 1 ($y=0$),

$$E_x(x,0^+)=E_x(x,0^-)=E_x(x,0) \tag{5.1a}$$

$$E_z(x,0^+)=E_z(x,0^-)=E_z(x,0) \tag{5.1b}$$

$$H_x(x,0^+)=H_x(x,0^-) \qquad |x|<a/2 \tag{5.1c}$$

$$H_z(x,0^+)=H_z(x,0^-) \qquad |x|\leq a/ \tag{5.1d}$$

2. At interface 2 ($y=-h_1$),

$$E_x(x,-h_1^+)=E_x(x,-h_1^-)=E_x(x,-h_1) \qquad |x|<a/2 \tag{5.2a}$$

$$E_z(x,-h_1^+)=E_z(x,-h_1^-)=E_z(x,-h_1) \qquad |x|<a/2 \tag{5.2b}$$

and

$$E_x(x,-h_1)=E_z(x,-h_1)=0 \qquad |x|<w/2 \tag{5.2c}$$

5.4.1 FORMULATION OF OPERATORS FOR THE FIELDS AT $y=-h_1$

The fields in each of the individual circuits of Figure 5.6 can be rigorously analyzed by the methods detailed in Chapter 2 and 3. Circuit 1 of Figure 5.6, for example, is the slot region of IDG, circuit 3 is the air region of IDG, while circuit 2 is a boxed microstrip structure. The analysis of these circuits will not be repeated in detail in this section.

The tangential electric fields at $y=-h_1$ are given by

$$E_x(x,-h_1)=E_x^{(1)}(x,-h_1)+E_x^{(2)}(x,-h_1) \tag{5.3a}$$

$$E_z(x,-h_1)=E_z^{(1)}(x,-h_1)+E_z^{(2)}(x,-h_1) \tag{5.3b}$$

where the superscript (i) denote fields in circuit (i).

Tangential electric fields for circuit 2

For circuit (2) (section 2.3.3)

$$\begin{bmatrix} E_x^{(2)}(x,-h_1) \\ E_z^{(2)}(x,-h_1) \end{bmatrix} = \begin{bmatrix} \tilde{Z}_{xx}^{(2)}(\beta) & \tilde{Z}_{xz}^{(2)}(\beta) \\ \tilde{Z}_{zx}^{(2)}(\beta) & \tilde{Z}_{zz}^{(2)}(\beta) \end{bmatrix} \begin{bmatrix} I_x(x,-h_1) \\ I_z(x,-h_1) \end{bmatrix} \tag{5.4}$$

where the impedance operators $\tilde{Z}_{ii}^{(2)}$ are given by

$$\tilde{Z}_{xx}^{(2)} I_x(x,-h_1)=\sum_n \left(\cos^2\theta \overleftarrow{Z''}_2^{(2)}(n)+\sin^2\theta \overleftarrow{Z'}_2^{(2)}(n)\right)\phi_{hn}(x)\prec I_x,\phi_{hn}(x)\succ \tag{5.4a}$$

$$\hat{Z}^{(2)}_{xz} I_x(x,-h_1) = \sum_n -j\cos\theta\sin\theta\left(\tilde{Z}''^{(2)}_2(n) - \tilde{Z}'^{(2)}_2(n)\right)\phi_{hn}(x) \prec I_z, \phi_{en}(x) \succ \qquad (5.4b)$$

$$\hat{Z}^{(2)}_{zx} I_x(x,-h_1) = \sum_n j\cos\theta\sin\theta\left(\tilde{Z}''^{(2)}_2(n) - \tilde{Z}'^{(2)}_2(n)\right)\phi_{en}(x) \prec I_x, \phi_{hn}(x) \succ \qquad (5.4c)$$

$$\hat{Z}^{(2)}_{zz} I_z(x,-h_1) = \sum_n \left(\cos^2\theta\tilde{Z}'^{(2)}_2(n) + \sin^2\theta\tilde{Z}''^{(2)}_2(n)\right)\phi_{en}(x) \prec I_z, \phi_{en}(x) \succ \qquad (5.4d)$$

$$\cos\theta = \frac{n\pi/a}{\sqrt{(n\pi/a)^2+\beta^2}} \qquad \sin\theta = \frac{\beta}{\sqrt{(n\pi/a)^2+\beta^2}} \qquad (5.5)$$

and

$$\tilde{Z}^{(2)}_2(n) = Z^{U(2)}_2(n) + Z^{D(2)}_2(n) \qquad (5.6)$$

where $Z^{U(2)}_2$ and $Z^{D(2)}_2$ are the input impedances looking up and down respectively, at interface 2, for the e-modes and the h-modes of circuit 2.

Tangential electric fields for circuit 1

The fields in circuit 1 are given by the expression (see Appendix 2A for example);

$$E_x(x,y)^{(1)} = \sum_n E'^{(1)}_{xn}\phi_{hn}(x)\frac{Y'_1(n)\cos k_{1n}(y+h_1) + jY'^{D(1)}_2(n)\sin k_{1n}(y+h_1)}{Y'_1(n)\cos k_{1n}h_1 + jY'^{D(1)}_2(n)\sin k_{1n}h_1} + E''^{(1)}_{xn}\phi_{hn}(x)\frac{Y''_1(n)\cos k_{1n}(y+h_1) + jY''^{D(1)}_2(n)\sin k_{1n}(y+h_1)}{Y''_1(n)\cos k_{1n}h_1 + jY''^{D(1)}_2(n)\sin k_{1n}h_1} \qquad (5.7a)$$

$$E_x(x,y)^{(1)}=\sum_n E'^{(1)}_{zn}\phi_{en}(x)\frac{Y'_1(n)\cos k_{1n}(y+h_1)+jY'^{D(1)}_2(n)\sin k_{1n}(y+h_1)}{Y'_1(n)\cos k_{1n}h_1+jY'^{D(1)}_2(n)\sin k_{1n}h_1}$$
$$+E''^{(1)}_{zn}\phi_{en}(x)\frac{Y''_1(n)\cos k_{1n}(y+h_1)+jY''^{D(1)}_2(n)\sin k_{1n}(y+h_1)}{Y''_1(n)\cos k_{1n}h_1+jY''^{D(1)}_2(n)\sin k_{1n}h_1} \qquad (5.7b)$$

where $0<y<-h_1$

Thus (see section 3.3)

$$E_x^{(1)}(x,0)=\sum_n E_{xn}^{(1)}\phi_{hn}(x) \qquad (5.8a)$$

$$E_z^{(1)}(x,0)=\sum_n E_{zn}^{(1)}\phi_{en}(x) \qquad (5.8b)$$

where

$$E_{xn}^{(1)}=E'^{(1)}_{xn}+E''^{(1)}_{xn} \qquad (5.8c)$$

$$E_{zn}^{(1)}=E'^{(1)}_{zn}+E''^{(1)}_{zn} \qquad (5.8d)$$

and

$$\begin{bmatrix}E_{xn}^{(1)}\\-E_{zn}^{(1)}\end{bmatrix}=\begin{bmatrix}\cos\theta & -j\sin\theta\\-j\sin\theta & \cos\theta\end{bmatrix}\begin{bmatrix}Z'^{D(1)}_1(n) & 0\\0 & 1\end{bmatrix}\begin{bmatrix}-I'^{(1)}_{1n}\\V''^{(1)}_{1n}\end{bmatrix}$$
$$=T_n\begin{bmatrix}Z'^{D(1)}_1(n) & 0\\0 & 1\end{bmatrix}\begin{bmatrix}-I'^{(1)}_{1n}\\V''^{(1)}_{1n}\end{bmatrix} \qquad (5.9)$$

where $I'^{(1)}_{1n}, V''^{(1)}_{1n}$ are the amplitudes of the TE-to-y and TM-to-y potential functions for circuit 1 for $0<y<-h_1$.

On the other hand, it can be seen from (5.7a, 5.7b) that the tangential fields at $y=-h_1$ are given by

$$E_x^{(1)}(x,-h_1)=\sum_n E_{xn}^{(1)}(-h_1)\phi_{hn}(x) \tag{5.10a}$$

$$E_z^{(1)}(x,-h_1)=\sum_n E_{zn}^{(1)}(-h_1)\phi_{en}(x) \tag{5.10b}$$

where

$$E_{xn}^{(1)}(-h_1)=E_{xn}^{I(1)}\frac{Y^I{}_1(n)}{Y^I{}_1(n)\cos k_{1n}h_1+jY_2^{ID(1)}(n)\sin k_{1n}h_1} +E_{xn}^{II(1)}\frac{Y_2^{IID(1)}(n)}{Y^{II}{}_1(n)\cos k_{1n}h_1+jY_2^{IID(1)}(n)\sin k_{1n}h_1} \tag{5.10c}$$

$$E_{zn}^{(1)}(-h_1)=E_{zn}^{I(1)}\frac{Y^I{}_1(n)}{Y^I{}_1(n)\cos k_{1n}h_1+jY_2^{ID(1)}(n)\sin k_{1n}h_1} +E_{zn}^{II(1)}\frac{Y_2^{IID(1)}(n)}{Y^{II}{}_1(n)\cos k_{1n}h_1+jY_2^{IID(1)}(n)\sin k_{1n}h_1} \tag{5.10d}$$

The expressions for the amplitude functions $E_{xn,zn}^{(1)}(-h_1)$ in (5.10) can be rearranged in matrix form to give

$$\begin{bmatrix} E_{xn}^{(1)}(-h_1) \\ -E_{zn}^{(1)}(-h_1) \end{bmatrix} = T_n \cdot A_n \cdot \begin{bmatrix} Z_1^{ID(1)}(n) & 0 \\ 0 & 1 \end{bmatrix} \begin{bmatrix} -I_{1n}^{I(1)} \\ V_{1n}^{II(1)} \end{bmatrix} \tag{5.11a}$$

where

$$A_n = \begin{bmatrix} \dfrac{Y^I{}_1(n)}{Y^I{}_1(n)\cos k_{1n}h_1+jY_2^{ID(1)}(n)\sin k_{1n}h_1} & 0 \\ 0 & \dfrac{Y^{II}{}_1(n)}{Y^{II}{}_1(n)\cos k_{1n}h_1+jY_2^{IID(1)}(n)\sin k_{1n}h_1} \end{bmatrix} \tag{5.11b}$$

Eliminating $I'^{(1)}_{1n}, V''^{(1)}_{1n}$ from (5.11a) and (5.9) gives

$$\begin{bmatrix} E^{(1)}_{xn}(-h_1) \\ E^{(1)}_{zn}(-h_1) \end{bmatrix} = T_n \cdot \begin{bmatrix} \dfrac{Y'_1(n)}{Y'_1(n)\cos k_{1n}h_1 + jY'^{D(1)}_2(n)\sin k_{1n}h_1} & 0 \\ 0 & \dfrac{Y''_1(n)}{Y''_1(n)\cos k_{1n}h_1 + jY''^{D(1)}_2(n)\sin k_{1n}h_1} \end{bmatrix} \cdot T_n^{-1} \begin{bmatrix} E^{(1)}_{xn}(0) \\ E^{(1)}_{zn}(0) \end{bmatrix} \tag{5.12}$$

From (5.8a) and (5.10a), the tangential electric fields at $y=-h_1$ can thus be expressed in terms of the tangential electric fields at $y=0$ as

$$\begin{bmatrix} E^{(1)}_x(x,-h_1) \\ E^{(1)}_z(x,-h_1) \end{bmatrix} = \begin{bmatrix} \tilde{A}^{(1)}_{xx}(\beta) & \tilde{A}^{(1)}_{xz}(\beta) \\ \tilde{A}^{(1)}_{zx}(\beta) & \tilde{A}^{(1)}_{zz}(\beta) \end{bmatrix} \begin{bmatrix} E^{(1)}_x(x,0) \\ E^{(1)}_z(x,0) \end{bmatrix} \tag{5.14}$$

where $\tilde{A}^{(1)}_{ij}$ are linear integral operators defined by

$$\tilde{A}^{(1)}_{xx} E_x(x,0) = \sum_n \left(\cos^2\theta A'^{(1)}_{21}(n) + \sin^2\theta A''^{(1)}_{21}(n)\right) \phi_{hn}(x) \prec E_x, \phi_{hn}(x) \succ \tag{5.15a}$$

$$\tilde{A}^{(1)}_{xz} E_z(x,0) = \sum_n j\cos\theta\sin\theta \left(A'^{(1)}_{21}(n) - A''^{(1)}_{21}(n)\right) \phi_{hn}(x) \prec E_z, \phi_{en}(x) \succ \tag{5.15b}$$

$$\tilde{A}^{(1)}_{zx} E_x(x,0) = \sum_n j\cos\theta\sin\theta \left(A'^{(1)}_{21}(n) - A''^{(1)}_{21}(n)\right) \phi_{en}(x) \prec E_x, \phi_{hn}(x) \succ \tag{5.15c}$$

$$\tilde{A}^{(1)}_{zz} E_z(x,0) = \sum_n \left(\cos^2\theta A''^{(1)}_{21}(n) + \sin^2\theta A'^{(1)}_{21}(n)\right) \phi_{en}(x) \prec E_z, \phi_{en}(x) \succ \tag{5.15d}$$

and

$$A'^{(1)}_{12}(n)=\frac{Y'_1(n)}{Y'_1(n)\cos k_{1n}h_1+jY'^{D(1)}_2(n)\sin k_{1n}h_1} \tag{5.16a}$$

$$A''^{(1)}_{12}(n)=\frac{Y''_1(n)}{Y''_1(n)\cos k_{1n}h_1+jY''^{D(1)}_2(n)\sin k_{1n}h_1} \tag{5.16b}$$

Finally substituting (5.14) and (5.4) into (5.3) gives

$$\begin{bmatrix}E_x(x,-h_1)\\E_z(x,-h_1)\end{bmatrix}=\begin{bmatrix}\tilde{A}^{(1)} & \tilde{Z}^{12}\end{bmatrix}\cdot\begin{bmatrix}E_x(x,0)\\E_z(x,0)\\I_x(x,-h_1)\\I_z(x,-h_1)\end{bmatrix} \tag{5.17}$$

where

$$\tilde{A}^{(1)}=\begin{bmatrix}\tilde{A}^{(1)}_{xx}(\beta) & \tilde{A}^{(1)}_{xz}(\beta)\\\tilde{A}^{(1)}_{zx}(\beta) & \tilde{A}^{(1)}_{zz}(\beta)\end{bmatrix} \qquad \tilde{Z}^{(2)}=\begin{bmatrix}\tilde{Z}^{(2)}_{xx}(\beta) & \tilde{Z}^{(2)}_{xz}(\beta)\\\tilde{Z}^{(2)}_{zx}(\beta) & \tilde{Z}^{(2)}_{zz}(\beta)\end{bmatrix} \tag{5.18a}$$

5.4.2 FORMULATION OF OPERATORS FOR THE FIELDS AT $y=0$

In order to impose the boundary conditions (5.1c, 5.1d) on the tangential magnetic fields at $y=0$, the following expressions can be obtained for the latter at $y=0^+$ and $y=0^-$.

5.4.2.1 The tangential magnetic fields at $y=0^+$

The fields in circuit 3 of Figure 5.6, can be analyzed in

the same way as the fields in IDG for the air region were analyzed (section 3.3). Thus the tangential magnetic fields at $y=0^+$ are given by

$$-\begin{bmatrix} H_z(x,0^+) \\ H_x(x,0^+) \end{bmatrix} = \begin{bmatrix} \tilde{Y}^{(3)}_{zx}(\beta) & \tilde{Y}^{(3)}_{zz}(\beta) \\ \tilde{Y}^{(3)}_{xx}(\beta) & \tilde{Y}^{(3)}_{xz}(\beta) \end{bmatrix} \begin{bmatrix} E_x(x,0) \\ E_z(x,0) \end{bmatrix} \tag{5.19}$$

where the operators $\tilde{Y}^{(3)}_{ij}$ are given by

$$\tilde{Y}^{(3)}{}_{zx}E_x(x,0) = \int_0^\infty \left(\cos^2\alpha\, Y_1'^{U(3)}(\rho) + \sin^2\alpha\, Y_1''^{U(3)}(\rho)\right) \phi_h(x,\rho) \int_0^\infty E_x \phi_h(x,\rho)\, dx\, d\rho \tag{5.20a}$$

$$\tilde{Y}^{(3)}{}_{zz}E_z(x,0) = \int_0^\infty j\cos\alpha\sin\alpha\left(Y_1'^{U(3)}(\rho) - Y_1''^{U(3)}(\rho)\right) \phi_h(x,\rho) \int_0^\infty E_z \phi_e(x,\rho)\, dx\, d\rho \tag{5.20b}$$

$$\tilde{Y}^{(3)}{}_{xx}E_x(x,0) = \int_0^\infty -j\cos\alpha\sin\alpha\left(Y_1'^{U(3)}(\rho) - Y_1''^{U(3)}(\rho)\right) \phi_e(x,\rho) \int_0^\infty E_x(x) \phi_h(x,\rho)\, dx\, d\rho \tag{5.20c}$$

$$\tilde{Y}^{3}{}_{xz}E_z(x,0) = \int_0^\infty \left(\sin^2\alpha\, Y_1'^{U(3)}(\rho) + \cos^2\alpha\, Y_1''^{U(3)}(\rho)\right) \phi_e(x,\rho) \int_0^\infty E_x \phi_e(x,\rho)\, dx\, d\rho \tag{5.20d}$$

and

$$\cos\alpha=\frac{\rho}{\sqrt{(\rho^2+\beta^2)}} \qquad \sin\alpha=\frac{\beta}{\sqrt{(\rho^2+\beta^2)}} \tag{5.20e}$$

5.4.2.2 The tangential magnetic fields at $y=0^-$

The tangential magnetic fields at $y=0^-$ are given by

$$H_{x,z}(x,0^-)=H_{x,z}^{(1)}(x,0^-)+H_{x,z}^{(2)}(x,0^-) \tag{5.21}$$

where the fields are the superposition of the fields from circuit 1 and circuit 2.

Tangential magnetic fields for circuit 1

These are given by the same expressions obtained for the IDG slot (section 3.3):

$$\begin{bmatrix} H_z^{(1)}(x,0^-) \\ H_x^{(1)}(x,0^-) \end{bmatrix} = \begin{bmatrix} \tilde{Y}_{zx}^{(1)}(\beta) & \tilde{Y}_{zz}^{(1)}(\beta) \\ \tilde{Y}_{xx}^{(1)}(\beta) & \tilde{Y}_{xz}^{(1)}(\beta) \end{bmatrix} \begin{bmatrix} E_x(x,0) \\ E_z(x,0) \end{bmatrix} \tag{5.22}$$

Where the operators $\tilde{Y}^{(1)}{}_{ij}$ are defined by

$$\tilde{Y}^{(1)}{}_{zx}E_x(x,0)=\sum_n\left(\cos^2\theta Y_1'^{D(1)}(n)+\sin^2\theta Y_1''^{D(1)}(n)\right)\phi_{hn}(x)\int_0^{\infty}E_x\phi_{hn}(x)\,dx \tag{5.23a}$$

$$\tilde{Y}^{(1)}{}_{zz}E_z(x,0)=\sum_n j\cos\theta\sin\theta\left(Y_1'^{D(1)}(n)-Y_1''^{D(1)}(n)\right)\phi_{hn}(x)\int_0^{\infty}E_z\phi_{en}(x)\,dx \tag{5.23b}$$

$$\tilde{Y}^{(1)}{}_{xx}E_x(x,0)=\sum_n -j\cos\theta\sin\theta\left(Y_1'^{D(1)}(n)-Y_1''^{D(1)}(n)\right)\phi_{en}(x)\int_0^{\infty}E_x\phi_{hn}(x)\,dx \tag{5.23c}$$

$$\tilde{Y}^{(1)}{}_{xz}E_z(x,0)=\sum_n\left(\sin^2\theta Y_1'^{D(1)}(n)+\cos^2\theta Y_1''^{D(1)}(n)\right)\phi_{en}(x)\int_0^{\bar{x}}E_x\phi_{en}(x)\,dx \qquad (5.23d)$$

Tangential magnetic fields for circuit 2

The fields for $0<y<h_1$ are given by

$$H_x^{(2)}(x,y)=\sum_n H_{xn}^{(2)}\phi_{en}(x)\frac{\cos k_{1n}(-y)}{\cos k_{1n}h_1} \qquad (5.24a)$$

$$H_z^{(2)}(x,y)=\sum_n H_{zn}^{(2)}\phi_{hn}(x)\frac{\cos k_{1n}(-y)}{\cos k_{1n}h_1} \qquad (5.24b)$$

$$E_x^{(2)}(x,y)=\sum_n E_{xn}^{(2)}\phi_{hn}(x)\frac{\sin k_{1n}(-y)}{\sin k_{1n}h_1} \qquad (5.24c)$$

$$E_z^{(2)}(x,y)=\sum_n E_{zn}^{(2)}\phi_{en}(x)\frac{\sin k_{1n}(-y)}{\sin k_{1n}h_1} \qquad (5.24d)$$

where the fields are normalised to unity at $y=-h_1$. The tangential magnetic fields at $y=-h_1^+$ are thus given by

$$H_x^{(2)}(x,-h_1^+)=\sum_n H_{xn}^{(2)}\phi_{en}(x) \qquad (5.25a)$$

$$H_z^{(2)}(x,-h_1^+)=\sum_n H_{zn}^{(2)}\phi_{hn}(x) \qquad (5.25b)$$

The magnetic field components H_{xn}, H_{zn} can be expressed in terms of the electric field components E_{xn}, E_{zn} (see section 2.3.2) as

$$-\begin{bmatrix} H_{zn}^{(2)} \\ H_{xn}^{(2)} \end{bmatrix} = T_n \begin{bmatrix} Y_2'^{U(2)}(n) & 0 \\ 0 & Y_2''^{U(2)}(n) \end{bmatrix} T_n^{-1} \begin{bmatrix} E_{xn}^{(2)} \\ -E_{zn}^{(2)} \end{bmatrix} \tag{5.26}$$

However,

$$\begin{bmatrix} E_{xn}^{(2)} \\ -E_{zn}^{(2)} \end{bmatrix} = T_n \begin{bmatrix} \overleftarrow{Y_2'^{(2)}}(n) & 0 \\ 0 & \overleftarrow{Y_2''^{(2)}}(n) \end{bmatrix} T_n^{-1} \begin{bmatrix} I_{xn} \\ -I_{zn} \end{bmatrix} \tag{5.27}$$

where

$$I_{xn} = \langle I_x(x, -h_1), \phi_{hn}(x) \rangle \qquad I_{zn} = \langle I_z(x, -h_1), \phi_{en}(x) \rangle \tag{5.28}$$

Substituting (5.27) into (5.26) gives

$$-\begin{bmatrix} H_{zn}^{(2)} \\ H_{xn}^{(2)} \end{bmatrix} = T_n \begin{bmatrix} \dfrac{Y_2'^{U(2)}(n)}{\overleftarrow{Y_2'^{(2)}}(n)} & 0 \\ 0 & \dfrac{Y_2''^{U(2)}(n)}{\overleftarrow{Y_2''^{(2)}}(n)} \end{bmatrix} T_n^{-1} \begin{bmatrix} I_{xn} \\ -I_{zn} \end{bmatrix} \tag{5.29}$$

From (5.24a, 5.24b),

$$H_x^{(2)}(x, 0^-) = \sum_n H_{xn}^{(2)} \phi_{en}(x) \frac{1}{\cos k_{1n} h_1} \tag{5.30a}$$

$$H_z^{(2)}(x, 0^-) = \sum_n H_{zn}^{(2)} \phi_{hn}(x) \frac{1}{\cos k_{1n} h_1} \tag{5.30b}$$

Thus

$$H_x^{(2)}(x, 0^-) = \sum_n H_{xn}^{(2)}(0^-) \phi_{en}(x) \tag{5.31a}$$

$$H_z^{(2)}(x,0^-)=\sum_n H_{zn}^{(2)}(0^-)\,\phi_{hn}(x) \tag{5.31b}$$

where from (5.31a, 5.31b), (5.25a, 5.25b), and (5.29) the following expression is obtained

$$-\begin{bmatrix}H_{zn}^{(2)}(0)\\ H_{xn}^{(2)}(0)\end{bmatrix}= T_n \begin{bmatrix}\dfrac{Y_2'^{U(2)}(n)}{\tilde{Y}_2'^{(2)}(n)\cos(k_{n1}h_1)} & 0\\ 0 & \dfrac{Y_2''^{U(2)}(n)}{\tilde{Y}_2''^{(2)}(n)\cos(k_{n1}h_1)}\end{bmatrix} T_n^{-1}\begin{bmatrix}I_{xn}\\ -I_{zn}\end{bmatrix} \tag{5.32}$$

Finally from (5.31a, 5.31b) and (5.28) the following expression is obtained for the tangential magnetic fields at $y=0^-$:

$$-\begin{bmatrix}H_z^{(2)}(x,0^-)\\ H_x^{(2)}(x,0^-)\end{bmatrix}=\begin{bmatrix}\tilde{L}_{zx}^{(2)}(\beta) & \tilde{L}_{zz}^{(2)}(\beta)\\ \tilde{L}_{xx}^{(2)}(\beta) & \tilde{L}_{xz}^{(2)}(\beta)\end{bmatrix}\begin{bmatrix}I_x(x,-h_1)\\ I_z(x,-h_1)\end{bmatrix} \tag{5.33}$$

where the operators $\tilde{L}_{11}^{(2)}$ are given by

$$\tilde{L}_{zx}^{(2)} I_x(x,-h_1)=\sum_n \left(\cos^2\theta\,\tilde{L}_{12}''^{(2)}(n)+\sin^2\theta\,\tilde{Z}_{12}'^{(2)}(n)\right) \phi_{hn}(x)\prec I_x,\phi_{hn}(x)\succ \tag{5.34a}$$

$$\tilde{L}_{zz}^{(2)} I_x(x,-h_1)=\sum_n -j\cos\theta\sin\theta\left(\tilde{L}_{12}''^{(2)}(n)-\tilde{L}_{12}'^{(2)}(n)\right) \phi_{hn}(x)\prec I_z,\phi_{en}(x)\succ \tag{5.34b}$$

$$\tilde{L}_{xx}^{(2)} I_x(x,-h_1) = \sum_n j\cos\theta\sin\theta\left(\overleftarrow{L}_{12}^{//(2)}(n) - \overleftarrow{L}_{12}^{/(2)}(n)\right) \phi_{en}(x) \prec I_x, \phi_{hn}(x) \succ \tag{5.34c}$$

$$\tilde{L}_{xx}^{(2)} I_z(x,-h_1) = \sum_n \left(\cos^2\theta \overleftarrow{A}_{12}^{/(2)}(n) + \sin^2\theta \overleftarrow{A}_{12}^{//(2)}(n)\right) \phi_{en}(x) \prec I_z, \phi_{en}(x) \succ \tag{5.34d}$$

and

$$L_{12}^{/(2)} = \frac{Y_2^{/U(2)}(n)}{\overleftarrow{Y}_2^{/(2)}(n)\cos(k_{n1}h_1)} \tag{5.35a}$$

$$L_{12}^{//(2)} = \frac{Y_2^{//U(2)}(n)}{\overleftarrow{Y}_2^{//(2)}(n)\cos(k_{n1}h_1)} \tag{5.35b}$$

Finally, enforcing the boundary conditions (5.1c, 5.1d) gives

$$0 = \left[\tilde{Y} - \tilde{L}^{(2)}\right] \cdot \begin{bmatrix} E_x(x,0) \\ E_z(x,0) \\ I_x(x,-h_1) \\ I_z(x,-h_1) \end{bmatrix} \tag{5.36}$$

where

$$\tilde{Y} = \begin{bmatrix} \tilde{Y}_{zx}(\beta) & \tilde{Y}_{zz}(\beta) \\ \tilde{Y}_{xx}(\beta) & \tilde{Y}_{xz}(\beta) \end{bmatrix} \qquad \tilde{L}^{(2)} = \begin{bmatrix} \tilde{L}_{zx}^{(2)}(\beta) & \tilde{L}_{zz}^{(2)}(\beta) \\ \tilde{L}_{xx}^{(2)}(\beta) & \tilde{L}_{xz}^{(2)}(\beta) \end{bmatrix} \tag{5.37}$$

and

$$\tilde{Y}_{ii}=\tilde{Y}_{ii}^{(1)}+\tilde{Y}_{ii}^{(3)} \tag{5.38}$$

5.5 SOLUTION OF DISPERSON RELATION

The solutions of the dispersion relation for the Partially filled MLIDG, can now be obtained using the same method which has been used in the previous chapters.

Expressions (5.17) and (5.36) can be combined together to give

$$\begin{bmatrix} E_x(x,-h_1) \\ E_z(x,-h_1) \\ 0 \\ 0 \end{bmatrix} = \begin{bmatrix} \tilde{A}^{(1)} & \tilde{Z}^{(2)} \\ \tilde{Y} & -\tilde{L}^{(2)} \end{bmatrix} \cdot \begin{bmatrix} E_x(x,0) \\ E_z(x,0) \\ I_x(x,-h_1) \\ I_z(x,-h_1 \end{bmatrix} \tag{5.39}$$

Through (5.39), a relationship is thus obtained relating the tangential magnetic fields at interface 1 ($y=0$) and tangential electric fields at interface 2 ($y=-h_1$) in terms of the tangential electric fields at interface 1 and the current at interface 2. The latter variables thus become independent variables, whereas the former variables are dependent.

In order to obtain the solutions for the required propagating modes, the unknown currents and tangential electric fields are discretised by applying the Galerkin procedure, where each of these variables is expressed in terms of a set of normalised basis functions:

$$E_x(x,0)=\sum X_{1i}E_{xi}(x) \tag{5.40a}$$

$$E_z(x,0)=\sum Z_{1i}E_{xi}(x) \tag{5.40b}$$

$$I_x(x,0)=\sum X_{2i}I_{xi}(x) \tag{5.40c}$$

$$I_z(x,0)=\sum Z_{2i}I_{zi}(x) \tag{5.40d}$$

The Galerkin procedure is then completed by taking the inner product of the basis functions with (5.39). This reduces the LHS of (5.39) to zero since the tangential electric fields at $y=-h_1$ must be zero where the strip current is non-zero and vice-versa, and at the same time imposes the boundary conditions (5.2c). All of the boundary conditions ((5.1) and (5.2)) will thus be obeyed by the fields in the final expression:

$$\begin{bmatrix} A & Z \\ Y & L \end{bmatrix} \cdot \begin{bmatrix} \underline{X_1} \\ \underline{Z_1} \\ \underline{X_2} \\ \underline{Z_2} \end{bmatrix} = 0 \tag{5.41}$$

where for example

$$A=\begin{bmatrix} A_{xx} & A_{xz} \\ A_{zx} & A_{zz} \end{bmatrix} \tag{5.42}$$

and

$$|A_{xx}|_{ij}=\langle I_{xi}, \tilde{A}_{xx}E_{xj}\rangle \tag{5.42a}$$

$$|A_{xz}|_{ij}=\langle I_{xi}, \tilde{A}_{xz}E_{zj}\rangle \tag{5.42b}$$

$$|A_{zx}|_{ij}=\langle I_{zi}, \tilde{A}_{zx}E_{xj}\rangle \tag{5.42c}$$

$$|A_{zz}|_{ij}=\langle I_{zi}, \tilde{A}_{zz}E_{zj}\rangle \tag{5.42d}$$

and in a similar fashion

$$Z=\begin{bmatrix} Z_{xx} & Z_{xz} \\ Z_{zx} & Z_{zz} \end{bmatrix} \tag{5.43}$$

where

$$|Z_{xx}|_{ij}=\langle I_{xi}, \tilde{Z}_{xx}I_{xj}\rangle \tag{5.43a}$$

$$|Z_{xz}|_{ij}=\langle I_{xi}, \tilde{Z}_{xz}I_{zj}\rangle \tag{5.43b}$$

$$|Z_{zx}|_{ij}=\langle I_{zi}, \tilde{Z}_{zx}I_{xj}\rangle \tag{5.43c}$$

$$|Z_{zz}|_{ij}=\langle I_{zi}, \tilde{Z}_{zz}I_{zj}\rangle \tag{5.43d}$$

The required propagation wavenumber can now be obtained by searching for the zeros of the determinant of (5.41).

In order to achieve fast convergence, the singular behaviour of the tangential electric fields and currents at $y=0, y=-h_1$ respectively, should be modelled by the basis functions. The following inner products must be computed

in (5.41):

$$\langle E_{xi}, \phi_{hn}(x) \rangle \tag{5.44a}$$

$$\langle E_{zi}, \phi_{en}(x) \rangle \tag{5.44b}$$

$$\langle I_{xi}, \phi_{hn}(x) \rangle \tag{5.44c}$$

$$\langle I_{zi}, \phi_{en}(x) \rangle \tag{5.44d}$$

Since $I_z(x,-h_1)$, $\partial_x I_x(x,-h_1)$ have the same singular behaviour (of the type $r^{-1/2}$) at the edge of the conducting strip at $y=-h_1$, we integrate the inner products (5.44c) by parts (section 2.3.3). $I_{zi}(x)$, $\partial_x I_{xi}(x)$ can then be represented in terms of the basis functions (2.46).

Similarly since $E_x(x,0)$ ∂_x, $E_z(x,0)$ have same singular behaviour at the metallic corners (of the type $r^{-1/3}$) we integrate the inner products (5.44b) by parts and then represent $E_{xi}(x)$, $\partial_x E_{zi}(x)$ in terms of the basis functions (3.26).

5.6 VARIATION OF DISPERSION WITH SUBSTRATE THICKNESS

Figure 5.7 gives the dispersion curves obtained for the fundamental mode of partially filled MLIDG where the thickness of the substrate h_2 was varied and all other dimensions where kept fixed.

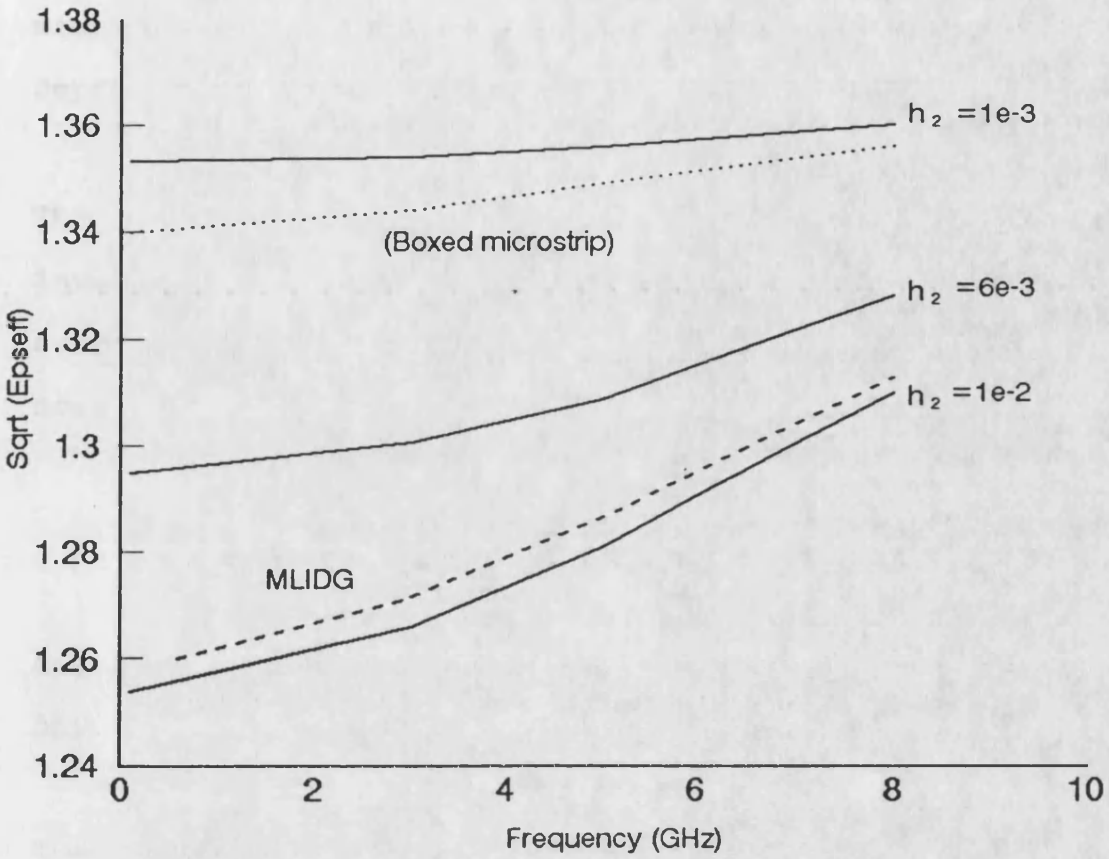

Figure 5.7 Dispersion curves obtained for the fundamental mode of partially filled MLIDG, for various values of substrate thickness. h=1.016e-2, a=2.286e-2, w=5e-3, ϵ_{r2}=2.04 (all dimensions in metres).

As the thickness of the substrate, h_2, approaches the depth of the slot, h, we expect dispersion in partially filled MLIDG to approach that of MLIDG, where the dielectric fills the slot completely. The dispersion curve obtained for MLIDG is included in the figure for comparison, and it can be seen that this does occur as expected.

As the thickness of the substrate becomes much smaller than the height of the slot, however, the fields will be

strongly confined within the slot and we expect dispersion in partially filled MLIDG to approach that of boxed microstrip with the height of the box set equal to the depth of the slot.

The dispersion curve obtained for boxed microstrip is included in Figure 5.7 for comparison, and again it can be seen that for $h_2 < h$ dispersion in partially filled MLIDG does approach that of boxed microstrip as expected.

5.7 VARIATION OF MONOMODE BANDWIDTH WITH SUBSTRATE HEIGHT AND STRIP WIDTH

The cutoff frequency of the first higher order mode as a function of stripwidth in partially filled MLIDG is given in Figure 5.8 for an example geometry. It can be seen from the figure that as with MLIDG, the monomode bandwidth decreases as the stripwidth approaches the slotwidth.

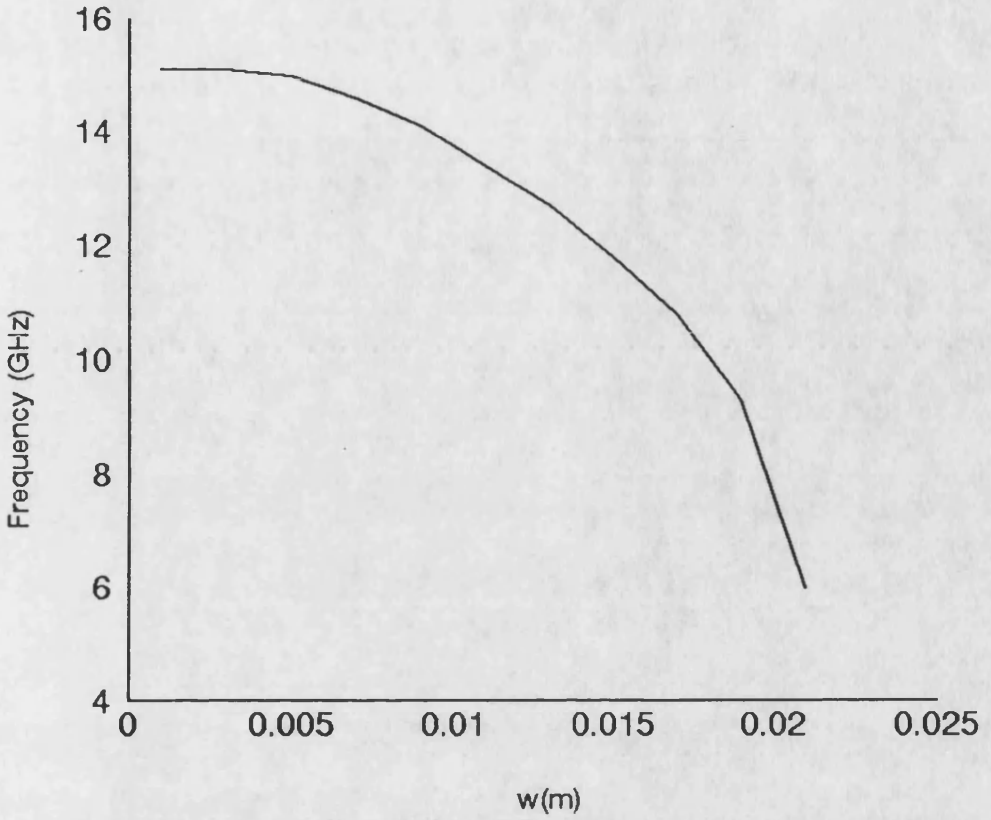

Figure 5.8 Cutoff frequency of the first higher order mode as a function of strip width in partially filled MLIDG. a=2.286e-2, h_2=5e-3, h=1.016e-2, ϵ_r=2.04 (all dimension in metres).

The cutoff frequency of the first higher order mode as a function of substrate thickness for a particular geometry is given in Figure 5.9. As with MLIDG, it can be seen that there is an improvement in monomode bandwidth as the substrate thickness is reduced.

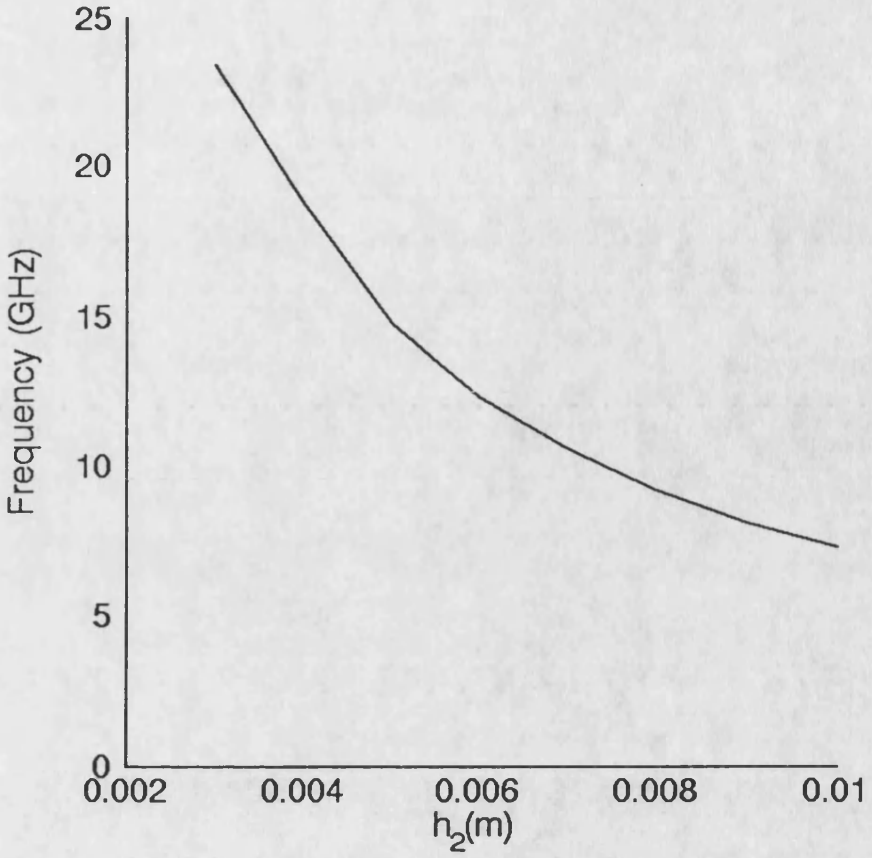

Figure 5.9 Cutoff frequency of first higher order mode as a function of substrate thickness in partially filled MLIDG. a=2.286e-2, h=1.016e-2, w=5e-3, ϵ_r=2.04 (all dimensions in metres).

5.8 CLOSING THE APERTURE IN PARTIALLY FILLED FILLED MLIDG

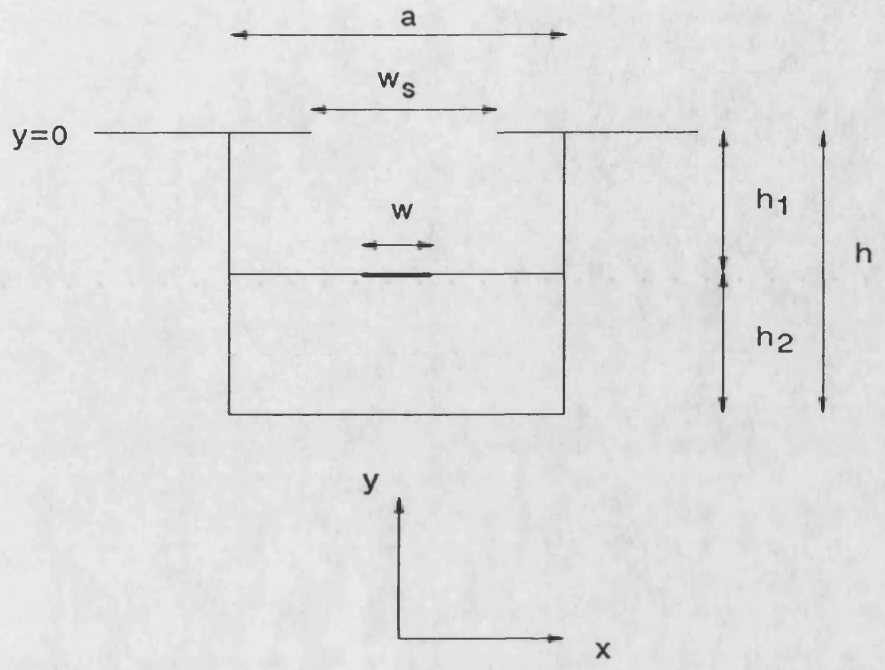

Figure 5.10 Cross section of partially filled MLIDG with the aperture at y=0 partly closed

Figure 5.10 gives the cross section of partially filled MLIDG with the aperture at $y=0$ partly closed.

The boundary conditions for this structure will be modified by the presence of the conducting surfaces at $y=0$. The boundary conditions at interface 1 now become

$$E_x(x,0)=E_z(x,0)=0 \qquad |x|>w_s \tag{5.45a}$$

while for the tangential magnetic fields

$$H_x(x,0^+)=H_x(x,0^-) \qquad |x|<w_s \tag{5.45b}$$

$$H_z(x,0^+)=H_z(x,0^-) \qquad |x|<w_s \tag{5.45c}$$

and

$$H_z(x,0^+)-H_z(x,0^-)=I_x(x) \tag{5.45d}$$

$$H_x(x,0^+)-H_x(x,0^-)=-I_z(x) \tag{5.45e}$$

Applying these boundary conditions to (5.36) and (5.39) gives

$$\begin{bmatrix} E_x(x,-h_1) \\ E_z(x,-h_1) \\ I_x(x,0) \\ I_z(x,0) \end{bmatrix} = \begin{bmatrix} \tilde{A}^{(1)} & \tilde{Z}^{(2)} \\ \tilde{Y} & -\tilde{L}^{(2)} \end{bmatrix} \cdot \begin{bmatrix} E_x(x,0) \\ E_z(x,0) \\ I_x(x,-h_1) \\ I_z(x,-h_1 \end{bmatrix} \tag{5.46}$$

where $E_x(x,0)$, $E_z(x,0)$ must be chosen to be zero for $|x|>w_s$. The dispersion relation can now be obtained and solved using the same method of section 5.5. It is noted however that the singularity in $E_x(x,0), \partial_x E_z(x,0)$ at edge of the conducting strips is now of the order $r^{-1/2}$. Thus upon discretisation, a suitable choice of basis functions for $E_{xi}(x), \partial_x E_{zi}(x)$ would be the functions (2.46).

The dispersion curves obtained for the fundamental mode for various values of aperture width is given in Figure 5.11. As $w_s \to 0$ we expect dispersion in the structure to approach that of boxed microstrip and the dispersion curves obtained for boxed microstrip are included in the figure for comparison. On the other hand, as $w_s \to a$ we expect dispersion to approach that of partially filled MLIDG and the dispersion curves obtained for the latter are also included for comparison.

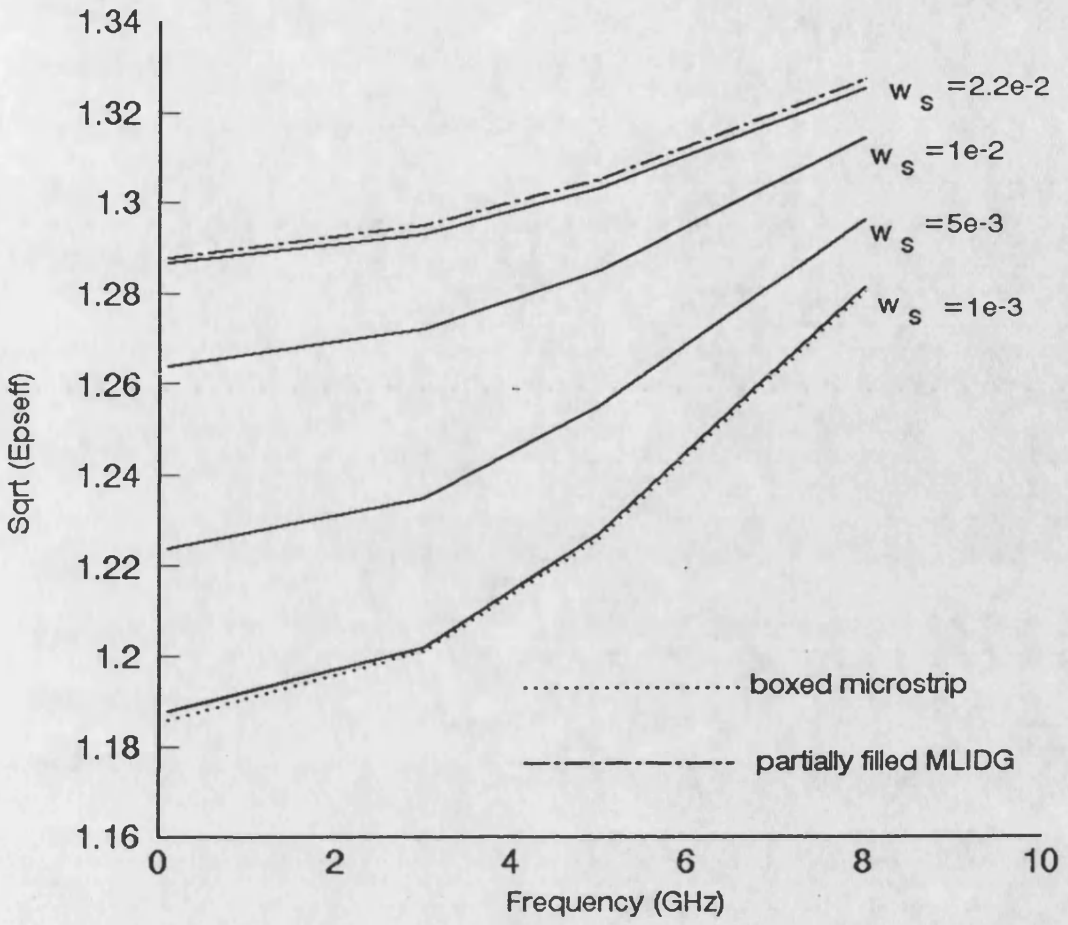

Figure 5.11 Dispersion curves obtained for t h e fundamental mode of partially filled MLIDG with the aperture at $y=0$ partly closed. a=2.286e-2, h=1.016e2, w=5e-3, $\epsilon_r=2.04$ (all dimensions in metres).

5.9 ANALYSIS OF EMBEDDED STRIP AND MULTIPLE STRIP IDG

5.9.1 ANALYSIS OF EMBEDDED STRIP IDG

The analysis of embedded strip IDG, proceeds in the same way that partially filled IDG was analysed. An equivalent structure for the guide can be setup as was done for the

partially filled IDG (see Figure 5.12). Each of the individual circuits of the equivalent structure of Figure 5.12b, can then be rigorously analyzed and the fields in the original guide are then the expressed as the superposition of the fields from these individual circuits.

5.9.2 ANALYSIS OF MULTIPLE STRIP IDG

For multiple strip IDG (Figure 5.13a), the same equivalent circuit of Figure 5.12b is used but with different boundary conditions being imposed on the tangential electric fields and the tangential magnetic fields at $y=0$:

The boundary condition on the tangential electric and magnetic fields at $y=0$ are:

$$E_x(x,0)=E_z(x,0)=0 \qquad |x|<w_1 \tag{5.47a}$$

$$H_z(x,0^+)-H_z(x,0^-)=I_x(x) \tag{5.47b}$$

$$H_x(x,0^+)-H_x(x,0^-)=-I_z(x) \tag{5.47c}$$

where $I_x(x,0)$, $I_z(x,0)$ are the x- and z-directed current components on the strip at $y=0$. The following relationship is then obtained for the fields at interface 1 and interface 2:

$$\begin{bmatrix} E_x(x,-h_1) \\ E_z(x,-h_1) \\ I_x(x,0) \\ I_z(x,0) \end{bmatrix} = \begin{bmatrix} \tilde{A}^{(1)} & \tilde{Z}^{(2)} \\ \tilde{Y} & \tilde{L}^{(2)} \end{bmatrix} \cdot \begin{bmatrix} E_x(x,0) \\ E_z(x,0) \\ I_x(x,-h_1) \\ I_z(x,-h_1) \end{bmatrix} \tag{5.48}$$

The generalisation from embedded strip IDG to multiple strip IDG is thus analogous to the generalisation that was used from IDG (Chapter 3) to MLIDG (Chapter 4), where the same admittance operators where used but the boundary conditions on the tangential and magnetic fields were modified. In addition the presence of the conducting strip modifies the singular behaviour of the fields at $y=0$, and thus the basis functions of section 4.3.1 are now used to model the tangential electric fields at $y=0$

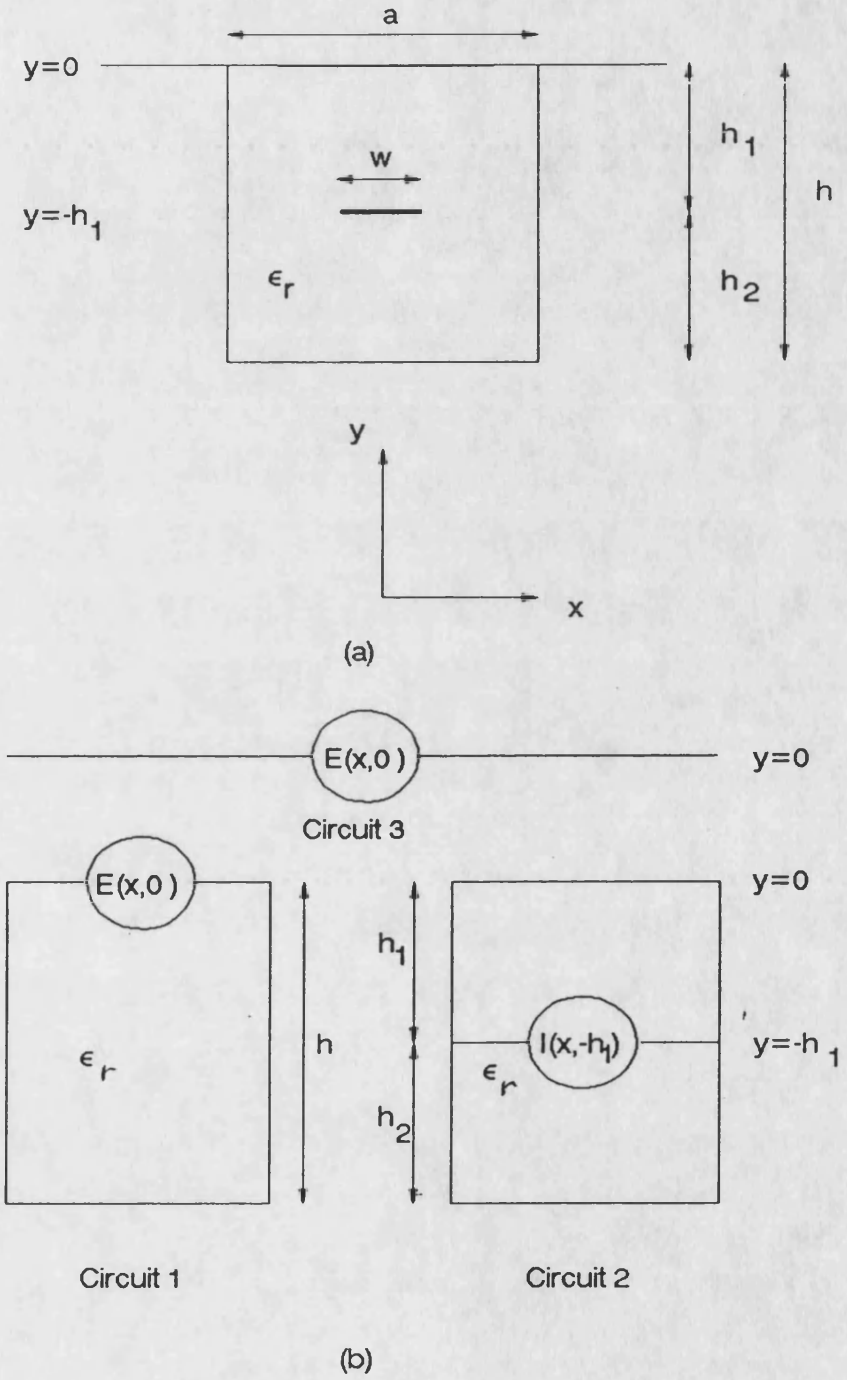

Figure 5.12 Cross-section of embedded strip IDG (a) and its equivalent circuit (b)

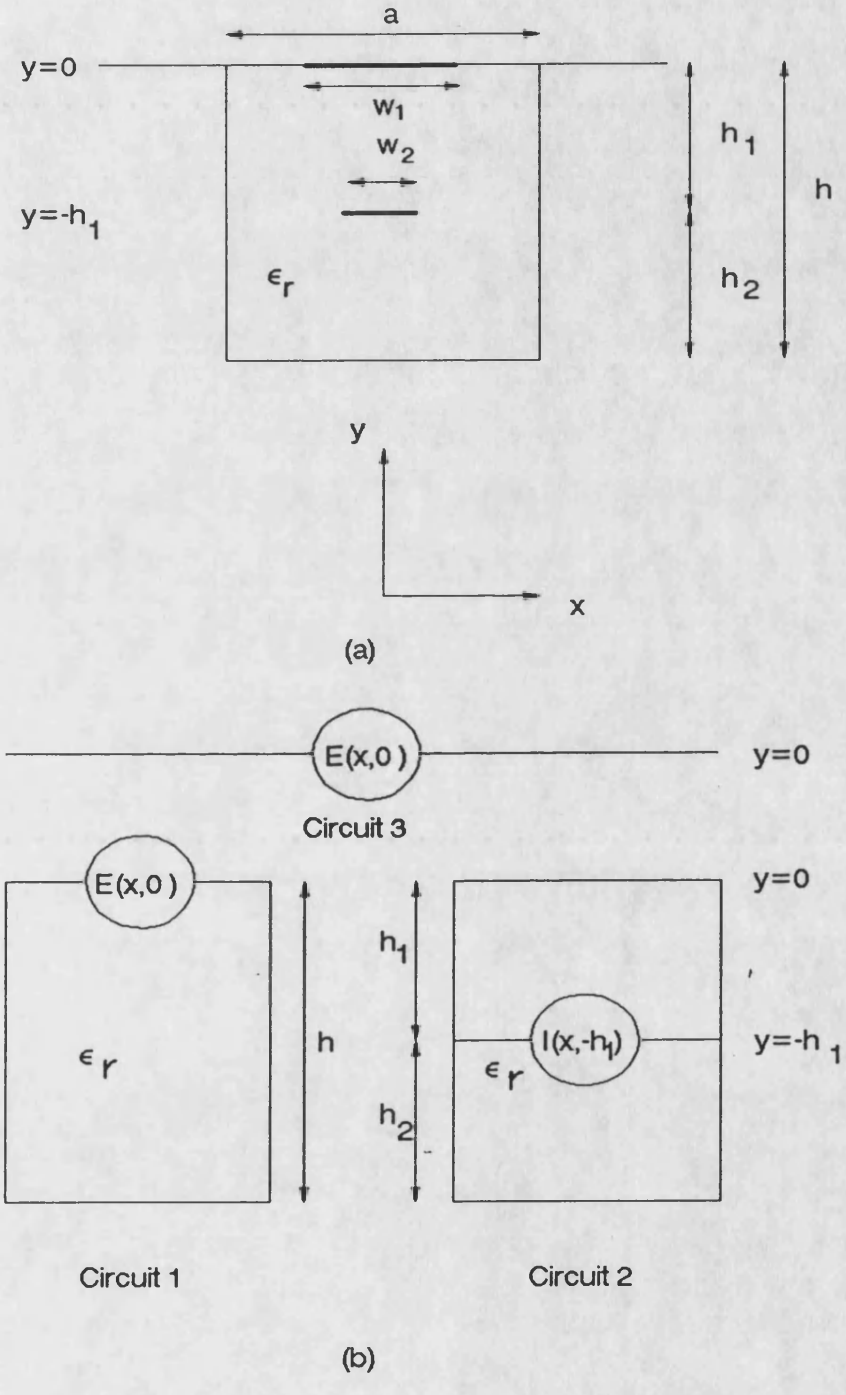

Figure 5.13 (a) Cross section of multiple strip IDG and (b) its equivalent circuit.

5.10 EXPERIMENTAL MEASUREMENT OF DISPERSION

Dispersion for several cross-sectional geometries was measured using the resonant section technique and the results obtained are compared with the computed values in Figure 5.15-5.17. It can be seen from the figures that the measured results are in good agreement with the computed results. In these results convergence to three significant figures was achieved using two basis functions for the basis expansions in (5.42).

It is noted that for the multiple strip IDG of Figure 5.17, two modes propagate down to DC, thus two sets of resonant frequencies were observed, each set associated with one of the propagating modes (Figure 5.14).

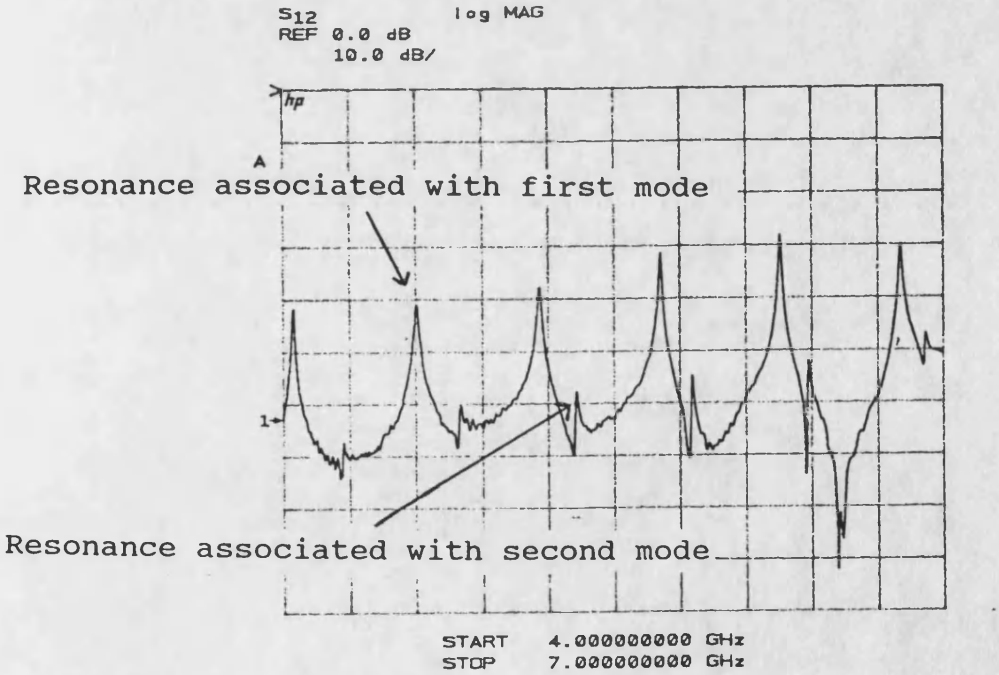

Figure 5.14 Insertion loss of a resonant section of multiple-strip IDG, measured on the HP8510A network analyzer.

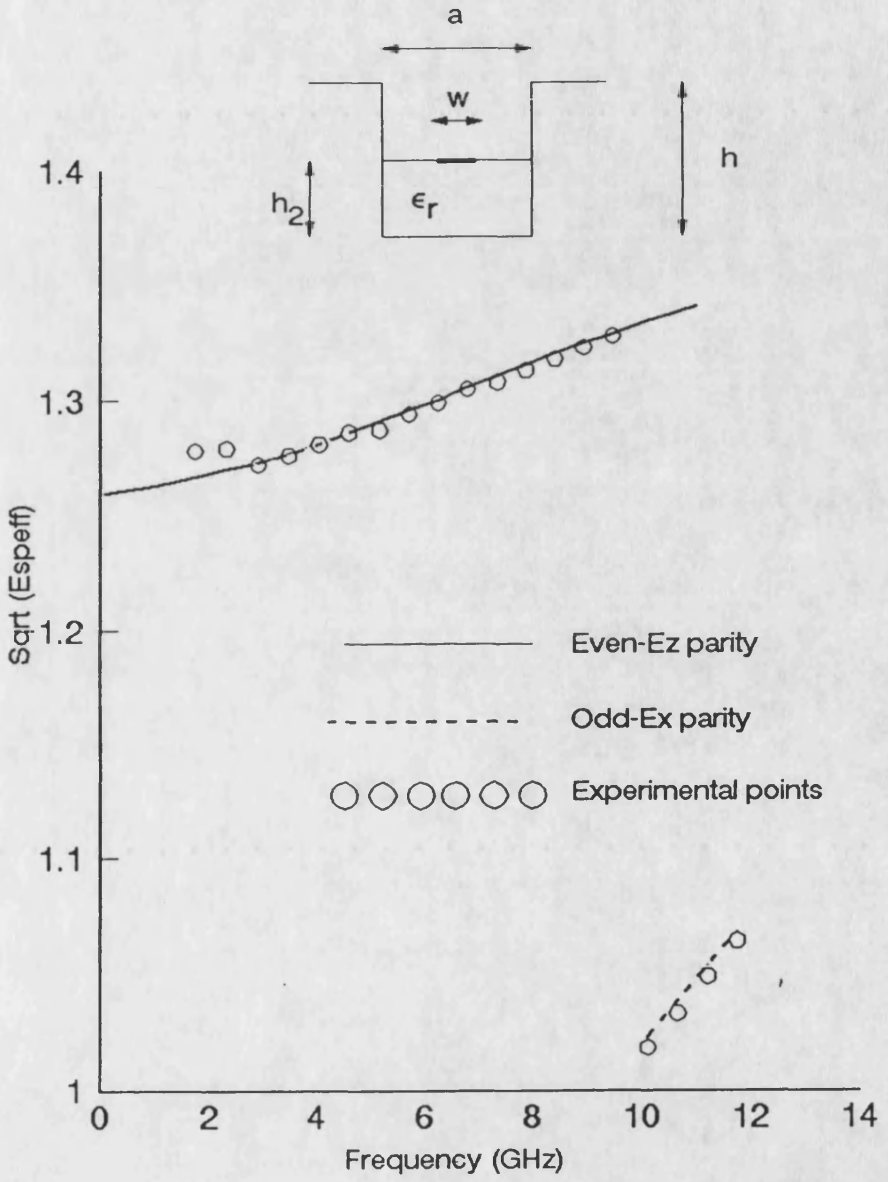

Figure 5.15 Dispersion characteristics of partially filled MLIDG. a=2.286e-2, w=6.5e-3, h=1.016e-2, h_2=7e-3, ϵ_r=2.04 (all dimension in metres).

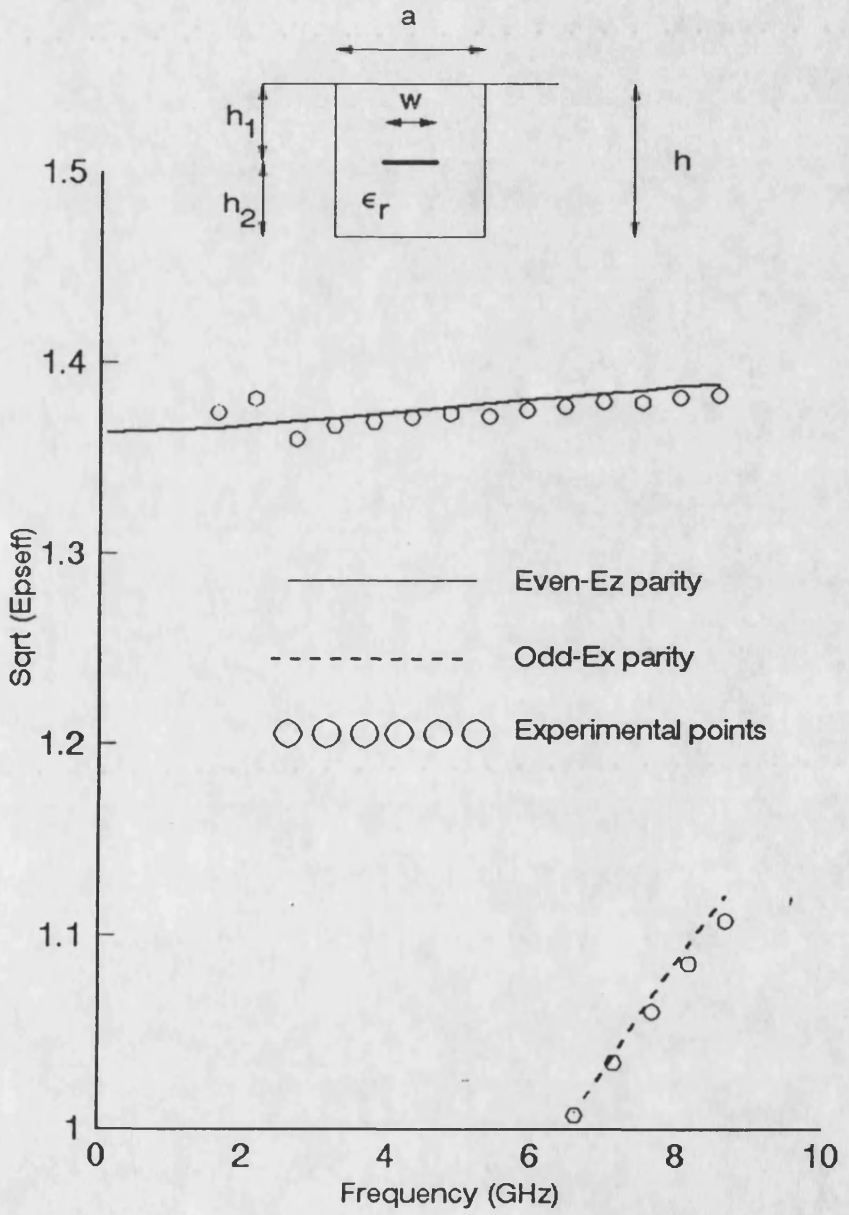

Figure 5.16 Dispersion characteristics of Embedded strip IDG. a=2.286e-2, h=1.016e-2, h_2=7e-3, ϵ_r=2.04 (all dimensions in metres)

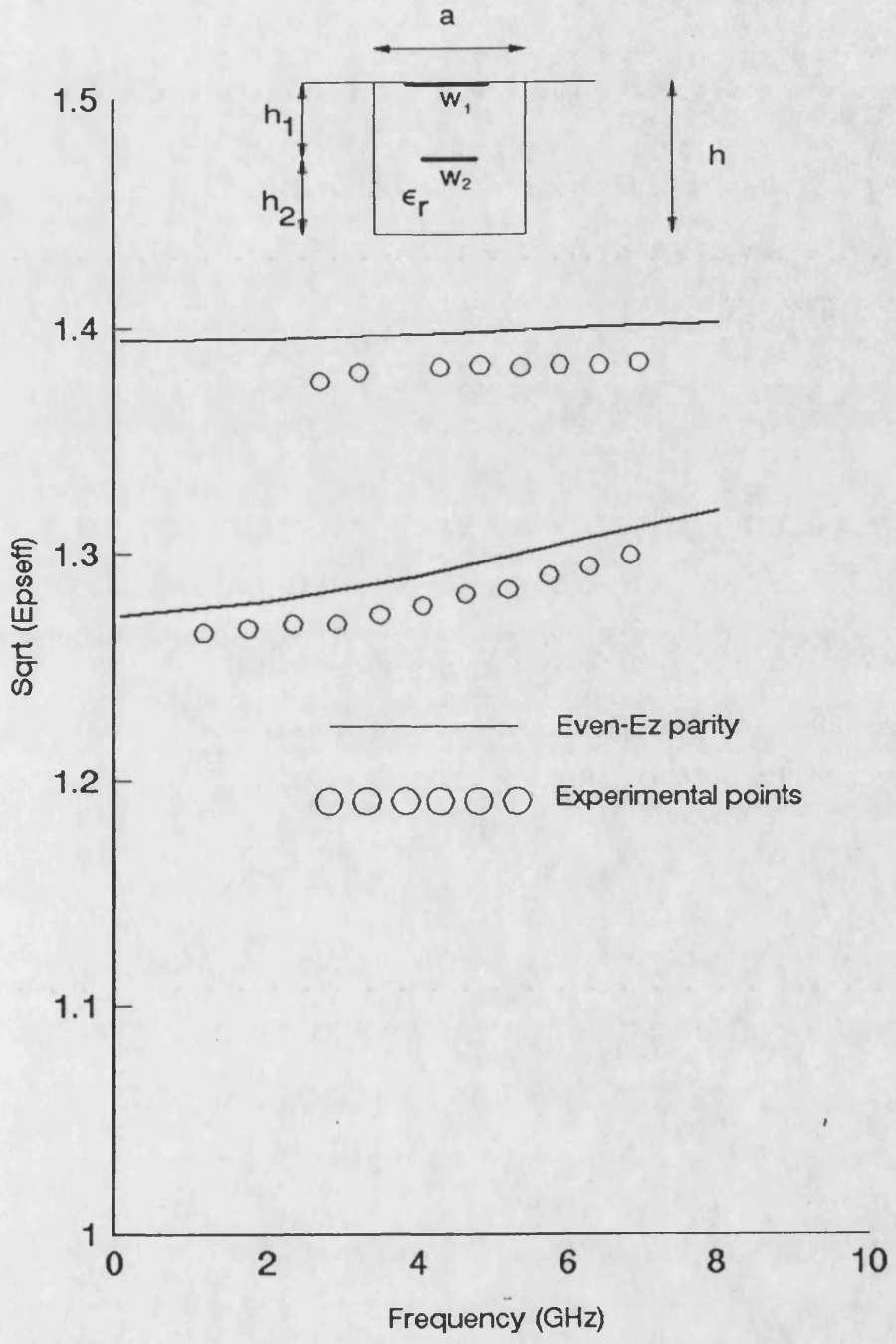

Figure 5.17 Dispersion characteristics of multiple-strip IDG. a=2.286e-2, h=1.016e-2, h2=8e-3, ϵ_r=2.04, w_1=5e-3, w_2=1e-2 (all dimensions in metres).

CONCLUSION

A rigorous method of analysis has been presented for the analysis of partially filled MLIDG, embedded strip IDG and multiple strip IDG. The advantage of these structures is the possibility of controlling stray coupling which arises in open microstrip circuits and these structures have a potential applications as antenna media.

Although the derivation of the integral operators required in the technique is elaborate, once the form of these operators is obtained, they can be readily setup for a generalised circuit almost upon inspection.

REFERENCES

1. J. R. James, P. S. Hall, and C. Wood, "Microstrip Antenna Theory and Design", IEE Electromagnetic Wave Series 12, Peter Pereguins Ltd., 1981.

2. T. Itoh, "Spectral Domain Immitance Approach for Dispersion Characteristics of Generalized Printed Transmission Lines", IEEE Trans. Microwave Theory Tech., Vol. MTT-28, 1980, pp. 981-985.

3. C.H. Chan, K.T. Kwong and A.B. Kouki, "A Mixed Spectral-Domain Approach for Dispersion Analysis of Suspended Planar Transmission Lines with Pedestals", IEEE Trans. Microwave Theory Tech., Vol. MTT-37, 1989, pp. 1716-1722.

4. C.J. Boukamp, "Diffraction Theory", Rep. Prog. Phys., Vol. 17, 1954, pp. 35-100.

5. J. Van Bladel, "Electromagnetic Fields", New York, McGraw-Hill 1964.

6. C.M. Butler, Y. Rahmat-Samii and P. Mittra, "Electromagnetic Penetration through Apertures in Conducting Surfaces", IEEE Trans. Antenna Propagat., Vol. AP-26, 1978, pp. 82-93.

7. C.M. Butler and K.R. Umashankar, "Electromagnetic Penetration through an Aperture Separating two half-spaces of Different Electromagnetic Properties", Radio Sci., Vol. 11, pp. 611-619, July 1976.

CHAPTER 6

CONCLUSION AND FURTHER WORK

6.1 DISCUSSION OF THE WORK PRESENTED IN THIS THESIS

This thesis has been concerned with the analysis of several different waveguide structures and identifying any potential advantages that these guides may have as transmission line media and as antenna media.

Microstrip was considered in Chapter 1. The generalised case of boxed, open or covered microstrip were considered with particular emphasis on covered and open microstrip. The cutoff condition for bound modes and radiation modes has been examined leading to the characterisation of the continuum into substrate modes and radiation modes. The presence of the substrate modes has important implications on stray coupling in microstrip circuits. The effect of dielectric thickness on the propagation of the substrate mode has been highlighted. In addition the effect of multi-layering on the substrate modes and on the higher order microstrip modes has also been highlighted.

Multilayered IDG was considered in Chapter 2. Here a novel

feature of IDG is identified and that is the large degree of control over the monomode bandwidth of this structure. Monomode bandwidth in single-layered IDG and in two-layered IDG were considered. Mechanisms for bandwidth control were identified and it was shown that by suitable choice of cross sectional dimensions and dielectric fillings, significant improvement in bandwidth can be achieved in twin-layered IDG.

In Chapter 4, the microstrip-loaded IDG was considered. In particular the characteristic impedance was calculated for this guide using the commonly adopted power-current formulation. Together with the analysis of dispersion, antenna and transmission line circuits may now be realised.

In Chapter 5, novel waveguide structures which involve the housing of microstrip circuits within an IDG structure. The potential advantages of these structures is control of stray coupling. A novel method of analysis presented. This method has the advantage of ease of adaptation to general circuits.

A particular feature of the method of analysis used in this thesis is its applicability to a large number of different configurations. The analysis of the wide variety of structures that were considered was substantially similar, and simple adaption allowed dispersion in the different cases to be efficiently characterised.

6.2 FURTHER WORK

Most of the devices that have been considered in this thesis are, open, radiating devices. The complete characterisation of these devices requires analysis of the bound dispersive modes which is presented in this thesis but in addition the radiation spectrum of these guides must be systematically characterised. Without the latter, a full investigation of these devices and systematic realisation of antenna circuits is not possible.

In particular the last class of waveguides to be considered - partially filled MLIDG, embedded strip IDG and multiple strip IDG may used to design a useful class of antennas.